MICROWAVE DYNAMICS

OF

QUASIPARTICLES AND CRITICAL FIELDS

IN

SUPERCONDUCTING FILMS

Thesis by

SRINIVAS SRIDHAR

In Partial Fulfillment of the Requirements

for the Degree of

Doctor of Philosophy

California Institute of Technology

Pasadena, California

1983

(Submitted December 21, 1982)

To

My Parents

Ranga and Iyengar

Acknowledgements

This work, like any other of a similar nature, had its inevitable accompaniment of labor, torment and joy. The peaks of success were made more enjoyable and the valleys of depression more bearable by the kind and generous support of teachers, friends and family. In particular I would like to thank :

Prof. Jim Mercereau, for sharing his critical insight, his invaluable encouragement and support and for his concern toward my development as a physicist

Dr.John Dick, experimental guide and philosophical bête noire, who was always ready to discuss any question - be it practical or eternal.

Ed Boud, to whom I could always turn to when in an experimental jam

Drs. Harris Notarys, Jean Delayen, Jeff Greif , Tadashi Yogi and Gerd Schon - who were generous of their time and knowledge

Dave Bell, Henry Mormile and the late Sandy Santantonio for invaluable technical assistance

My parents Ranga and Iyengar, Mala and to Usha and my larger family - for their affection and faith in me and my endeavours

Finally I would like to thank the California Institute of Technology for providing an excellent education and financial support.

Abstract

The microwave response of the superconducting state in equilibrium and non-equilibrium configurations was examined experimentally and analytically. Thin film superconductors were mostly studied in order to explore spatial effects. The response parameter measured was the surface impedance.

For small microwave intensity the surface impedance at 10 GHz was measured for a variety of samples (mostly Sn) over a wide range of sample thickness and temperature. A detailed analysis based on the BCS theory was developed for calculating the surface impedance for general thickness and other experimental parameters. Experiment and theory agreed with each other to within the experimental accuracy. Thus it was established that the samples, thin films as well as bulk, were well characterised at low microwave powers (near equilibrium).

Thin films were perturbed by a small dc supercurrent and the effect on the superconducting order parameter and the quasiparticle response determined by measuring changes in the surface resistance (still at low microwave intensity and independent of it) due to the induced current. The use of fully superconducting resonators enabled the measurement of very small changes in the surface resistance ($< 10^{-9}\ \Omega/$ sq.). These experiments yield information regarding the dynamics of the order parameter and quasiparticle systems. For all the films studied the results could be described at temperatures near T_c by the thermodynamic depression of the order parameter due to the static current leading to a quadratic increase of the surface resistance with current.

For the thinnest films the low temperature results were surprising in that the surface resistance *decreased* with increasing current. An explanation is proposed according to which this decrease occurs due to an additional high frequency quasiparticle current caused by the combined presence of both static and high frequency fields. For frequencies larger than the inverse of the quasiparticle relaxation time this additional current is out of phase (by π) with the

microwave electric field and is observed as a decrease of surface resistance. Calculations agree quantitatively with experimental results. This is the first observation and explanation of this non-equilibrium quasiparticle effect.

For thicker films of Sn, the low temperature surface resistance was found to *increase* with applied static current. It is proposed that due to the spatial non-uniformity of the induced current distribution across the thicker films, the above purely temporal analysis of the local quasiparticle response needs to be generalised to include space and time non-equilibrium effects.

The nonlinear interaction of microwaves and superconducting films was also examined in a third set of experiments. The surface impedance of thin films was measured as a function of the incident microwave magnetic field. The experiments exploit the ability to measure the absorbed microwave power and applied microwave magnetic field absolutely. It was found that the applied surface microwave field could not be raised above a certain threshold level at which the absorption increased abruptly. This critical field level represents a dynamic critical field and was found to be associated with the penetration of the applied field into the film at values well below the thermodynamic critical field for the configuration of a field applied to one side of the film. The penetration occurs despite the thermal stability of the film which was unequivocally demonstrated by experiment. A new mechanism for such penetration via the formation of a vortex-antivortex pair is proposed. The experimental results for the thinnest films agreed with the calculated values of this pair generation field. The observations of increased transmission at the critical field level and suppression of the process by a metallic ground plane further support the proposed model.

Contents

CH.I Introduction

The phenomenon of superconductivity is a manifestation of quantum mechanics on a macroscopic scale. As described in the BCS theory (B1) superconductivity arises due to the condensation of pairs of electrons into a coherent macroscopic quantum mechanical state. As a consequence of this coherence superconductors possess several unique properties - one of which is the absence of resistance to current flow.

The pairing of electrons leads to the formation of a ground state which is separated in energy by a gap Δ from a continuum of excited states. At zero temperature electrons in a region near the Fermi level are paired and occupy the ground state. At a finite temperature some of the excited states are occupied by excitations called quasiparticles. The quasiparticles constitute an electronic gas like system which is in thermodynamic equilibrium with the condensed pairs.

The two-component picture summarized above is a direct consequence of the BCS theory of the many-body interaction resulting in superconductivity and describes an astonishing range of phenomena when the quasiparticles and the pairs can be considered to be in equilibrium.

In situations where the quasiparticle and pair systems are out of equilibrium with each other and/or with the background lattice one might expect that the unique macroscopic quantum mechanical nature might manifest interesting features. The equilibrium BCS description would have to be modified in order to include non-equilibrium situations. This question has been the subject of intense research recently (G1) resulting in the elucidation of a variety of interesting phenomena.

Non-equlibrium situations are usually induced by an external (drive) perturbation and studied with a probe perturbation. The nature and amount of disequilibrium is determined by the strength of the drive and the time scale of observation relative to the characteristic relaxation times of the system. Thus

non-equilibrium phenomena are intimately determined by time-dependent processes in the superconductor.

Viewed in this context the study of effects due to time-dependent perturbations (drive and probe) would seem to be ideal tools to examine non-equilibrium questions. While several investigations have been carried out in superconductivity , rather surprisingly a coherent picture has not emerged. A problem that has been studied extensively and yet lacks a satisfactory theoretical explanation (P1) is the dependence on an applied static magnetic field of microwave absorption in bulk superconductors in the presence of a static magnetic field (see Ch.III). Nonlinear effects at high frequencies have been sparsely examined. The stability of non-equilibrium states (Ch.10,11 of G1) promises to pose interesting problems for the future.

The work reported here is the outcome of experimental and analytical investigations of the interaction of superconductors with high frequency radiation in the microwave range. Recent progress in technology has enabled us to examine this interaction with greatly enhanced sensitivity, control and precision. The experiments utilise superconducting high Q ($10^4 - 10^9$) microwave cavities and have resulted in the measurement of changes in surface resistance as small as $10^{-9}\ \Omega$/sq.!! The experimental configuration allows for the measurement of absolute impedance (see later for definitions) and microwave power and field enabling us to arrive at quantitative conclusions.

Three situations concerning the microwave superconductor interaction were examined :

(1) At low microwave intensity the transport parameter called surface impedance was measured for a variety of superconductors (Ch.II). This is an equilibrium configuration where the microwaves act as a probe of the superconducting state. The experimental results agreed with calculations based on the equilibrium BCS theory. This work forms an essential foundation to the subsequent investigations of non-equilibrium and nonlinear effects.

(2) The effect of a static supercurrent on the surface resistance of thin superconducting films was examined. The microwave intensity was kept low and the results were independent of it.(Ch.III) The use of fully superconducting high

Q cavities enabled us to detect extremely small changes ($\gtrsim 10^{-9}\Omega$/sq.) in the surface resistance.

Under certain conditions the results (increased surface resistance or absorption) could be described by thermodynamic (equilibrium) effects of the static current on the superconducting film. The observed quadratic increases of the surface resistance at high temperature (red. temp. $t > 0.9$) could be explained by the mechanism of order parameter depression due to the static current.

When the temperature was reduced ($t < 0.9$ for the thinnest Sn films $d \leq 500\text{Å}$) a surprising result was obtained. The absorption decreased with increasing static current whereas equilibrium considerations (at low static current) only predict increases. It was as if application of the static current resulted in "cooling" of the superconductor. It was found that such an effect could be described by a non-thermal quasiparticle distribution function which is produced if there is both a static current and high frequency current. This gives rise to an additional quasiparticle current which is out of phase with the microwave electric field and results in reduced absorption. The microwaves cease to be a mere probe of the superconductor even though the results are independent of microwave field. This is the first observation of the non-equilibrium quasiparticle distribution function effect described above. The results of this experiment also raise several important and interesting questions whose examination should yield further information regarding dynamic processes at short time scales ($\sim 10^{-10}$ sec).

One interesting outcome of this investigation is the reinterpretation of measurements of this class (i.e. dependence of surface impedance on static magnetic field or current) as measurements of supercurrent and quasiparticle current components whose phases relative to the applied high frequency fields determine whether the measured surface impedance increases or decreases. These components arise due to the action of the static and high frequency fields on the order parameter, density of states and quasiparticle energy spectrum. They are nonlinear versions of the well-known quasiparticle backflow current (or "anti-backflow" depending on phase).

The result that has emerged from the present experimental and analytical considerations (Ch.III) is that the temporal or dynamic response of quasiparticles plays an important role in experiments of this type. For the thinnest films studied in this work the spatial uniformity of the perturbations simplifies the considerations to purely time-dependent effects in a (vanishingly) small region of the superconductor. Under conditions of spatial non-uniformity a more comprehensive (and complicated) analysis of the mixed space and time effects would be required. Our experimental results for thicker Sn films indicate that this is indeed the case. It is suggested that such effects are likely to be crucial in understanding the hitherto unexplained results for bulk superconductors for the dependence of impedance on magnetic field.

(3) Another set of investigations was designed to exploit the ability to measure absolutely powers and magnetic fields at high frequency. This is possible again because of the precise geometry of the resonator which enables us to quantify the microwave intensity and hence the superconductor - microwave interaction. Here there was no static current but the microwave intensity was larger and expected to significantly perturb the superconductor. Experimentally an unexpected limitation on the maximum microwave magnetic field that could be applied to the thin films was observed. This high frequency (dynamic) critical field was well below the thermodynamic thin film critical field. The thermal stability of the films was demonstrated and it was observed that at this field level the films were unstable to flux penetration. A model which allows such flux penetration via the dissociation of vortex-anti vortex pairs is proposed. An interesting outcome of this work was the realization that this type of experiment could be used to study formation dynamics of macroscopic excitations (vortices or flux lines).

1. Equilibrium and Non-equilibrium superconductivity

We now describe what is meant by the terms "equilibrium" and "non-equilibrium" with special reference to superconductivity.

A system is said to be in equilibrium with its surroundings when it can be described by single values for the macroscopic thermodynamic variables (eg.

temp. T) and which are unchanging in time. The system will be in equilibrium when it is not acted upon by any external force - the equilibrium state is the state of lowest free energy.

Microscopically the system is characterised by the distribution function $f(\varepsilon_k)$ which is the occupation number for the particles having an energy ε_k where k is a variable characterising the energy level. The distribution function is arrived at by minimising the free energy associated with different configurations of the system, incorporating all the particle interactions (or scattering processes). For a given equilibrium state, f may be parameterised by the thermodynamic variables T, P, etc.

Under the influence of an external perturbation which acts on the constituents of the system, their energies, momenta and distribution are altered. The driving force is balanced by relaxation and diffusion and (if the driving force is not too large) the system reaches a *steady state* or one of *dynamic equilibrium*. The characteristic of this state is that the distribution function f^* is generally different from that of the equilibrium or thermal function f. Further f^* is determined by the balance of drive and relaxation rates. Such a state characterised by a nonthermal distribution function and in dynamic equilibrium is referred to as a *non-equilibrium steady state*.

Having given this very brief definition of what the terms equilibrium and non-equilibrium mean in a general context we turn to the system of interest in this work - superconductivity - and discuss superconductors in equilibrium and non-equilibrium states.

In contrast to the case of normal metals, superconductors are easily driven out of equilibrium by relatively weak perturbations. The simple reason for this is the small magnitude of the energy gap Δ compared to the Fermi energy ε_F. Superconductors display a rich variety of phenomena when acted on by different perturbations driving them out of equilibrium - the details of the response being dependent on the details of the perturbation.

The BCS model describes very well the ground state or unperturbed state at a given temperature. Weak perturbations have been used to study superconductors and have confirmed the BCS model in a spectacular way. Since the

perturbation is very weak the superconductor is not altered from the BCS state. An excellent example is the study of the surface impedance at low microwave powers discussed in Ch.II When a static current is superposed on the high frequency measuring current or as the strength of the perturbation is raised one has to consider how the BCS state itself is altered by the perturbation.

2. Classification of Nonequlibrium States in Superconductors

The fundamental parameter that may be used to characterise the state is the distribution function $f_{\vec{k}}(\varepsilon_{\vec{k}})$ of quasiparticles of momentum $\vec{k}$ and energy $\varepsilon_{\vec{k}}$. In the BCS model $f(\varepsilon_{\vec{k}})$ is simply the Fermi function at the ambient temperature. In studying the response to weak perturbations the Fermi function is used to compute quantities of interest. (For example this leads to $R_s \alpha e^{-\Delta/kT}$ at low temperature where Δ is the equilibrium gap at temperature T). In the nonequilibrium state $f^*(\varepsilon_{\vec{k}}) \neq f(\varepsilon_{\vec{k}})$ (the thermal distribution function) and depends on the details and strength of perturbation.

The nature of the perturbation determines the properties of f^*. It is possible to categorise the perturbation and the resulting f^* into two types determined by the symmetry of f^* with respect to local inversion through the Fermi surface i.e w.r.t $\varepsilon_{\vec{k}}$ (S4,T2). A further subdivision determined by the symmetry w.r.t. $\vec{k}$ is also carried out.

I "EVEN, LONGITUDINAL, ENERGY OR TEMPERATURE MODE" f^* even in $\varepsilon_{\vec{k}}$

(a) f^* even in $\varepsilon_{\vec{k}}$ and odd in $\vec{k}$: This can be caused by a current of density J flowing in a "clean" superconductor and can be studied by measuring the electromagnetic response in the current carrying state. This leads to a dependence of R_s on J for which results are reported in Ch.3.

(b) f^* even in both $\varepsilon_{\vec{k}}$, $\vec{k}$: Strong electromagnetic radiation falls under this class. Typical phenomena associated with this type are the gap-enhancement of Eliashberg and the dependence of surface impedance on the microwave field. This latter effect was studied in this work and is described in Ch.IV

In a "dirty" superconductor impurity scattering randomises the

quasiparticle momenta and the distribution function has a weak dependence on the direction of $\vec{k}$. Thus a current acting on a dirty superconductor is more appropriately characterised as a type (b) perturbation.

This mode is also called the temperature mode because the symmetry is similar to that of a change in temperature : the population of both the $\vec{k} > \vec{k}_F$ ($\varepsilon_{\vec{k}} > 0$,electron-like) and $\vec{k} < \vec{k}_F$ ($\varepsilon_{\vec{k}} < 0$,hole-like) branches of the quasiparticle energy spectrum are equally changed.

One of the interesting effects associated with this mode is a "cooling effect" in which the superconductor reacts to the perturbation *as if it's temperature were decreased*. The intuitively reasonable "heating effect" in which the temperature is *apparently increased* is also observed.

In Ch.II we describe an experiment in which, depending on experimental conditions, both the heating and cooling effects are observed as apparent increases or decreases of the microwave absorption caused by a static current.

II ODD OR TRANSVERSE MODE : f^* odd in $\varepsilon_{\vec{k}}$

(c) f^* odd in $\varepsilon_{\vec{k}}$, even in $\vec{k}$: Branch imbalance falls under this class.

(d) f^* odd in both $\varepsilon_{\vec{k}}$, $\vec{k}$: Thermoelectric phenomena.

Perturbations associated with the transverse mode have been extensively studied and the results are described in ref.(G1).

3. Relationship of this work to the scheme of classification

In this work the applied perturbations result in non-equilibrium distribution functions which are characteristic of the energy or longitudinal mode. The perturbations were of two types :

(a) Static + High frequency (small) fields (Ch.III) applied to thin superconducting films resulting in induced currents

(b) Strong microwave radiation i.e. "large" high frequency fields applied to thin films (Ch.IV)

We briefly discuss the effects associated with these two perturbations in relation to general theoretical considerations and to other experiments of a similar type.

3.1. Static + High Frequency Currents

In Ch.III we describe experimental and analytical results for the dependence of the surface impedance on induced static current in thin films. In the presence of both static and high frequency currents the high frequency conductivity (and hence impedance) is different than if the high frequency measuring current alone were present. Such measurements yield important information regarding quasiparticle dynamics in superconductors.

Scattering of quasiparticles by impurities (elastic) and phonons (inelastic) plays an important role in determining the nature of the non-equilibrium distribution function. The distribution function can be decomposed into static and high frequency components. The static component is largely determined by elastic impurity scattering. The high frequency or dynamic component is determined by the relation between the frequency ω and the elastic (τ_{imp}) and inelastic (τ_{in}) scattering times. For weak scattering ("clean" limit) the quasiparticles remain in their momentum state but change energy with the high frequency field for frequencies smaller than $1/\tau_{imp}$. For strong elastic scattering ("dirty" limit) the momentum distribution is randomised and the energy distribution is determined by the relative magnitudes of ω and $1/\tau_{in}$ (ref.02). In the latter case this leads to novel effects discussed in Ch.III.

While this type of perturbation is easily produced by applied or induced current, there are few studies of its time dependence. The experiment of Peters and Meissner (P2) in which they measured a gap relaxation time was confined to a very narrow region near T_c. Because the number of quasiparticles decreases rapidly below T_c experiments that look directly for dynamic quasiparticle effects are almost nonexistent. Early experiments on the dependence of surface impedance on an applied magnetic field required large fields in order to observe any effects. The results have not led to any understanding of the basic phenomena (P1).

The experiments carried out in this work (Ch.III) have the great advantage of extremely high sensitivity which is maintained at all temperatures. Furthermore the ability to vary film thickness enables us to separate out local time dependent effects from more complicated space-time effects. A novel "cooling"

effect was observed which is explained by non-equilibrium effects on the distribution function. Such non-equilibrium considerations have been included for the the first time in the analysis of such experiments and it is clear that they play a major role in the dynamics of quasiparticles.

3.2. Strong Microwave Radiation

The gap enhancement under strong microwave irradiation predicted by Eliashberg (E1) is an important example of effects associated with such a perturbation. In the experiments designed to observe this effect the superconductor is irradiated with microwaves and the gap measured by tunnelling. Since the coupling to the microwaves is not well defined the actual strength of the perturbation is not quantitatively known. The effect on the gap is usually plotted versus the incident microwave power which is quoted in arbitrary units.

One can devise an experiment in which the coupling of the superconductor to the incident radiation is well defined and the strength of the perturbation measured quantitatively. By this we mean that the surface magnetic field B_ω and the power absorbed P_{abs} can be measured absolutely. In such an experiment which is described in detail in Ch.IV, the response of the superconductor is determined by measuring the surface impedance Z_s as a function of B_ω or P_{abs}. Theoretical analysis indicates (S2) that under appropriate conditions it should be possible to observe a cooling effect in which the surface resistance decreases with increasing high frequency field. The experimental observation effect of such an effect seems to be hampered by experimental limitations (see Ch.IV).

3.3. High Frequency or Dynamic Critical Fields

Beyond the possible nonlinear effects just discussed, there exists the question of critical currents and fields at high frequencies. This is largely uncharted land where experiments are few and theoretical understanding limited. There have been no measurements of high frequency critical currents in thin films. One important question is whether it is possible to observe the superheating fields at high frequencies reported in Ref.(Y1) . Along with this there is a very practical concern as to the maximum fields attainable in high frequency

superconducting structures. This has relevance to a host of problems in accelerator design and energy storage.

With these questions in mind we report the first clear results for high fields incident on thin films at microwave frequencies in Ch.4 where we have measured a dynamic critical field. A new model is proposed for the inhomogeneous destruction of superconductivity at fields well below the thermodynamic critical field via the formation of a vortex-antivortex pair. Experiments and calculations indicate that this mechanism is responsible for the observed dynamic critical field.

4. The Superconductor - Microwave Interaction

In the experiments described in this work microwave fields were used to probe the superconductor. A brief description of the interaction of microwaves with superconductors is now provided.

Consider a magnetic field B_ω oscillating at a frequency $f = \omega/2\pi$ applied at the surface of a *bulk* superconductor (Fig.1.1 a). Due to the Meissner effect (which is operative as long as $\omega < 2\Delta$, the energy gap) the field is screeened out from the interior and decays exponentially into the metal. A screening supercurrent (non-dissipative) is induced at right angles to the magnetic field (Fig.1.1 (b)). This screening current is due to the response of the condensate (Cooper pair) electrons *and* the quasiparticles ("backflow").

Due to the changing magnetic field there exists an electric field E_ω which is out of phase by $\pi/2$ with B_ω. The electric field accelerates the quasiparticles resulting in absorption of energy. (At zero frequency there is no absorption because E_ω is absent). Associated with the electric field is a quasiparticle (normal dissipative) current.

The current field relationship can be written in terms of a complex conductivity (M1). For the simple case in which the fields and currents are locally related (see later for more general cases), this relation can be written :

$$J_\omega = \sigma_s E_\omega = (\sigma_1 - i \sigma_2) E_\omega = -i \omega (\sigma_1 - i \sigma_2) A_\omega \qquad (1.1)$$

where σ_2 determines the supercurrent and σ_1 the quasiparticle current. These

are functions of frequency and temperature relative to the temperature-dependent energy gap. For a normal metal, $\Delta = 0$ and $\sigma_1 = \sigma_n$, $\sigma_2 = 0$. We call the real part of eqn.(1.1) $J_{s\omega}$ and the imaginary dissipative part $J_{q\omega}$.

For frequencies much smaller than the gap the eqn for $J_{s\omega}$ (the σ_2 part) reduces to London's eqn.: $J_s = -(c^2/4\pi\lambda_L^2)\,A$ because $\sigma_2 = n_s e^2/m\omega = c^2/4\pi/\omega\lambda_L^2$ where n_s is the density of condensate electrons (Cooper pairs) and λ_L is the London penetration depth. This is a good approximation at all frequencies $\omega < 2\Delta$ and hence is applicable at microwave frequencies.

The phase (or temporal) relationship between the currents and fields is depicted in Fig.(1.1(c). using eqn.(1.1). The quasiparticle normal current $J_{q\omega}$ whose magnitude is determined by σ_1 is out of phase by $\pi/2$ from the supercurrent $J_{s\omega} \propto \sigma_2$. In the experiments carried out here $\sigma_2 \gg \sigma_1$. However since we are directly measuring the effects of absorption the effects of the quasiparticles are important.

4.1. Generalization to Nonlocal Situations

The simple discussion given above was based upon a *local* relation between current and field i.e. the current in a small region is determined by the field in the same region. Even in normal metals this situation is invalid if the mean free path (m.f.p.) $l \gg \delta$, the skin depth. This limit is usually called the anomalous skin effect. The current is then determined by a spatial average of the fields over a region of size l.

In superconductors the size of the contributing region is determined by the Pippard coherence length ξ. The m.f.p. dependence of ξ can be described by $\xi^{-1} = \xi_0^{-1} + l^{-1}$ where ξ_0 is the pure bulk coherence length. The resulting J-A relation can be compactly expressed in Fourier space as ($\vec{q}$ = wavevector):

$$\vec{J}_\omega(\vec{q}) = -K(\vec{q},\omega,T)\,\vec{A}_\omega = -i\,\omega\,\sigma_s(\vec{q},\omega,T)\,\vec{A}_\omega \qquad (1.2)$$

This is a generalization of Eq.(1.1). Two limits are interesting and simple:

Local Limit	$l \ll \xi_0$	$K(\vec{q}) \rightarrow$ constant
Extreme Anomalous Limit	$\lambda \ll \xi_0$	$K(\vec{q}) \rightarrow 1/q\xi$

The latter case is just the Pippard case mentioned above. In either limit the expressions for σ_1 and σ_2 are independent of wavevector when normalised to σ_n. Expressions for them have been given by Mattis and Bardeen (M1).

$K(\vec{q},\omega,T)$ has been given for general $\vec{q},\omega,T$ by Khalatnikov and Abrikosov (K2) using the BCS theory. We have used their results to calculate the surface impedance of thin films in order to compare with experimental results (Ch.II)

5. Time and length scales relevant to this work

The superconducting energy gap Δ represents a fundamental time (frequency) scale which is the correlation time of a Cooper pair. At frequencies much greater than Δ the distinction between the normal and superconducting states is blurred. In the present experiments the frequency (10 GHz) $\omega < \Delta$ in the temperature range in which the experiments were carried out (except for $T > 0.98T_c$).

The presence of impurities resulting in elastic scattering of the *electrons* introduces an additional time scale $\tau_{el} = l/v_F$ (l = mean free path, v_F = Fermi velocity). Anderson (A1) has shown that non-magnetic impurities do not drastically affect the thermodynamic properties of the superconductor, i.e. the thermodynamic parameters T_c, bulk critical field B_c etc. are nearly the same. However the electrodynamic response is considerably dependent on the amount of impurity scattering (T1). The penetration depth λ and Pippard coherence length ξ in the "dirty" limit ($l \ll \xi_0$, $\tau_{el} \ll \Delta$) are changed from their values in the pure or "clean" limit ($l >> \xi_0$, $\tau_{el} >> \Delta$) limit λ_p and ξ_0 respectively by :(T1)

$$\lambda(l) = \lambda_p \left(1 + \frac{\xi_0}{1.33\, l}\right)^{1/2} \tag{1.3}$$

$$\xi^{-1} = \xi_0^{-1} + l^{-1} \tag{1.4}$$

The Ginzburg-Landau coherence length ξ which is $\approx \xi_0$ in pure materials at low temperature is given in the dirty limit by :

$$\xi = 0.855 \frac{(\xi_0 l)^{1/2}}{(1-t)^{1/2}} \qquad (1.5)$$

For the material Sn ξ_0 = 2300 Å. The pure bulk penetration depth λ_p is slightly different than the London penetration depth $\lambda_L(0)$ (H1) :

$$\lambda_p(0) \approx 510\ Å \qquad \lambda_L(0) \approx 350\ Å$$

In practise the clean limit is realised only in pure bulk samples. Except in the bulk samples of Ch.II in almost all the thin films studied here the dirty limit is applicable and we use eqns.(1.1) to (1.3) where necessary. The relation of the magnitudes of ω^{-1} ($\sim 10^{-9}$) , Δ^{-1} ($\sim 10^{-13}$) and τ_{el} ($10^{-13} - 10^{-14}$) (in secs) are depicted in Fig.1.2 These time and length scales are adequate for the equilibrium description of transport processes.

Under non-equilibrium conditions a new set of relaxation times determined by inelastic scattering processes enters into the picture. If the quasiparticles and pairs systems are out of equilibrium within themselves, with each other or with the phonon system due to the influence of a perturbation then they tend to relax back into equilibrium via a variety of channels :

(a) Inelastic Scattering with phonons of all frequencies

(b) Recombination processes involving phonons of frequency $\Omega \geq 2\Delta$ which change the number of quasiparticles above the gap. In equilibrium this process is determined by the number of thermal phonons but the recombination rate can be changed by any driving mechanism which causes an excess of phonons with $\Omega \geq 2\Delta$. The paired electrons also participate in the recombination process.

(c) Electron - Electron scattering - this is important at high energies

(d) Branch mixing which arises if the branches $+\vec{k}$ and $-\vec{k}$ are unequally populated as in tunnel injection but not with microwaves.

The respective relaxation rates are called τ_s , τ_R , τ_{ee} and τ_Q.

For a quasiparticle of energy E the net relaxation rate will be the sum of contributions due to all processes. As mentioned above the latter channels can be ignored for the cases of interest here. The net rate then can be written as :

$$\frac{1}{\tau(E)} = \frac{1}{\tau_s(E)} + \frac{1}{\tau_R(E)} \qquad (1.6)$$

For quasiparticles at the gap edge ($E = \Delta$) and at low temperature ($\Delta >> T$) τ_s and τ_R can be written as (K1) :

$$\tau_s(\Delta,T) = \tau_0 \frac{1}{\Gamma(7/2)\zeta(7/2)} \left(\frac{2\Delta(0)}{kT}\right)^{1/2} \left(\frac{T_c}{T}\right)^{7/2} \qquad (1.7)$$

$$\tau_R(\Delta,T) = \tau_0 \frac{1}{\sqrt{\pi}} \left(\frac{kT_c}{2\Delta(0)}\right)^{5/2} \left(\frac{T_c}{T}\right)^{1/2} \exp\left(\Delta(0)/kT\right) \qquad (1.7)$$

τ_0 is a characteristic time of the material. The values of τ_0 for several materials of interest are :

VALUES OF τ_0 FOR SOME MATERIALS

Al	4.4×10^{-7} sec
Sn	2.3×10^{-9} sec
In	7.8×10^{-10} sec
Pb	2.0×10^{-10} sec

At $t = 0.5$ and for material Sn we get :

$t = 0.5$ $\quad \tau_s(\Delta,T) = 1.1 \times 10^{-8}$ sec $\quad \tau_R(\Delta) = 2.0 \times 10^{-9}$ sec

In the temperature range $0.4 < t < 1$ $\tau_R < \tau_s$ at $E = \Delta$ and consequently dominates the relaxation rate in eqn.(1.4). In this temperature range $\tau(\Delta) \sim 10^{-9}$ sec.

The relationship of all the relevant times τ_s , τ_R , ω^{-1} , Δ^{-1} , and τ_{el} are depicted in Fig.1.2. At 10 GHz $\omega\tau \sim 50$ for Sn and this implies that insofar as inelastic processes are concerned the quasiparticles cannot be described as adiabatically following the high frequency fields. This is a necessary criterion for producing non-equilibrium situations. (Ch.IV,S1, G1).

Most of the work described here was with the material Sn along with some examination of Pb, Al and In. These must be some of the most widely studied superconductors - a fact which itself is of advantage since the main interest here is in the fundamental dynamics of superconductivity rather than in exotic material properties. In addition the following criteria dictated the choice of

materials :

(a) ability to fabricate high quality specimens

(b) critical temperatures in the accessible range of 1.5 - 4.2 K .The T_c 's of the various materials are :

Sn 3.7 K, In 3.4 K, Pb 7.2 K, Granular Al 2.1 K.

(c) A convenient microwave resonator size determines the microwave frequency (10 GHz). For producing non-equilibrium situations we have mentioned that $\omega \tau$ must be >> 1 which is valid at 10 GHz for Sn, Al and In.

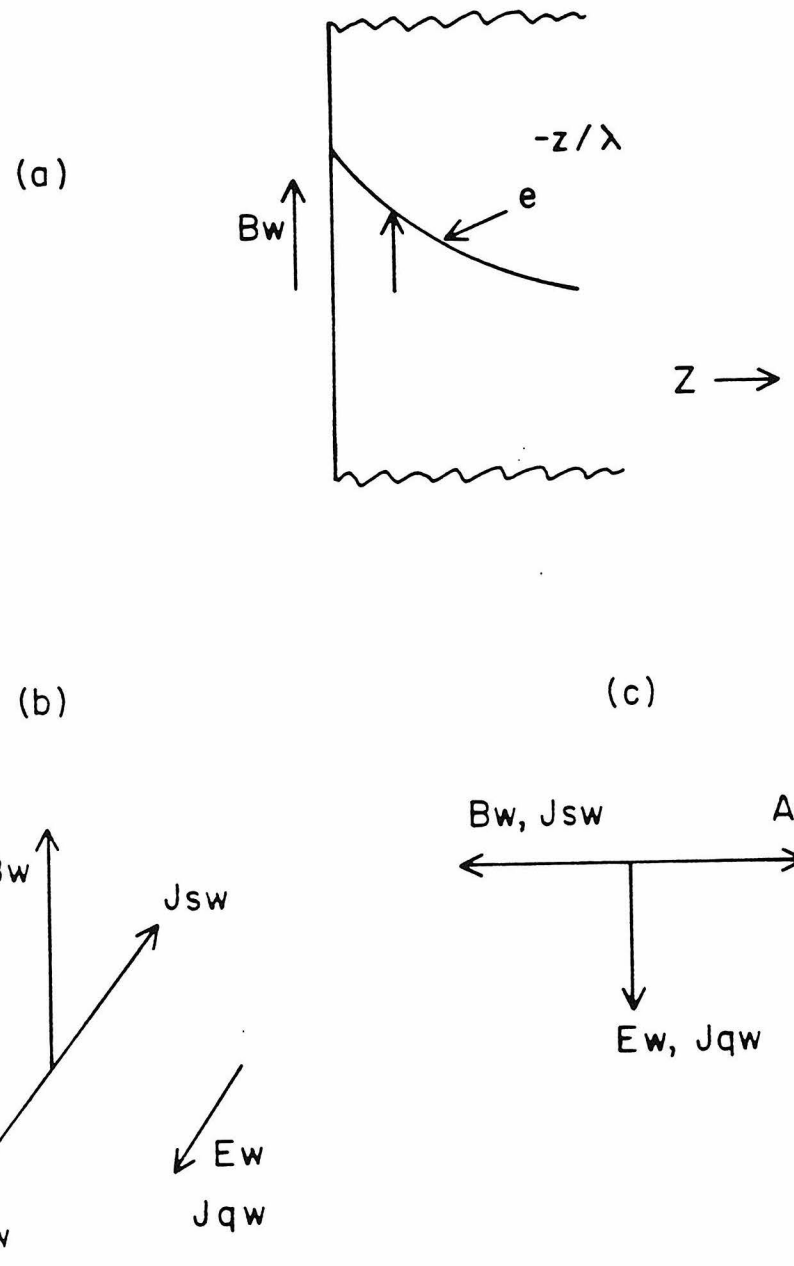

Fig.1.1

(a) Oscillating magnetic field B_ω applied at the surface of a metal and its spatial decay into metal.

(b) Instantaneous field and current directions.

(c) Phase (Time) relationship between different fields and currents

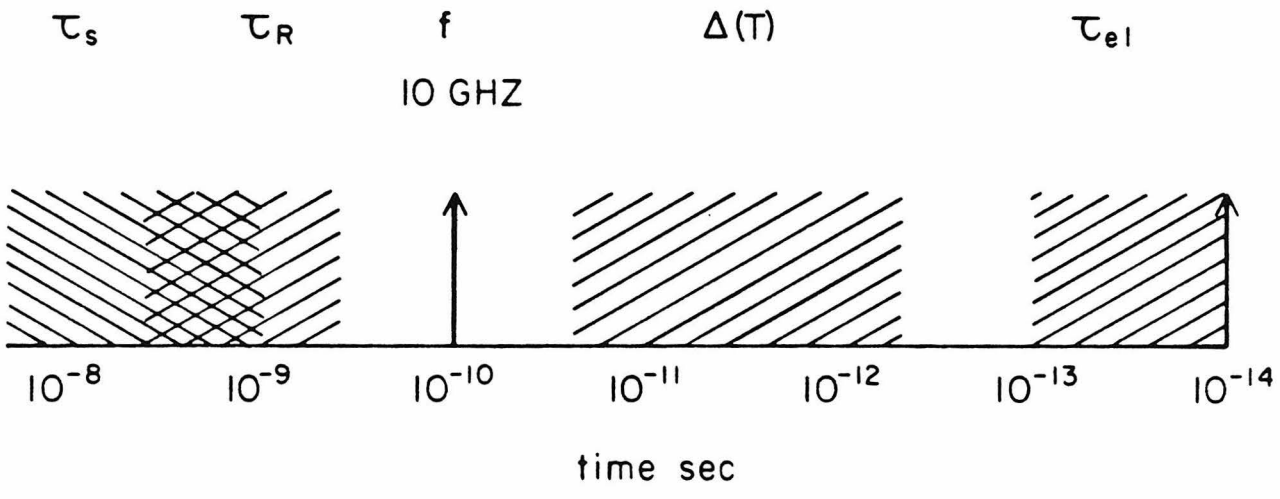

Fig.1.2 Interrelation of various time scales relevant to this work (see Sec.4 Ch.I)

CH. II Microwave response of superconductrors at low microwave powers

A transport measurement is usually carried out by applying a small perturbation to the system and measuring its response. For small values of the perturbation the response is linear and the response coefficient independent of the strength of the perturbation (Ch.I)

In this chapter we examine the response of superconductors (in the form of films and bulk specimens) to low microwave fields incident on one surface. The transport coefficient is called the surface impedance Z (a complex quantity) and at low microwave fields is independent of the field magnitude.

A general definition of the surface impedance of a metal is now provided. Consider plane electromagnetic radiation (of frequency ω) incident on the plane interface between vacuum and the metal with a tangential magnetic field strength B_ω at the surface. Then the real and imaginary parts of $Z = R + i X$ relate B_ω to the amount of power involved in the metal - radiation interaction :

$$P_{abs} = \frac{1}{2\mu_0} \int_S dS \; R \; B_\omega^2 \qquad (2.1)$$

$$P_{reac} = \frac{1}{2\mu_0} \int_S dS \; X \; B_\omega^2 \qquad (2.2)$$

where the integral is over the surface.

P_{abs} is the power that is absorbed by the metal from the radiation and R is a measure of this. X is a measure of the rate P_{reac} at which energy is exchanged between the radiation and the metal.

When the metal is a superconductor and $\omega < 2\Delta$ (Δ = energy gap) the radiation cannot directly break Cooper pairs. The Meissner effect leads to a shielding current at the surface which causes the field to decay exponentially into the metal with a characteristic penetration depth λ. This shielding effect determines the superconducting surface reactance X_s. Absorption can occur due to

excited quasiparticles at a finite temperature and determines the surface resistance. At low temperature the number of quasiparticles is proportional to $\exp(-\Delta/T)$ and consequently R_s also decreases with temperature ($R_s \propto 1/T \exp(-\Delta/T)$.

In the experiments reported here we have measured R_s of a variety of superconductors forming part of a microwave resonator by utilising the fact that the resonator Q is a measure of the absorption in the cavity. The reactance X_s was measured for thin films by measurements of the power transmitted by the film which determines X_s.

The impedance which is a measured quantity is related to the fundamental properties of the material since a solution of the radiation - metal interaction requires :

1) Maxwell's equations with appropriate boundary conditions
2) Boundary conditions for the momentum of the electrons at the interface
3) A constitutive current-field equation specific to the material. For a normal metal this is just Ohm's law.

For a superconductor the constitutive equation is a generalization of London's eqn :

$$\vec{J}_\omega(\vec{q},\omega,T) = -K(\vec{q},\omega,T)\,\vec{A}_\omega(\vec{q}) \qquad (2.3)$$

where $\vec{q}$ is the wavevector, T = temp. The kernel K embodies all the microscopic processes relevant to the superconductor - radiation interaction. Note that this eqn.(2.3) is a linear relation. Using a relation like eqn.(2.3) R_s and X_s can be calculated if requirement (2) is also specified. Thus R_s and X_s can be calculated in terms of K. Because eqn.(2.3) is linear Z_s is independent of $\vec{A}_\omega$ i.e. independent of microwave field B_ω.

Conversely measurements of R_s and X_s yield information concerning K. For this reason the interaction of microwaves with superconductors has played an important tole in understanding the phenomenon of superconductivity. Since the first experiments of Pippard numerous investigators have measured the impedance of different superconductors.

All of these previous investigations have been concerned with two extreme limits of thickness of the superconductor - very thin films where there is substantial transmission of microwaves through the films - and bulk superconductors. In the former case one does not measure the surface resistance or the surface reactance independently but rather a combination of the two.

Recently both the questions of physics and the demands of technology seem to call for a more detailed understanding of the microwave properties of thin superconducting films. For example : non-equilibrium physical situations (G1) are most easily produced and studied in thin films since often one does not have to worry about the spatial variation of quantities (this is the primary interest of this work) ; sapphire resonators coated with superconducting films have been proposed for use as stable clocks and gravity wave detectors ; there is also an interest in the possible use of thin films as high power microwave switches.

In this chapter results are reported of extensive measurements of surface resistance R_s and surface reactance X_s (surface impedance $Z_s = R_s + i X_s$) over a wide range of temperatures T and thickness d of superconducting Sn films. The thickness d was varied from d = 200 Å to bulk (d = 2.4 μ) - the corresponding change in R_s being almost a factor of 10. This range brackets the length scales involved since the superconducting penetration depth λ_p = 510Å and bulk coherence length ξ_0 = 2300Å. Measurements are also reported for 1 - 5μ Sn films plated on Cu and for a 3/8 ins. thick Sn disc.

A numerical program was also developed for computing the surface impedance of thin film superconductors. The usual calculation of Z_s for bulk superconductors was adapted to the case of thin films by incorporating the electrodynamic boundary conditions due to the presence of both surfaces and assuming specular reflection for electrons at both the interfaces. The Khalatnikov-Abrikosov (K1) formulation of the kernel K was used in its general form. The calculation is expected to be applicable over a wide range of thicknesses and material parameters.

The experimental results for $R_s(T,d)$ and $X_s(T,d)$ compare excellently with the results of the calculation for all the thicknesses and temperatures studied.

Only measured quantities viz. T_c , ω , d and the mean free path (denoted m.f.p.) l measured from the normal state microwave surface resistance R_n were used as input to the calculation. *There were thus no adjustable parameters.*

This chapter is organized in the following way.

1. Description of Apparatus and Resonator mode geometry
2. Principle of measurement of R_s
3. Experimental Procedure
   - 3.1 Calibration of Resonator
   - 3.2. Method of Sample preparation
   - 3.3. Characterization of Samples
4. Theory of Surface Impedance of thin films
5. Measurement of Sample Parameters
6. Experimental results and comparison with theory
7. Measurements of surface reactance $X_s(T,d)$
8. Conclusions

1. Description of Apparatus

A right cylindrical cavity resonating in the TE_{011} mode was employed for measuring the surface impedance. The cavity was constructed in two sections (Fig.2.1): - one, the upper part consisting of the cylinder and the top plate was machined out of a single OFHC Cu block. This part which had two symmetric holes for coupling microwave power and a central pumping hole used to evacuate the resonator was electroplated with superconducting Pb employing a procedure described in Ref.D2.

The second section of the cavity is a bottom disc 2.25 in. dia. which was pressed against the upper part with an In O-ring to ensure vacuum sealing and electrical contact. This design allows for great flexibility since a variety of sample configurations can be obtained by evaporation or electrodeposition on a variety of disc substrates - dielectric (sapphire, glass etc.) or metallic (OFHC) or can even be bulk Sn disc.

Microwaves were coupled into and out of the resonator through two 50 Ω coaxial lines terminated in a loop. The magnetic field lines in the loop "look into" the resonator through small circular waveguide sections ending in symmetrically placed coupling holes 0.156 in. dia. each and at a distance of 0.700 in. from the center. These holes were located in a low field section of the resonator.

One unique and very useful feature of the design was the ability to vary the coupling to the resonator by moving the lines. Thus it was possible to achieve critical coupling and weak coupling over a wide range (estimated to be between 10^3 and 10^{11}) of resonator Q (see next section for some relevant definitions).

The resonator was usually evacuated though there was a provision for condensing liq.He_4 inside. The apparatus was immersed in liq. He_4 in a stainless steel dewar and shielded by a μ-metal can (residual earth's magnetic field $\approx 10^{-3}$ Gauss). Temperature was varied by pumping on the He bath and could be regulated to within 5mK.

1.1. **Resonator Mode Geometry**

All measurements were done using the TE_{011} mode of the resonator (H5). This mode was chosen as it has no electrical fields normal to the surface thus minimising spurious absorption due to dielectric surface layers and also possible electron loading. Further there are no currents traversing the In joint connecting the two cavity sections. The dimensions of the cavity were chosen to produce maximum H fields in the end plate on a ring of radius 0.411 in.

It is essential to lift the degeneracy between the TE_{011} and the $TM_{\pm 111}$ modes in order to maintain the advantages listed above. The central pumping hole depresses the frequency of the TM modes. The lack of azimuthal symmetry because of the coupling holes further splits the two TM modes.

The final mode configuration for the resonator is depicted in Fig.2.1. From an examination of the R_s of a fully Pb-plated cavity the cross coupling between the modes was shown to contribute no more than 1% to the TE_{011} absorption. (This was deduced from the fact that in going through the In transition there was no measurable effect on R_s). Further the contribution of the Pb surface to the absorption is < 1% at all temperatures. Thus the contribution of the In joint to

the measurements of R_s were completely negligible.

2. Principle of Measurement of R_s

The intrinsic unloaded Q called Q_0 of a resonator whose energy content is U is a measure of the rate of energy decay in the resonator :

$$\frac{1}{Q_0} = -\frac{1}{\omega U}\frac{dU}{dt} \tag{2.4}$$

It is assumed that the time scale τ_U governing dU/dt is much slower than the frequency ω. If Q_0 is independent of U (i.e. independent of the field B_ω) this leads to an exponential decay of U : $U = U_0 \exp(-t/\tau_U)$ where $\tau_U = Q_0/\omega$ is the time constant for energy decay. Determining τ_U yields Q_0 (see next section).

Since the energy content U decays due to absorption in the walls of the resonator, $-dU/dt = P_{abs}$. Using eqns.(2.1), (2.4) and the relation between U and B_ω (from the Maxwell eqns. solution for the mode) we get (H5,J1) :

$$Q_0 R_s = \Gamma = \omega \frac{\int(\varepsilon_0 E_\omega^2 + \mu_0^{-1} B_\omega^2)\, dV}{2\int B_\omega^2\, dS} \tag{2.5}$$

where ε_0 and μ_0 are respectively the permittivity and the permeability of free space (we assume the resonator is evacuated). E_ω is the electric field, $\int dV$ is over the resonator volume. Γ is called the geometric factor of the mode and is determined by it's geometry.

Γ is different between the two cases of a completely homogeneous resonator and the case where the top section does not contribute to the losses. The latter case occurs when the top section is Pb plated and the bottom plate is covered with Sn or a lower T_c material. The *calculated* geometrical factors for the two cases are :

$$\Gamma_{H011} = 709 \ \frac{\Omega}{sq.} \tag{2.6}$$

$$\Gamma_{P011} = 2990 \ \frac{\Omega}{sq.} \tag{2.7}$$

$$\frac{\Gamma_{P011}}{\Gamma_{H011}} = 4.22 \tag{2.8}$$

Measurement of the resonator Q requires a means of coupling power into and out of the resonator. These could introduce additional losses which can be included in the form of a coupling factor β yielding a "loaded" Q (T3) :

$$Q = \frac{Q_0}{1 + \beta}$$

At weak coupling $\beta << 1$ and $Q = Q_0$. This is achieved by moving the coupling lines away from the cavity until the measured Q is independent of probe position (β varies exponentially with probe position relative to the cavity if $\beta << 1$). There is an upper limit to the measurable Q determined by the radiation losses of the pumping and probe holes. This is estimated to be $> 10^{11}$ and since we are mostly interested in $Q < 10^9$ does not affect the measurements. In the results reported in this chapter $\beta < 0.01$ for both input and output coax lines - they are always weakly coupled.

The basic principle of the measurements is as follows :

A pulse of microwaves Fig.(2.2a) is sent down one coax line and detected with the other. Due to the time constant τ the resultant pulse shape is as in Fig.(2.2b). This was detected and observed on a fast scope. The time difference $(t_1 - t_3)$ between two points on the decay curve whose amplitudes are in the ratio 3:1 was measured and the time constant $\tau_v = (t_3 - t_1)/\ln 3$ was calculated. Since the heterodyne system measures voltage (not power) $\tau_U = \tau_v/2 = Q_0/\omega$. Using also eqn.(2.5) R_s was determined from :

$$R_s = \frac{\Gamma}{\pi f \tau_v} \qquad (2.9)$$

3. Scheme of Microwave measurements

Eq.(2.9) was used to determine the surface resistance by a measurement of the resonator Q. Pulsed microwave power was fed through one probe and the cavity field amplitude was picked up with the other and detected (Fig.2.3). The detection was carried out by heterodyning to an intermediate frequency of approx. 25 Mhz. and the pulse shape observed in real time on a fast scope. The time constant τ_v of the cavity amplitude envelope was measured and R_s

calculated from eqn.(2.9). and (2.7). Weak coupling was ensured by verifyng that the Q was independent of the probe positions. A typical power transmission factor (ratio of power in to power out) in this configuration was 40dB while the absorbed powers are < 100μW and maximum surface fields are < 50 mG.

For Q > 10^4, the 10GHz source was stabilized with an external frequency stabilizer referenced to an oven-controlled 15 MHz crystal oscillator . For Q > 10^8 this scheme was inadequate because of the frequency noise limitations of the stabilized source and an additional method was employed. The phase change across the cavity was detected and changes in the phase were compensated for by a feedback mechanism which fed a correction voltage to the stabilised source (acting as a VCO). In all these schemes the cavity was essentially driven in a fixed-source-frequency mode. Yet another scheme of exciting the cavity by means of a self-locked loop is described in Ch III and is applicable for all Q $\gtrsim 10^3$.

The absorption of microwaves can result in the film being driven out of equlibrium. This can lead to a dependence of the impedance of the microwave field strength or power due either to a rearrangement of quasiparticles of due to simple heating. In the results quoted here, care was taken to ensure that such effects were minimal by determining that the results were independent of field strength and pulse length.

3.1. Resonator calibration

To measure the absolute surface resistance it was necessary to verify eqns.(2.6) and (2.8) by independent measurements. For the homogeneous case, the resonator with polished OFHC Cu walls (i.e. without deposition of superconductor) was employed at room temperature. The dc resistivity of the OFHC Cu was measured and R_s was calculated using the measured dc resistivity. By measuring the Q it was found *experimentally* that in the TE_{011} mode :

$$\Gamma_{H011} = 709 \pm 35 \ \frac{\Omega}{\text{sq.}} \quad \text{(Expt.)} \qquad (2.10a)$$

The ratio $\Gamma_{P011}/\Gamma_{H011}$ was determined by measuring Q_{P011}/Q_{H011} where Q_{H011} was the unloaded Q measured at 4.2 K with a full Cu resonator and Q_{P011} the Q measured with the same Cu endplate but with the rest of the resonator plated

with Pb. It was found that :

$$\frac{\Gamma_{P011}}{\Gamma_{H011}} = 3.9 \pm 0.4(\text{Expt.}) \qquad (2.10b)$$

The agreement with the expected calculated values eqn.(2.6) and (2.8) is excellent. For the TM_{111} modes the measured and expected values differed by 20% at room temperature, indicating that the joint was lossy even at room temp.

3.2. Sample Preparation

Three types of superconducting configurations were studied :

(a) Thin films evaporated on sapphire, glass or OFHC Cu.

(b) Thick (2-5 μ) films plated on OFHC Cu.

(c) Bulk 2.25 in. dia x $\frac{3}{16}$ in. thick Sn disc.

The substrates were all 2.25 in. dia. x $\frac{1}{8}$ in. thick.

Thin films of Sn were evaporated from Mo boats at a pressure of 5 $x10^{-6}$ torr. The substrates were cooled to 70 K by means of liq N_2 . Optically reflecting mirror perfect films were obtained (with polished sapphire substrates) which had no visible structure on a resolution scale of 500 Å on examination with a Scanning Electron Microscope at a magnification of 20000.

Samples of type(b) were obtained by electroplating Sn onto polished discs of OFHC Cu in a $Sn(BF_2)_2$ bath to which HBF_4, β- napthol and gelatin were added (the recipe is described in ref.(G6)). The plating current density used was typically $5x10^{-2}$ A/sq.in.. The resultant coating was optically bright in appearance but had surface structure approx. 2μ in size. The specimen was rinsed with water and acetone and preserved in vacuum before assembly.

The Sn disc was made by melting and casting 99.99% Sn sheet into a disc. The disc was machined and polished with 1 - 3μ levigated alumina. The surface had clearly observable grain size ~ few mm.

4. Theory of the surface impedance of thin films

The derivation of the surface impedance of bulk metals is based upon two sets of equations. One is the Maxwell equations with appropriate interface boundary conditions which specifies the electrodynamics. The other is the material or constitutive equation (the analog of Ohm's law) which gives the relation between current and applied field.

To derive the surface impedance for a corresponding thin film we assume that only the boundary conditions are modified and that the second interface influences the electrodynamics. The assumption here is that the constitutive equation (2 3) is the same as that for bulk provided the appropriate thin film material parameters like mean free path l are used.

For superconductors the constitutive equation is eqn.(2.3). In addition it is necessary to specify the nature of the reflection of the electrons at the interfaces. We consider only the case of specular reflection at the film surfaces as the expressions for diffuse reflection are quite intractable.

For specular reflection, the problem of a plane wave incident on a semi-infinite metal is solved by replacing the metal by a current sheet at the interface, the magnitude of the current being determined by the B field at the surface. Use of this artifice leads to the following expression for the surface impedance for a bulk metal (H3) :

$$Z_s = \frac{i\mu_0\omega}{\pi} \int_{-\infty}^{\infty} \frac{dq}{q^2+K(\omega,l,\vec{q})} \qquad (2.11)$$

For a thin film filling the space $0 \leq x \leq d$ with the electromagnetic field incident on one side of the film at x=0, the film can be replaced by an infinite set of current sheets spaced 2d apart covering the entire space (Fig.2.4). We assume that there is no transmission through the film so that B(x=d)=0. This assumption is true provided that $2\pi\lambda^2/d\nu \ll 1$ where λ is the bulk penetration depth and ν is the free space wavelength. If this condition is satisfied then $B(d) \approx 2\pi\lambda^2/d\nu$ B(0) and is negligible. Thus the magnetic field decays (linearly for a thin film) to zero across the film. It is perhaps worthwhile to emphasise that counter to intuition, even films with $d \approx \lambda$ have negligible transmission (see

also Sec.6). In the cases of interest here d~ 10^{-5} cm. ,$\lambda \sim 10^{-5}$cm. , $\nu \sim$ 3cm. B(d) ~ 10^{-5} B(0).

The simple case of local electrodynamics may be used to illustrate the spatial profile of fields and currents in thin films. In bulk both the fields and currents decay exponentially into the metal. As the thickness is decreased the current density is greater because the current is squeezed into a narrower region. The total current is determined by the field and hence has to remain fixed. In a very thin film the current becomes almost uniform and the field decays linearly to zero across the film. Fig.2.5 displays the current and field profiles calculated for various values of d/λ where λ is the bulk penetration depth. The spatial profiles depicted are approximately the same for both normal and superconducting films - the magnitudes are quite different.

With the above transformation $Z_s(\omega,l,d)$ can be calculated in a manner exactly analogous to the bulk case.(Ref S3). The result is :

$$Z_s(\omega,l,d) = \frac{i\mu_0\omega}{d} \sum_{n=-\infty}^{\infty} \frac{1}{q_n^2+K(q_n,l,\omega)} \qquad (2.12)$$

where $q_n=n\pi/d$. Once the kernel is specified Z_s can be calculated.

Khalatnikov and Abrikosov(Ref.K1) have given an extensive theory of the interaction of electromagnetic radiation with superconductors in terms of the kernel and give detailed expressions for the kernel. Halbritter (Ref.H2,H3) has used these expressions to compute the kernel for all $\omega,\vec{q},l$ and has used the results to calculate Z_s for bulk superconductors.

Halbritter's computer program was used to compute $K(\omega,q_n,l)$ for $q_n=n\pi/d$. The results were then used in equation (2.12) to calculate $Z_s(\omega,l,d)$ numerically. The expression in eq.(2.12) converges fairly rapidly, typically for $n < 20$.

The inputs to the computation of $Z_s(\omega,l,d)$ are :

$$T_c,\ l,\ d,\ \Delta(0)/kT_c,\ \lambda_L(0),\ \xi_0$$

where T_c is the transition temperature, l is the mean free path, $\Delta(0)/kT_c$ is the gap ratio ($\approx$ 1.74 for weak coupling superconductors), $\lambda_L(0)$ is the London penetration depth at T = 0 and ξ_0 is the coherence length. Of these the calculation is

fairly insensitive to the material parameters $\Delta(0)/kT_c$, $\lambda_L(0)$, ξ_0. The bulk values for a superconductor reported in the literature (H1) were used for these parameters. The measurement of the important parameters is described in the next section. In this experiment $\omega = 2\pi\ 10.12\text{x}10^9$ rad/sec.

5. Measurement of Sample Parameters

From a measurement of the surface impedance in the normal state, the normal state resistivity was determined. The mean free path was then determined using the free electron expression :

$$\rho_n\ l \quad = \quad 0.061\mu\Omega\text{-cm.}\ \mu\text{m.} \tag{2.13}$$

where ρ_n is the normal state resistivity in $\mu\Omega$-cm. and l is in μm.

THIN FILMS

For d < 1000 Å , the normal films obey local electrodynamics because of the reduced mean free path. The resistivity was deduced from the thin film expression :

$$\rho_n \quad = \quad R_n\ d \tag{2.14}$$

THICK FILMS

For d>1000 Å and for samples of types (b) and (c) it was necessary to use the anomalous skin effect expressions. For $\alpha \geq 1.2$ Chambers(C1) gives the following extrapolated expressions :

$$R_n(\omega,l,d=\infty) \quad = \quad R_n(\omega,\infty,\infty)\ \left[1+1.157\alpha^{-0.2757}\right] \tag{2.15}$$

$$R_\infty \quad = \quad R_n(\omega,\infty,\infty) \quad = \quad \left[\sqrt{3}\pi(\rho_n l)\left(\frac{\mu_0\omega}{4\pi^2}\right)^2\right]^{\frac{1}{3}} \tag{2.16}$$

$$\alpha \quad = \quad \left[\frac{3}{4}\mu_0\omega\frac{(\rho_n l)^2}{\rho_n{}^3}\right] \tag{2.17}$$

where μ_0 is the permittivity of free space.

From these we deduce using eq.(2.13) and $\omega = 2\pi\ 10.12\text{x}10^9$:

$$\alpha = \left[0.864\left(\frac{R_n}{6.6\times10^{-3}} - 1\right)\right]^{-3.627} \tag{2.18}$$

$$\rho_n = \frac{0.285}{\alpha^{\frac{1}{3}}} \quad \mu\,\Omega - \text{cm.} \tag{2.19}$$

Independent measurements of the m.f.p. were also made by cutting a 1 cm. x 1 mm. area with banks for contacts after the microwave measurements were made. The resistivity was measured in the normal state by a 4-terminal method.

The transition temperature T_c of the films was determined by finding the temperature at which the surface resistance decreased by 2% from the normal state value R_n. The independent dc measurement agreed with this value to within 0.01 K.

The thickness of the films was determined at the time of evaporation by a Sloan Quartz crystal monitor.

The results for T_c and l for various thicknesses are given in Table I. The values of T_c from both the microwave and dc measurements agreed to within 0.01 K and only the average values are quoted. It will be noticed that l increases with d saturating at l = 2100 Å at the high end. The dependence of l on d and the small values of l are quite reasonable since the films are expected to be somewhat granular and boundary scattering is important at small thickness. However there is a systematic discrepancy between the dc m.f.p. l_{dc} and the microwave m.f.p. l_ω for thin films. The implications of this are discussed in Sec. 4.1. For the superconductor we take l_ω = l to be the appropriate m.f.p. at microwave frequencies.

Another observation is that T_c increases with decreasing l . One reason that has been advanced for this is that as l decreases the electron-phonon interaction gets stronger and T_c increases(B2,C2). This is consistent with the increase in T_c in granular Sn films reported in the literature (K4).

6. Comparison of experiment with theory

Samples prepared as described in Sec 2.5 were assembled into the cavity. A measurement of the normal state surface resistance R_n gave a measurement of the mean free path. The resonator was cooled below T_c and the surface resistance R_s determined from the resonator Q (Sec 2.3).

The measured parameters T_c,l,d and ω were then used in the calculation of the surface resistance (Sec. 3). For Sn the established values $\Delta(0)/kT_c = 1.74$, $\lambda_L(0) = 340$Å, $\xi_0 = 2300$ Å from the literature (H1) were used.

Fig 2.6 is a plot of $R_s(t,d)$ vs $t=T/T_c$ for some of the samples listed in Table 1. The bulk experimental results for $d > 3600$ Å for all configurations (a),(b) and (c) are identical to within experimental accuracy. The theoretical calculations also yield almost a single curve. This is because the surface resistance is insensitive to thickness and m.f.p. for large d.

The m.f.p. dependence is determined (T1) by the coherence length : $1/\xi = 1/\xi_0 + 1/l$ where ξ_0 is the Pippard coherence length in the pure bulk material. The dominant wavevectors entering into the kernel $K(q,\omega)$ are determined by $q \sim 1/\xi$. For $l \to \infty$, $\xi = \xi_0$, a property of the pure material. Hence as the m.f.p. becomes large the properties of the pure bulk material are independent of l. This is analogous to the anomalous skin effect in normal metals. The electrodynamics is non-local in this case.

The surface resistance increases as the thickness is reduced because :

(a) a higher current density is required to maintain a given value of the incident field at the surface.

(b) At the same time the mean free path is also reduced.

The combination of these two factors results in an increase by a factor ~ 10 for $d = 190$ Å above the bulk value at low temperatures.

The results of the calculation of $R_s(t,d)$ using the parameters listed in Table 2.1 are also plotted in Fig.2.6. *The agreement of the measured values to the calculated values is consistent to within the experimental accuracy. This agreement leads to the conclusion that the model described in Sec.3 which incorporates the BCS mechanism together with the appropriate thin film electrodynamics and the assumption of specular reflection describes very well the low power microwave absorption in the films. Since all the input parameters to the calculation are determined from the microwave measurements , there are no free parameters used in the comparison.*

One may ask whether these results are clear evidence that the electrons are specularly reflected at the interfaces. A quantitative calculation for the case of diffuse reflection is unfortunately difficult since the artifice of Fig.2.4 cannot be used. Instead one has to solve a complicated integro-differential equation. In bulk exact results can be obtained (H2) - the calculated difference between the cases lies within the typical experimental errors. For thin films in the normal state (C3,L1) the dc resistivity is calculated to be appreciably different for the two cases only for $l >> d$. In these experiments $l \lesssim d$ experimentally and hence in the normal state there is not an appreciable difference between the two cases. We expect the same to hold true for the superconducting case also i.e. by using the actual mean free path l (which is $\lesssim d$) the results for specular and diffuse reflection of the electrons at the interface should not be very different.

It was found that the m.f.p. l determined from the microwave resistivity was longer (by a factor < 2) than the dc m.f.p. l_{dc} for $d < 650$Å. For the thinner films eqn.(2.14) leads to a frequency independent R_n. In bulk R_n has a frequency dependence due to the skin depth , the conductivity being frequency independent well below the plasma frequency. The thinner films are likely to be inhomogeneous and to be characterised by an island structure with highly resistive paths joining the islands. Since the dc current is forced to traverse the highly resistive paths, the measured dc resistance is anomalously higher. On the other hand the microwave reactive displacement currents across the boundaries of the islands can short out the spurious highly resistive paths. The microwave resistivity correctly describes the scattering in the metal and the corresponding mean free path l_ω is the appropriate one to use for the superconducting

state.Thus an entirely consistent description of the superconducting surface resistance is possible *using the microwave measurements alone* and this description agrees very well with the experimental results.

7. Measurement of surface reactance $X_s(T,d)$

The usual method of measuring reactance (T3) is to measure the change in resonant frequency of the resonator as the temperature is lowered. This only yields the temperature dependent changes in the reactance and not its absolute value. However in the configuration employed in this experiment the shift in resonant frequency was dominated by a pressure dependent volume change and hence inapplicable to measuring X_s. Further the above method gives only the relative and not an absolute evaluation.

Consequently a new technique was developed which involves measuring the emission from the resonator. Emission comes about due to transmission through the film end-plate. By using the normal state as a normalization , this method enables the absolute measurement of the reactance. It is restricted to films of not too great thickness ($d < 1000\text{Å}$) in this experiment). Before the procedure is described, an estimate of the transmitted power is presented to show that the contribution to the Q due to this loss mechanism is negligible compared to the absorption in the film.

Now $P_{abs} = \frac{1}{2}R_s\, B(0)^2$ and $P_{xmitt} = \frac{1}{2}Z_0\, B(d)^2$ where Z_0 is the impedance of the substrate. Therefore :

$$\eta = \frac{P_{xmitt}}{P_{abs}} = \frac{Z_0}{R_s}\left|\frac{B(d))}{B(0)}\right|^2 = \frac{Z_0}{2990}Q\left|\frac{B(d)}{B(0)}\right|^2 \qquad (2.19)$$

As discussed in Sec.3 : $B(d)/B(0) \approx 2\pi\lambda^2/d\nu = 6\text{x}10^{-5}$ where $d \approx 300\text{A}$, $\lambda \approx 1000\text{Å}$, $\nu = 3\text{cm}$. has been assumed for the worst case. Using a large value for the $Q=10^7$

$$\eta = \frac{P_{xmitt}}{P_{abs}} < 6 \times 10^{-3}$$

This radiation loss is clearly an insignificant contribution to the surface resistance in this experiment. An interesting conclusion that arises from this

analysis is that there is an upper limit to the Q due to the radiation loss in a resonator which has a thin film constituting some portion of its walls.

The relation between impedance and fields is: $R + iX = E(0)/B(0)$ and $Z_0 = E(d)/B(d)$. Thus :

$$P_{xmitt} = \tfrac{1}{2}\frac{R^2+X^2}{Z_0}\left|\frac{E(d)}{E(0)}\right|^2 \left|B(0)\right|^2$$

For thin films, $E(d) \approx E(0) / \cosh(d/\lambda)$. This correction becomes significant for $d \gg \lambda$. Hence in the normal state: $P^n_{xmitt} = \tfrac{1}{2}R_n^2/Z_0 \ |H(0)|^2$. For the superconducting state $X_s \gg R_s$ except very near T_c.Hence : $P^s_{xmitt} = \tfrac{1}{2} X_s^2/Z_0 \ (\cosh(d/\lambda))^{-2} \ |H(0)|^2$

Hence except very near T_c :

$$X_s = R_n\left(\frac{P^s_{xmitt}}{P^n_{xmitt}}\right)^{\frac{1}{2}} \cosh(d/\lambda) \qquad (2.20)$$

P_{xmitt} was measured by pressing an X-band waveguide to the back of the sapphire and detecting the transmitted power. Starting from $T>T_c$, P^s_{xmitt} was measured for all T relative to the normal state value P^n_{xmitt}. λ was calculated for the dirty superconductor from $\lambda = \lambda_p \ (1+\xi_0/l)^{\frac{1}{2}}$. Using eq.(2.20), X_s was determined from the measured values of the transmission ratio $(P^s_{xmitt} / P^n_{xmitt})^{\frac{1}{2}}$.

The results for $X_s(t,d)$ for some of the films are displayed in Fig.2.7. These measurements are less accurate than those of R_s as they involve the measurements of very small microwave powers. It is estimated that relative error between values at different temperatures is ~ 25% and the error in the absolute magnitude is ~ 40%. Also shown in Fig.2.7 are the results of calculating $X_s(t,d)$ as described in Sec.3. The agreement between theory and experiment is consistent to within the experimental accuracy.

8. Conclusions.

We have measured the surface impedance $Z_s(T,d)=R_s(T,d) + i\, X_s(T,d)$ of thin superconducting films ranging in thickness from 200Å to bulk at 10GHz.The results were compared with calculations based on the BCS theory modified for thin films and assuming specular reflection at the surfaces. The agreement of the measured values with the calculations using no adjustable parameters is excellent.

The results described in this chapter lead to the conclusion that the thin films can be very well characterised insofar as their linear behaviour is concerned. This is an essential step towards an understanding of the more complicated nonlinear and nonequlibrium situations that were studied later and are described in the subsequent chapters.

Figures for Ch.II

Fig.2.1 Cavity Resonator Apparatus and Mode Geometry

(a) Cross-section of resonator and dewar insert

(b) Field Configuration of TE_{011} mode. The mode is cylindrically symmetric. The plot below is the radial dependence of the magnetic field at the end plate.

(c) Mode configuration. TM_{111} modes split off from TE mode by the holes for pumping and coupling.

Fig.2.2 Input and output pulse envelope shapes

(a) Input pulse envelope

(b) Output pulse envelope

Fig.2.3 Microwave Apparatus for measuring Q of a resonator (for discussion see Sec.3)

Fig.2.4 Field configuration used to calculate surface impedance assuming specular reflection of electrons at both interfaces.

Fig.2.5 Current and field profiles for various values of d/λ - current (dashed) and magnetic field (solid). d/λ = (a) 0.1 (b) 1.0 (c) 2.0

Fig.2.6 Measured Surface Resistance $R_s(t,d)$ vs. reduced temperature t for a variety of Sn samples studied. The solid lines represent calculations described in Sec.4. The dashed line represents the calculations for bulk.

Fig.2.7 Measured Surface Reactance $X_s(T,d)$ vs. temperature T for thin Sn films. The solid lines represent results of numerical calculation (Sec.4)

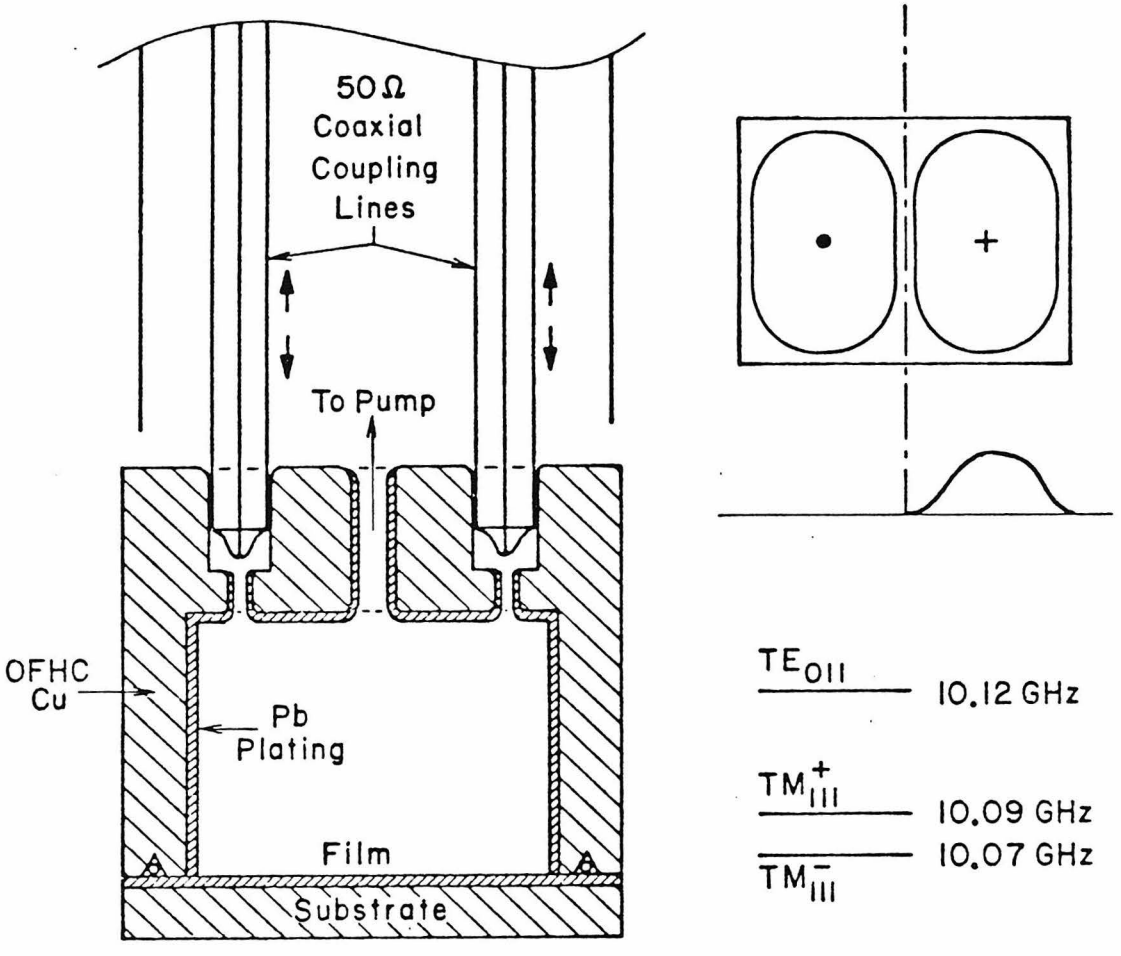

Cavity Resonator Apparatus and Mode Geometry

FIG.2.1

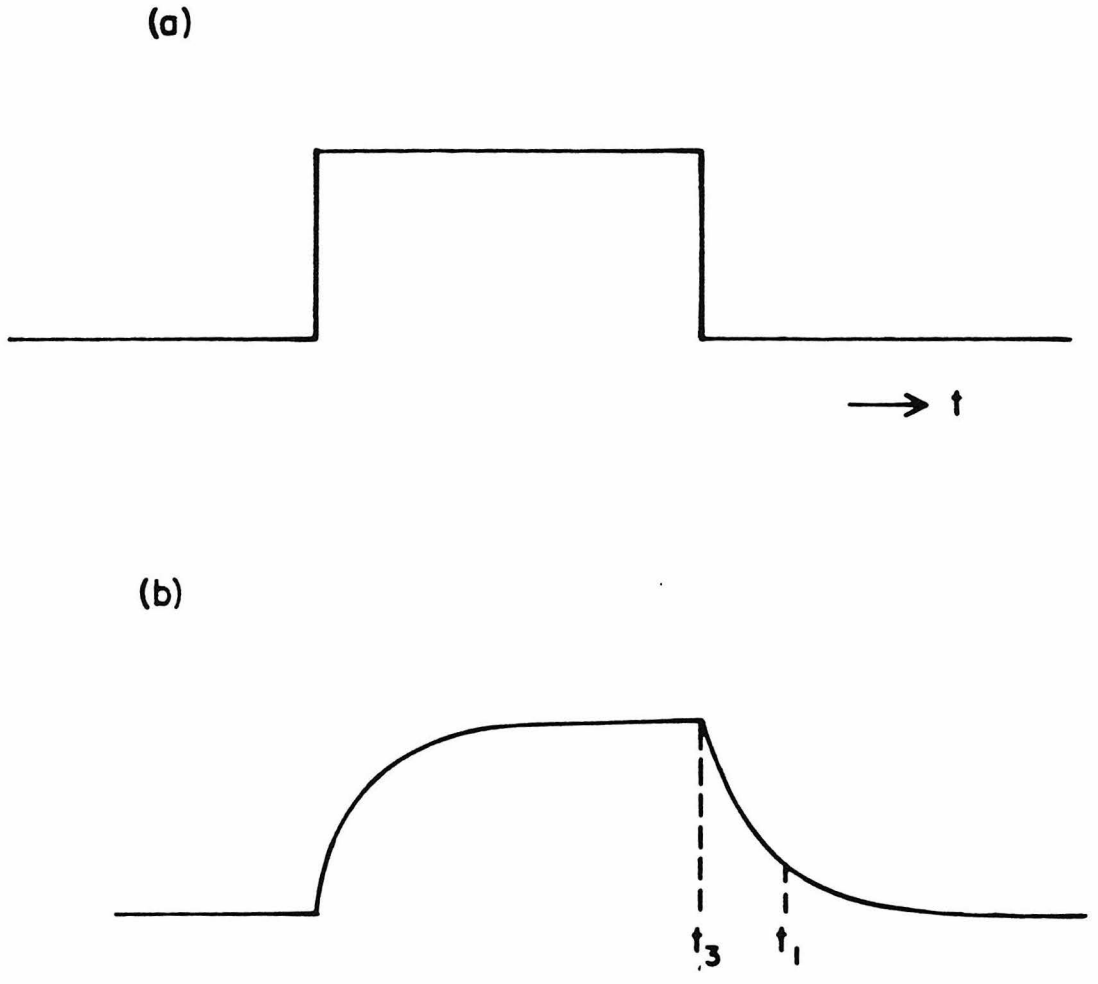

FIG.2.2

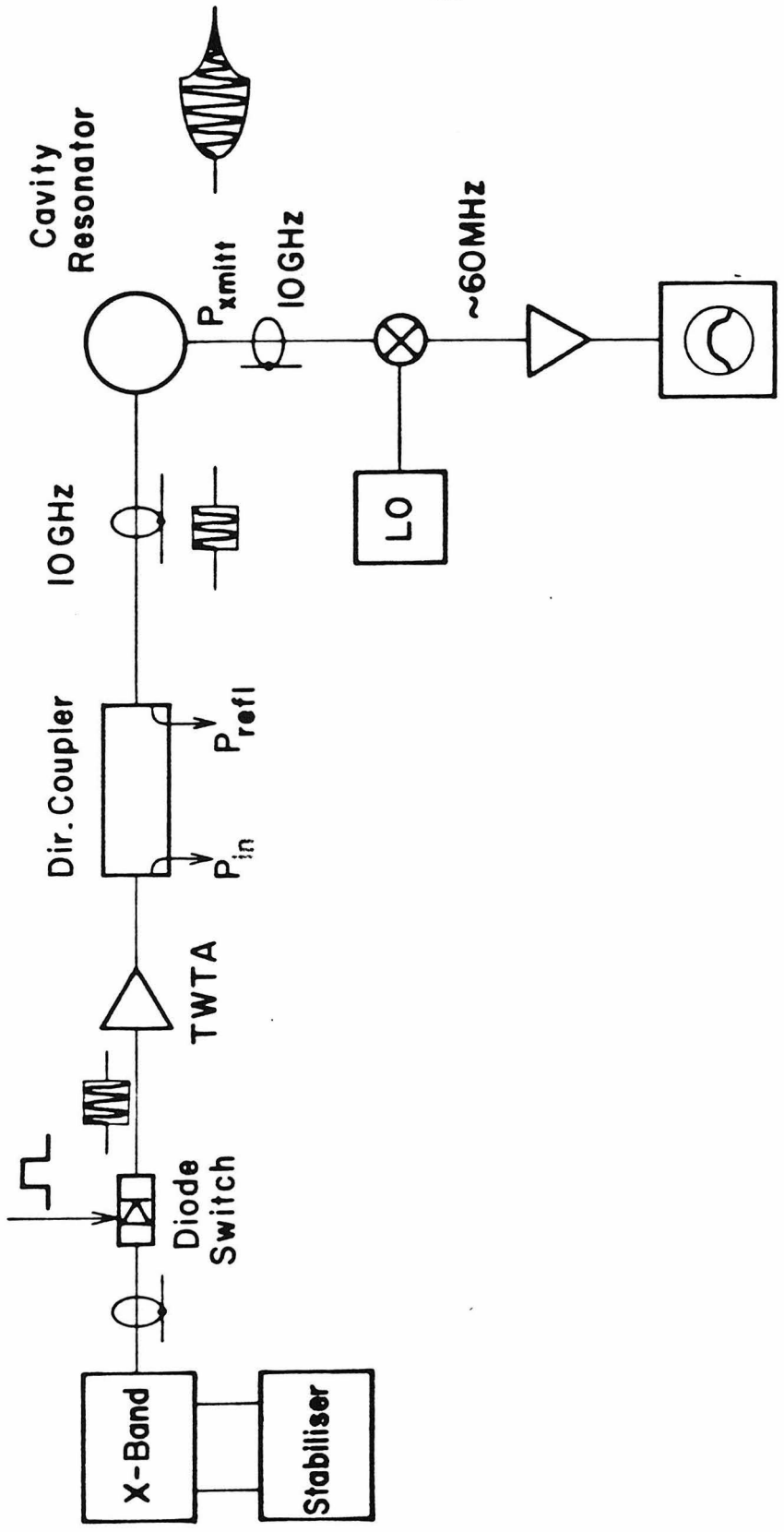

FIG.2.3

Microwave Apparatus for Measuring Q of a Cavity Resonator

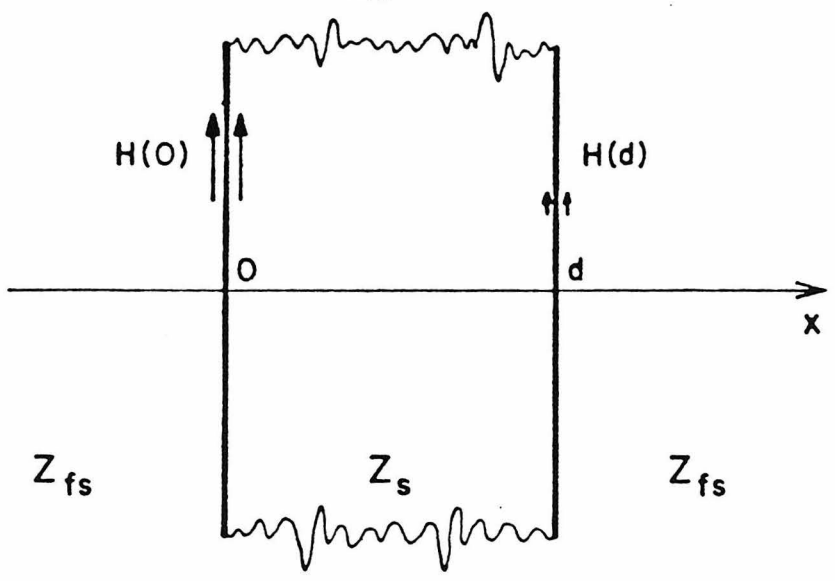

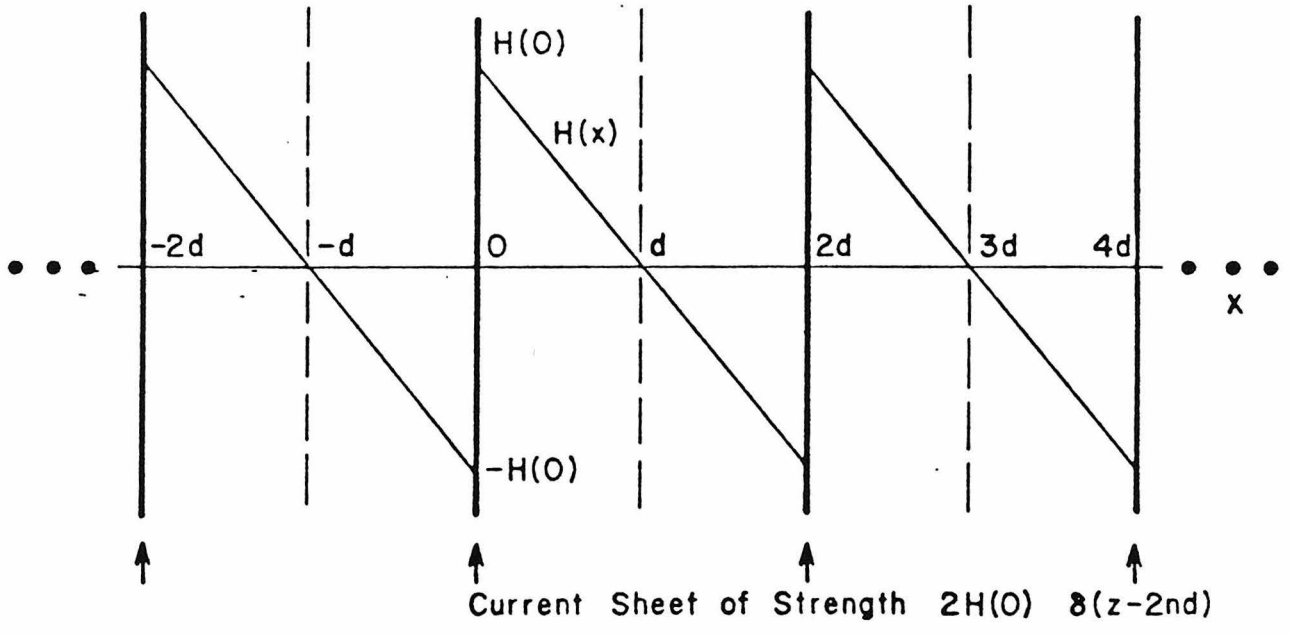

FIG.2.4

Field Configuration for Solving Thin Film Electrodynamics Problem.

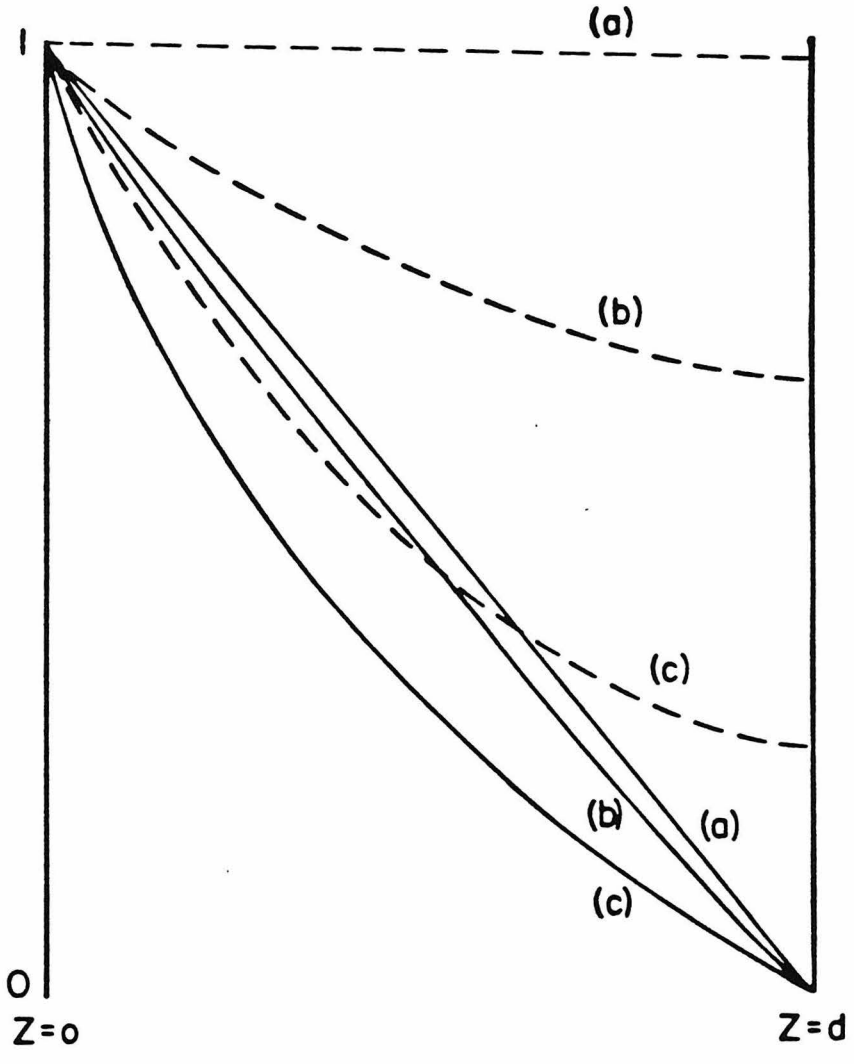

FIG.2.5

FIG.2.6

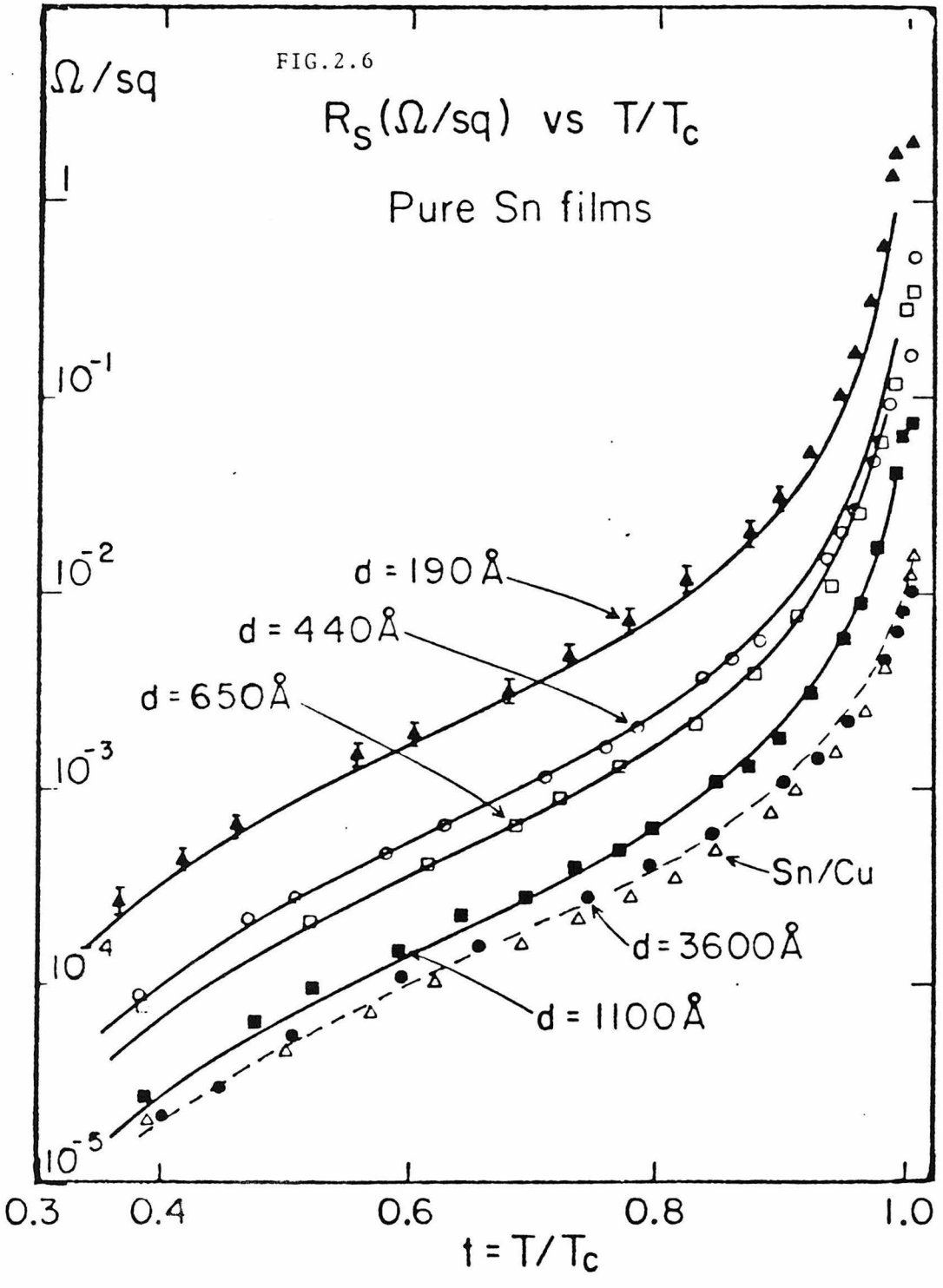
Ω/sq
$R_S(\Omega/sq)$ vs T/T_c
Pure Sn films
1
10^{-1}
10^{-2}
10^{-3}
10^{-4}
10^{-5}
d = 190 Å
d = 440 Å
d = 650 Å
Sn/Cu
d = 3600 Å
d = 1100 Å
0.3
0.4
0.6
0.8
1.0
$t = T/T_c$

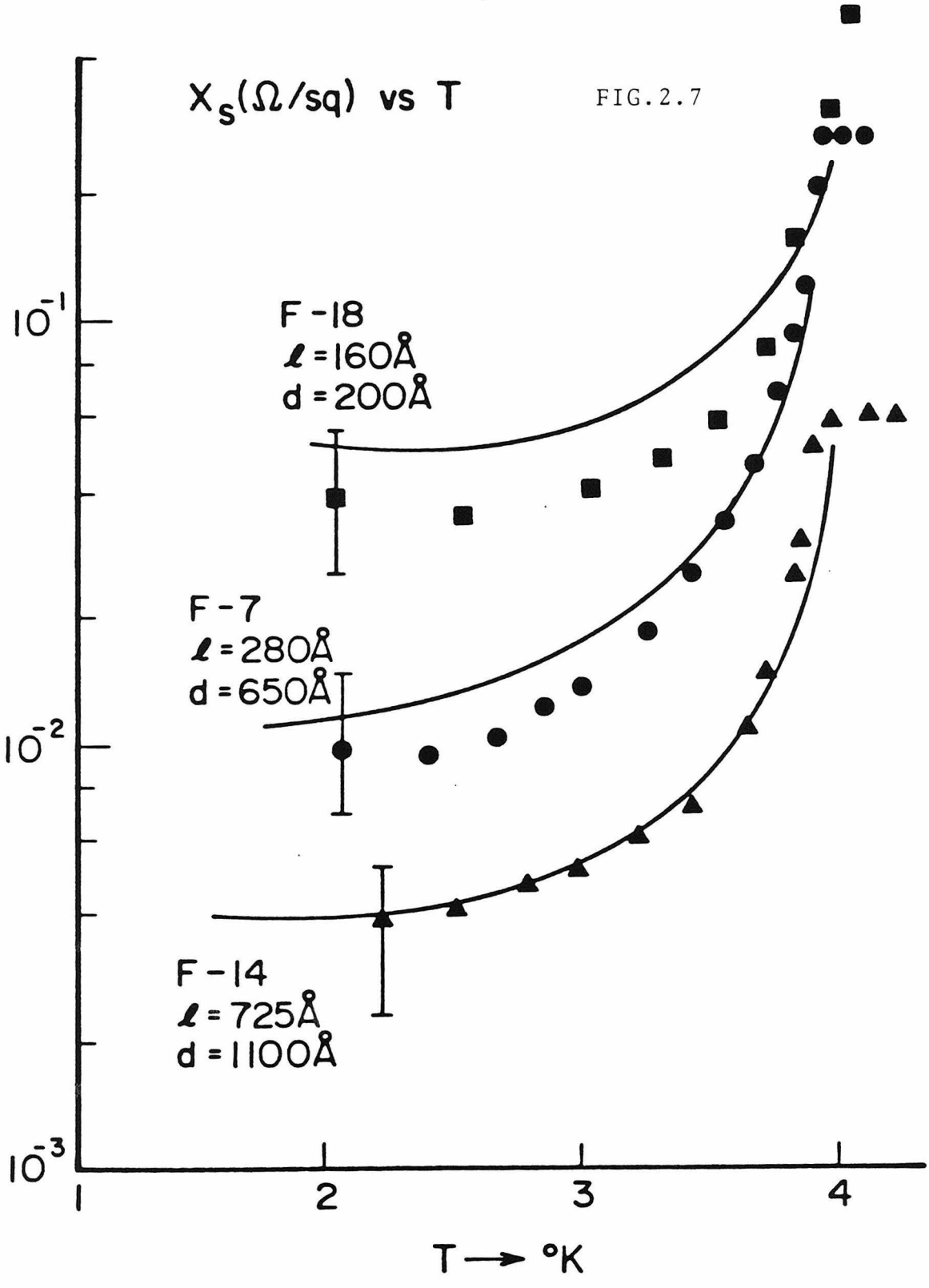
$X_s(\Omega/sq)$ vs T
FIG.2.7
F-18
ℓ = 160Å
d = 200Å
F-7
ℓ = 280Å
d = 650Å
F-14
ℓ = 725Å
d = 1100Å
10^{-1}
10^{-2}
10^{-3}
1
2
3
4
T → °K

TABLE 2.1 **Material Characteristics of the Films**

Film	d	l [(d)]	T_c	$R_{n,expt}$	ρ_n	λ_n [(e)]	λ_n / d	R_∞ [(f)]	$R_{n,exp} / R_\infty$
	(A)	(A)	(K)	$10^{-3}\Omega$/ sq	$\mu\Omega$-cm	μm		$10^{-3}\Omega$/ sq	
F-18 [(a)]	190	160	4.14	1930	7.03	1.30	68.4	54	35.7
F-15 [(a)]	440	200	4.00	510	3.10	0.89	20.2	35	14.6
F-7 [(a)]	650	277	3.93	320	2.20	0.75	11.5	30	10.8
F-14 [(a)]	1100	725	3.91	70	0.84	0.46	4.2	18	3.85
F-11 [(a)]	3620	1052	3.85	15	0.58	0.38	1.05	15	0.99
F-12 [(a)]	10200	2100	3.84	15.8	0.29	0.27	0.26	10.7	1.48
F-13 [(a)]	25000	2100	3.80	16.9	0.29	0.27	0.11	10.7	1.55
P-2 [(b)]	30000	6390	3.61	9.7	0.096 [(g)]	0.016			
B-1 [(c)]		33600	3.70	7.38	0.018 [(g)]	0.067			

(a) Type (a) sample , Sapphire substrate

(b) Type (b) sample , OFHC Cu substrate

(c) Type (c) sample , 3/16" thick disc

(d) $l = 0.061 / \rho_n$ (μm.) : mean free path

(e) $\lambda_n = 0.503 \sqrt{\rho_n}$ (μm.) : normal state skin depth

(f) Calculated using eq.(2.16)

(g) ρ_n calculated from measured R_n using eqs. (2.18).

CH.III Microwave Response of Superconducting Films in the Presence of a Static Supercurrent

In this chapter we examine the effects on the microwave surface resistance R_s of a static current of density J_0 in the film. The current is induced by a magnetic field B_0 applied on one side of the film and it's presence modifies the high frequency response of the superconductor.

It is important to view the results of this chapter in the context of the measurements of surface resistance in the *absence of static current* (Ch II). There we found that at low microwave fields the surface impedance was in excellent agreement with the BCS theory. Thus the linear material or constitutive B - J and the J - A relationship for the superconductor has been experimentally verified for thin films. This forms a firm foundation on which an attempt to understand nonlinear effects is based.

It was found that the surface resistance varied quadratically with J_0 (or B_0) except in narrow regions of temperature. The results for the surface resistance can be expressed as (t = red. temp. = T/T_c)

$$\frac{\delta R_s(B_0)}{R_s(0)} = \frac{R_s(B_0) - R_s(0)}{R_s(0)} = k(t)\, B_0^2 \qquad (3.1)$$

The changes in R_s are quadratic in B_0 and independent of the microwave field B_ω.

Conceptually this dependence of R_s on the static current can arise if one includes a non-linear cubic term in the constitutive current-vector potential relation of the superconductor. The part that is relevant to this experiment can be written in terms of the static ($\vec{A}_0$) and high frequency probe ($\vec{A}_\omega$) vector potentials :

$$\vec{J}_\omega(A_0^2) = -q_1(\omega,t)\,(\vec{A}_0\cdot\vec{A}_0)\,\vec{A}_\omega - q_2(\omega,t)\,(\vec{A}_0\cdot\vec{A}_\omega)\,\vec{A}_0 \qquad (3.2)$$

where q_1 and q_2 are to be determined from the theory. The total current is the

sum of eqn.(1.2) and (3.2).

Note that the resultant high frequency current is linear in $\vec{A}_\omega$ and quadratic in $\vec{A}_0$. The first term represents the modifications to the superconductor due to the static current alone (e.g. depressed order parameter, changed quasiparticle number). The second term is more complicated since it describes processes occurring due to the combined presence of both the static field and high frequency field. The second term is absent if $\vec{A}_0$ and $\vec{A}_\omega$ are perpendicular to each other. In this experiment they are parallel and hence this term cannot be ignored.

The basic aim of this research has been to experimentally measure k(t) at f = 10 GHz for a variety of Sn and In films in the temperature range $0.4 < t < 0.98$. The results are compared with calculations of equilibrium and non-equilibrium effects based on the microscopic theory.

The conclusions arrived at are :

(1) At high temperatures ($t > 0.9$) the dominant effect on the absorption is due to the depression of the order parameter by the static current. The experimental results for the sign (+), magnitude and temperature dependence agree with calculations based on the Ginzburg-Landau theory . This is true for all thicknesses of Sn films examined.

Inclusion of the second term , which enters if the order parameter oscillates with the microwave field would give results a factor of 3 larger than the experimental results. This implies that the order parameter does not "follow" the microwave field.

It was found that the order parameter effects were inadequate to explain the results at low temperature.

(2) At low temperature ($t < 0.9$) the dominant mechanism is the effect on the quasiparticle energy spectrum of the applied perturbations. The experimental results for k(t) for Sn films fall into two clearly distinguishable classes :

(a) Thin films ($d \leq 500$ Å): For thin films the surface resistance was *experimentally found to decrease with increasing static current* ($k(t) < 0$).

This startling result which is as if the superconductor was "cooled" by the current cannot be understood in terms of the equilibrium theories described above.

If the total quasiparticle number is constrained *not to follow the field* then the distribution function develops a high frequency component that is out of phase with the microwave electric field leading to a decrease of R_s. This is a purely non-equilibrium effect and an estimate of it agrees in sign (-ve) and approx. magnitude with the experimental results.

(b) Thick films ($d \geq 800\text{Å}$). Experimentally for thick films the surface resistance was found to *increase* with applied static current. A model based upon the equilibrium effect of current on the quasiparticle energy spectrum (in the "clean" limit) agrees with the experimental results for k(t) in sign (+ve) , magnitude and temperature dependence.

This analysis of the experimental results would imply that the quasiparticles are out of equilibrium with the phonons in the thinner films while they are in equilibrium in the thicker films. However the same results could arise if there were an additional current in phase with the electric field in the thicker films. From an examination of the material parameters it was found that $\lambda/\xi \gtrsim 1$ for $d \geq 800\text{Å}$. It is conjectured that inclusion of spatial effects effects might lead to such a current contribution.

The measurements reported here are unique in their sensitivity which enables the study of superconducting films for very small perturbations. Furthermore this work constitutes the first quantitative comparison between theory and experiments of this class regarding non-equilibrium effects.

The experiment described here falls in the same class as similar experiments carried out in the last 25 years to examine the static magnetic field dependence of the microwave impedance of bulk superconductors. The decreases in $R_s(B_0)$ observed in the bulk experiment were complicated functions of temperature, frequency ,orientation etc. and a satisfactory solution was never found.

This experiment has two significant and advantageous features in relation to the early bulk results which greatly facilitate analysis. One is the enormous

improvement in sensitivity which allows the study of effects due to small static current. The other is the ability to vary film thickness which allows the considerable manipulation of material parameters.

The use of a fully superconducting cavity in which the film dominates the absorption (Sec.2.2) enables us to achieve sensitivities orders of magnitude better than achieved before. We are able to measure $\delta R_s / R_s \sim 10^{-5}$ *(at low temperature,* $\delta R_s \sim 10^{-9}\ \Omega/$ sq.). The sensitivity of the bulk experiments was $\delta R_s / R_n > 10^{-4}$. Since $R_s / R_n \sim 10^{-3}$ at low temperature, we see that the lower limit on the sensitivity is 10^{-8} better than the previous experiments. The advantage of this increased sensitivity is that it allows the study of very small perturbations ($B_0 / Bc \sim 10^{-2} - 10^{-3}$). At these low perturbations $\vec{p}_F \cdot \vec{v}_0 \ll \omega, T, \Delta$ - an important limit for the relevant theories. In the bulk experiments to date the fields are comparable to the critical field so that typically $\vec{p}_F \cdot \vec{v}_0 \gg \omega$, T which greatly complicates the analysis. We believe that the understanding of similar experiments performed to date has been hampered by the high fields that were used. Indeed there is experimental (R2,K3) and theoretical evidence (Sec.9) that supports this assertion.

The second aspect concerns the ability to vary film thickness which allows us to explore the wavevector dependence of the superconductor - electromagnetic interaction and the effects of scattering (see Sec.3.5 and Ch.I). The bulk experiments did not have this flexibility since they were mostly confined to the case of large q (pure type I superconductors). This together with the spatial inhomogeneity of the fields would lead to complications in the analysis for those experiments.

We now proceed to describe experimental results and theoretical analysis for $\delta R_s(B_0)$. This chapter has been divided into the following sections :

1. Experimental configuration
2. Principle of the Measurement
3. Description of the Electronics

1. Experimental configuration

A current was induced in the film by applying a field generated by a coil carrying a current supplied from an external source. Fig.3.1(a) depicts the experimental configuration.

For a small coil placed coaxial with the resonator and close to it the film acts like a superconducting plane of infinite area. The effect of the finite size of the film is minimised by the remainder of the resonator which is also fully superconducting. Note that the resonator forms a fully connected superconducting enclosure. As a first approximation let us consider the film to be equivalent to an

infinite superconducting plane . Possible edge effects associated with the finite size will be examined later in greater detail.

When a coil is placed parallel to an infinite superconducting plane and a current is applied to it the superconductor shields out fields behind it due to the Meissner effect. For this to happen currents are induced in the superconductor. The problem may be analysed in terms of the method of images . In this method the superconducting plane is replaced by an imaginary coil which is the mirror image of the original one placed at the same distance behind the plane (Fig.3.1(b)). For the region I the resultant is the vector sum of the fields produced by the coil and its image .

Thus at the superconducting surface the resultant component perpendicular to the film plane is exactly zero while the parallel component is doubled. The assumption of a perfect Meissner effect makes this result true for arbitrary orientation of the coil (though we shall be concerned only with the case of the coil plane parallel to the film).

Replacing the multiturn coil by a single coil of dimensions shown in Fig.3.1(b) the radial dependence of the resutant parallel component of the field is plotted in Fig.3.1(c). Also shown in Fig.3.1(c) is the configuration of the microwave field which was applied to the opposite side of the film. The dimensions of the coil were deliberately chosen so that the coil field B_0 approximately had the same distribution as the microwave field B_ω so that the currents superpose. The maximum value of B_0 was equal to the field at the coil center (to within 10% from the calculation). All results in this chapter are quoted in terms of this maximum value. The field at the coil center was calibrated by an independent measurement.

As discussed above the resultant field configuration is the same as if a field were applied parallel to one side of the film and none on the other. Under this condition a current is induced in the film which is uniform if the film is thin (Ch.2.). For the superconductor this current is proportional to the applied field for the case of an ideal homogeneous film. This induced current J_0 then has the same spatial distribution as B_0 (the same argument applies to J_ω and B_ω). One expects that the primary quantity affecting the superconducor is J_0 but because

of the above proportionality it is justifiable to express the results in terms of B_0 which is the experimentally applied quantity.

2. Principle of the measurement

In the presence of a supercurrent in the film the surface resistance is expected to be different than for the case of no supercurrent. (The latter case was discussed extensively in Ch.2). The change in R_s can be measured as a change in the Q of the resonator.

In practise we shall be interested (see Sec.5 & 6) in the following dependence of R_s :

$$R_s(B_0) = R_s(0) (1 + k_\alpha B_0^\alpha) \tag{3.3}$$

$$\frac{\delta R_s(B_0)}{R_s} = k_\alpha B_0^\alpha \tag{3.4}$$

The experimental quantities of interest are α and k_α. We show below how a measurement of the change in Q with B_0 yields α and k_α. In the experiments to be described later $\Delta R_s / R_s < 10^{-2}$. i.e. the changes are very small.Now :

$$\frac{1}{Q(B_0)} = \frac{1}{\omega U} P_{abs} = \frac{1}{2 \omega U} \int R_s(B_0) B_\omega^2 \, dS \tag{3.5}$$

where U is the energy density in the cavity (which is independent of B_{dc}) and the integral is taken over the surface of the film. Now B_0 is cylindrically symmetric and the only dependence is on r the radial distance from the center of the film ($0 < r < a$, the film radius = 0.875 ins.).

If B_0 is not uniform we get :

$$\frac{\delta Q(B_0)}{Q_0} = - \frac{\delta R_s(B_0)}{R_s} = - \eta_\alpha k_\alpha B_0^\alpha \tag{3.6}$$

$$\eta_\alpha = \frac{\int_0^a r \, dr \, b_0^\alpha B_\omega^2}{\int_0^a r \, dr \, B_\omega^2} \tag{3.7}$$

where B_0 is the maximum value of $B_0(r)$ and $b_0 = B_0(r) / B_0$. We note that the

power dependence of δQ on B_0 is the same as that of R_s i.e. the exponent α is unchanged by the spatial profile. However the correction $\eta_\alpha \neq 1$ in general.

The principle of the measurement is as follows :

A magnetic field is applied to one side of the film in the form of a triangular wave of very low frequency (40 Hz) (Fig.3.3). The surface resistance changes due to the current induced by the field and this causes the resonator Q to change (by eqn.3.6). The change in Q causes the voltage V produced by a detector to change proportionately at the same frequency (see Sec.2.3). The voltage change is amplified , digitized and stored in a computer. Typical resulting plots of the voltage are as shown in Fig.3.4. These are analysed using a polynomial fitting program for the exponent α and coefficient k_α. and is related to $\delta R_s / R_s$ by the chain of relations :

$$\frac{\delta V}{V_0} = 2\frac{\delta Q}{Q_0} = -2\frac{\delta R_s}{R_s} = -2\,\eta_\alpha\, k_\alpha\, B_0^\alpha \qquad (3.8)$$

Experimentally it was found that $\alpha = 2$ i.e. the dependence of δV and hence R_s on B_0 was quadratic. For this $\eta_\alpha = 0.4 \pm 0.1$. A further correction = 0.6 is necessary to account for the use of a guard ring to minimise edge effects. The result is that k (we drop the subscript) is given by :

$$k = 2.1\,\frac{\gamma}{B_0^2}\left[\tfrac{1}{2}\frac{d^2}{dx^2}\left[\frac{\delta V}{V}\right]\right] \qquad (3.9)$$

where x parameterises the voltage waveform and γ is a conversion constant between B_0 and x. The quantity in brackets was calculated using a polynomial fit to the data. With reference to raw data as shown in Figs.3.4 and 3.5 x represents the horizontal axis and γ relates x to the instantaneous field value in Figs.3.4(a) and 3.5(a). B_0 is in units of Gauss and hence the units of k are $(\text{Gauss})^{-2}$.

The experimental procedure is summarized below (for details see later sections):

(1) The resonator was run in a C-W self excited loop (Fig.3.) with both probes weakly coupled. A steady dc voltage V_0 ($\approx$ 60 mV) was obtained at the output of the heterodyne detector.

(2) The low frequency (40 Hz) triangular wave magnetic field was applied. Due to the chain of relations $\delta R_s \rightarrow \delta Q \rightarrow \delta V$ the detector output had a small component (typically $1\mu V$) at 40 Hz.

(3) The small ac component was amplified and sent to a data acquisition computer which digitized and averaged the signal (to increase signal-to-noise). The resulting waveform was stored in the computer.

(4) Using a polynomial fitting program the coefficient of the quadratic was calculated. Thus the experimental quantity k(t) was determined using eqn.(3.9) at different temperatures.

The configuration of the electronics required for this scheme has two parts -

(a) a high frequency or rf part that was used to produce the voltage V having both the dc and ac components V_0 and δV respectively.

(b) the data acquisition system which acts as an ac voltmeter to measure δV at 40 Hz.

3. Description of the electronics

Fig. 3.2 is a block diagram of the electronics used for the measurement. The system may be divided into two parts - a high frequency subsystem used to produce a low frequency voltage whose magnitude was determined by the Q of the resonator (and hence by R_s) and a low frequency data acquisition subsytem designed to measure the voltage. We now describe in detail the operation of these subsystems .

3.1. High frequency subsystem

In order to compensate for random drifts in the source frequency the resonator was run in a self excited loop as shown in Fig.3.2. The amplified output of an X - band generator at a frequency $\omega_0 + \omega_{if}$ (ω_0 = resonator resonant frequency = 10.12 GHz, and ω_{if} = approx. 60 MHz) was split into two and fed into the L ports of two double balanced mixers A and B. The resonator output at ω_0 was fed into the R port of mixer A producing a heterodyned output of frequency ω_{if} . The ω_{if} signal was amplified (approx. 80 dB) and limited and fed into the X port

of mixer B. This signal on being recombined with the $\omega_0 + \omega_{if}$ signal produces a signal at ω_0 which was amplified and supplied to the input port of the resonator.

The condition for oscillation of the loop and consequent excitation of the resonator is :

$$\varphi_{out}(t) - \varphi_{in}(t) = \varphi_{loop} = 2\pi \qquad (3.13)$$

independent of frequency and where φ refers to a phase of the signal and φ_{loop} is the net phase difference introduced by the loop circuitry. φ_{loop} is determined by the phase shift introduced by the coaxial cables and various passive and active devices in the loop circuitry. Since these are not easily amenable to manipulation (except by changing cable lengths) the phase shifter had to be used in order to satisfy the conditon eqn.(3.13).

With all amplifiers activated the X-band source was set to 10.12 GHz + 60 MHz. The 60 MHz heterodyned output of mixer A was observed after amplification on a fast scope. The phase shifter was then adjusted to give maximum signal. The procedure was then repeated after adjusting the X-band source by a few MHz because of freqency dependent effects in the If circuitry. particularly the limiter.

Under these conditions the resonator was excited at resonance. Frequency shifts due to any cause were automatically compensated for by the loop circuitry. With both input and output probes weakly coupled the output and input powers are related at resonance by :

$$P_{out} = \beta P_{in} Q_0^2 \qquad (3.14)$$

where β is determined by the coupling of both probes to the resonator. When mixer A is operated in its linear mode the resultant output of the diode detector (operated as a square law detector) is

$$V = \alpha \gamma P_{out} = \alpha \beta \gamma P_{in} Q_0^2 \qquad (3.15)$$

where α is the amplification provided by the amplifier ($\approx$ 40dB) and γ is characteristic of the diode detector.

Since small changes ΔV were of interest :

$$\frac{\Delta V}{V_0} = 2 \frac{\Delta Q}{Q_0}$$

Typical magnitudes of $V \approx 60$ mv and since $\Delta V / V < 10^{-2}$, $\Delta V < 600$ nV.

3.2. Data acquisition subsystem

The ac part (at 40 Hz) of the detected voltage was amplified by a specially designed ac coupled low noise amplifier (gain approx. 1250.). This amplified signal together with the inherent noise had to be transmitted through 150 ft 50 Ω cable to the PDP-11 which was used to do an Analog-to-Digital conversion. In order to prevent the capacitance of the cable from loading the amplifier and making the latter oscillate a line driver (essentially a 1:1 current amplifier) was used after the amplifier to facilitate transmission. In order to isolate the electric grounds of the apparatus from the computer ground, since they were located in different rooms, a line receiver had to be constructed for use just before the computer

A timing or sync pulse had to be fed to the computer to initiate data taking. This pulse produced by the waveform generator which generated the triangular waveform for the magnetic field also had to be transmitted using a line driver and receiver for the reasons discussed above.

The sequence of events was as follows : The magnetic field was applied to the film as a triangular waveform at 40 Hz. The modulation of the surface resistance caused a corresponding voltage at 40 Hz in addition to the dc voltage. This 40 Hz signal was amplified and sent to Channel 0 of the computer.

The sync pulse applied to Channel 1 of the computer caused an upward going transition at this channel. When this happened the A/D was activated . The computer performed an A/D conversion of the signal (Ch 0) for 400 points separated by a specified interval. The A/D operation for each of the 400 points involves assigning an integer between 0 and 1023 as a result of the measurement of the voltage at Ch 0 (between ± 2.5V) and storing this result. When this was completed the computer waited for the next upward transition at Ch 1 caused by the sync pulse (Fig.3.3).The process was repeated n_1 times and the result

added for each point. In order to avoid integer overflow (max = + 32678, -32677) periodically the results were converted to real numbers and the entire process repeated n_2 times and the result divided by n_2. The final result was a set of 400 integers between +32678 , -32677 where :

$$1 \text{ integer unit} = 5./1023/ n_1 \text{ volts.}$$

The data acquisition system acted essentially like a multichannel signal averager with a gain of n_1 and reduction of white noise determined by n_1 and n_2. (Signal to noise is increased as $(n_1 n_2)^{1/2}$). n_1 was limited by integer overflow to values < 100 (depending on input signal level) while in principle n_2 could be arbitrarily large but was limited by reasonable data acquisition times and acceptable signal to noise level. For the largest values found necessary (n_1=100,n_2=100) the net time for data acquisition at a 40 Hz rate was approx. 2 x 10^4 /40 secs $\approx$ 4 mins., where the factor 2 takes into account some unavoidable dead time.

Typical results of such a measurement are shown in Fig.3.4. In Fig.3.4(a) the triangular waveform for the magnetic field is shown plotted vs. time. Fig.3.4(b) is a plot of the result of A/D conversion for 400 equidistant points over the same interval. It is apparent that the signal to noise ratio is more than adequate for data analysis.

4. Sample preparation, Errors and Experimental checks

4.1. Sample preparation

All samples studied were thin films evaporated into sapphire substrates at liq. Nitrogen temperature. The details are described in Ch.II. The parameters of the samples used in this experiment are given in Table 3.1.

4.2. Analysis of Errors in the measurement

The quantity that is measured experimentally is k(t) (see Sec. 3.2). Since the electronics is quite complex (Fig.3.2) great care was taken to ensure that the entire system was linear. The detector was operated in its square-law regime ($V \propto$ high frequency power). A test triangular wave was used to verify the linearity of the system. From a measurement of the slope and magnitude the linearity and accuracy of the A-D system were found to be better than 1%. Thus the errors introduced by the electronics are within 1% and can be ignored.

From an examination of eqn.(3.9.) we deduce three main sources of uncertainty in the measurement of k(t).

(a) *Uncertainty of Static field geometry - Temp. independent error* This is due to uncertainties in estimating B_0 and η_2. For a given current in the coil it is necessary to know B_0 (the maximum field at the film) and $B_0(r)$ it's spatial profile. This is easy to do for a single turn - as we have done. However the actual coil is of finite size which introduces an uncertainty into B_0 and η_2. We *estimate* this uncertainty to be 5% for B_0 and 20% for η_2 leading to a total contribution of 30% to k(t).

Note that this uncertainty is purely a geometric effect and is independent of temperature. It might vary slightly from film to film due to the slight geometric changes in assembling apparatus.

(b) *Relative Error (" Temp. Dependent" Error)* This arises because of random uncertainties in carrying out the experimental procedure described in Sec.3.2 used to measure the quantity $\frac{1}{2}\frac{d^2}{dx^2}(\delta V/V)$. This was estimated experimentally by repeating the procedure a few times and found to be

approx. 10%.

Thus we conclude that the relative error in measuring k(t) is ± 10% while the absolute error is ± 40%.

4.3. Examination of possible spurious effects

The repeatability of the results has been checked with 3 films with d = 500 Å.

EXAMINATION OF EDGE EFFECTS

In Sec.2 the film was regarded as an infinite plane . The reason this is possible is because of the remainder of the resonator which is also superconducting. An additional aspect is that the coil diameter is much smaller than the film diameter.

In Fig.3.1(c) it will be seen that the field at the film edge is $\approx 0.07B_c$ the maximum field at a distance r/a=0.469 from the center. In the pure TE_{011} mode the microwave field at the edge is strictly zero. These two factors greatly contribute to minimising any possible effects arising out of the finite film size.

In order to further ensure negligible edge effects a Sn ring was placed concentric with the coil and whose inner edge coincided with the dimension of the resonator.(Fig.3.1(a)).

Because of the flux quantization condition the ring acts to maintain zero total flux inside it. Thus it prevents the field from "peeking" out beyond the film edge since all the flux in the interior of the coil has to return in the area between the ring and the coil. This greatly reduces the field at the edge and only minimally reduces the maximum field. The ring may be imagined to be like an additional coil with an appropriate current flowing in it to maintain zero total flux and cancel fields outside the ring.

In this configuration the field distribution is slightly altered and the maximum field produced at the film for a given current in the coil is slightly reduced. It is easy to correct for this by experiment. By measuring $\Delta Q / Q$ (as discussed earlier) with and without the ring the correction to I_2 was determined for $\alpha = 2$:

$$\alpha = 2 : \qquad \eta_\alpha^{ring} = 0.6\, \eta_\alpha$$

This correction was used throughout the experiment as was the ring.

This factor of 0.6 implies that with the ring B_0 was approx. 80% of the value with no ring for the same coil current . This is the correct magnitude as can be seen by a simple argument considering the flux that would escape beyond the ring in its absence. For the above magnitude we expect that the field at the film edge would be reduced by perhaps a factor $\approx$ 5 - 10 from its already low value of $\approx$ 0.07 B_0. Since the outcome of the results was not affected (except for the small quantitative correction described above) we conclude that edge effects were negligible.

EXAMINATION OF TRAPPED FLUX EFFECTS

The results were clearly not due to flux trapped in the film. This was verified by examining situations where flux was deliberately introduced :

(a) The film was cooled with the coil carrying a current. The results for $\Delta R/R$ were always > 0 i.e. $\Delta R/R$ increased for all temperatures.

Data obtained with flux in the film were always dependent on the direction of the applied field. The quadratic data were always independent of field direction.

(b) With the film cooled in zero applied magnetic field (the ambient field < 10^{-3} G)flux was injected into the film by raising the applied field. (see Ch.5)

For high temperatures ($t \geq 0.9$ for Sn) the curves for $\Delta V / V$ at high fields were as shown in Fig.3.6.This plot leads to an easy interpretation of flux lines being driven into the film and pulled out. Fig.3.7(a) and 3.7(b) are a sketch of the applied field and the resultant data.

Fig.3.7(c) is a plot of the expected current density in the film .Remember that a continous triangular field was applied . Because of the presence of flux the condition of zero induced current occurs not at B = 0 but at some finite value of the field. On either side of this finite value the current is linearly proportional to the field until it rises to a critical value. Now the current cannot increase further but because the field is increasing flux lines are driven into the film. When the field reaches its maximum value and begins to decrease the current

begins to change and the process is repeated.

This picture lends considerable weight to the assumption that in the absence of flux the current was proportional to the field.

An important feature of the above result was that at high temperatures flux lines could be driven in and removed, i.e. when the applied field was removed the flux lines seemed to disappear since the resonator Q returned to its original value.

This was not the case at low temperatures where once flux was driven in it was irreversibly trapped (see Fig12.Ch.5) .When this happened the results for $\Delta R/R$ were different than Figs.3.4 and 3.5. in that stable plots like Figs.3.5 were not obtainable.

EXAMINATION OF "LEAKAGE" EFFECTS

We now examine the possible contribution of transmission through the film. We are effectively measuring changes in the resonator Q which has contributions both from the absorption and transmission. The changes in Q have been related thus far to changes in R_s rather than due to transmission.

In Ch.II it was shown that even for the thinnest films the ratio of the powers $P_{xmitt}/P_{abs} \approx 6x10^{-3}$. Thus the contribution to the Q is smaller than the absorption losses. This was experimentally verified as described in Ch.II. The effects of transmission continue to be negligible as in Ch.II.

5. Outline of Results

In Sec.3 we described the experimental procedure for measuring changes δR_s in the surface resistance R_s due to applied static magnetic field. Except in very narrow regions of temperature the raw data for $\delta R_s \propto -\delta V$ was as shown in Fig.3.4 and 3.5. *These results were independent of microwave intensity.*

In Fig.3.4 as the magnetic field was increased (in absolute magnitude) from zero the surface resistance increased. From curves (a) and (b) the relation between δR_s and B_0 is seen to be quadratic. These raw data were analysed on a computer and the exponent was found to be 2 ± 0.05. From a polynomial fit , the coefficient of the quadratic was extracted and k(t) computed from eqn(3.9)

where $\delta R_s = k(t)\, B_0^2$. *Note that k(t) > 0* in Fig.3.4.

Fig. 3.4 was typical of the results obtained for thicker films ($d \geq 800$ Å) for Sn at *all temperatures* (0.38 - 0.98T_c). The results for k(t) for these films is given as a function of temperature in Fig.3.8. Note the precipitous decrease for t near 1 (T near T_c). This steep behaviour seems to get arrested below $t \approx 0.9$ and is followed by a gradual rise as the temperature is lowered further.

For thinner films (d = 260 Å, 500Å) also of Sn the results at high temperature ($t \geq 0.9$) were represented by Fig.3.4. That is the surface resistance increased with increasing field ($k(t) > 0$) similar to the thick films and the temperature dependence was similar.

For these thinner films startling results were obtained when the temperature was lowered below $t \sim 0.9$. Fig.3.5 is typical of the data for these conditions. As the field was increased *the surface resistance decreased* quite unlike the other results. In other words $k(t) < 0$. The temperature dependence of the absolute value of k(t) for the thinner films is shown in Fig.3.9. The connected data points are for $k(t) < 0$. Note that at high temperature where $k(t) > 0$ the temperature dependence is quite similar to that of thicker films.

In the temperature region $0.88 < t < 0.90$ the field dependence of δR_s was not monotonic but nearly oscillatory. In this region the quadratic behaviour seems to be absent ($k(t) \sim 0$). It was decided to defer the analysis of these complicated data.

Summary of Results for Sn films

We summarize below the features of the results that should be described by relevant theories :

(a) The changes in δR_s are quadratic in the field strength i.e. $\delta R_s = k(t)\, B_0^2$ except for thin films between $t \approx 0.88$-0.90.

(b) The results were independent of microwave intensity.

(c) Thicker films ($d \geq 800$ Å): $k(t) > 0$ for all t, i.e. surface resistance increases with increasing applied field. k(t) decreases sharply below T_c and gradually rises at low temperature.

(d) Thinner films ($d \leq 500$ Å): At high temperature ($t > 0.9$) the results are similar to those of the thicker films i.e. $k(t) > 0$ and has a similar temperature dependence.

At low temperature $t < 0.9$, δR_s is still quadratic. However $\delta R_s < 0$ i.e. $k(t) < 0$. Thus this result differs qualitatively from the thicker film results at low temperature.

6. Theory of Static Current effects on Surface Resistance

Having described the features of the experimental results we now proceed to examine various theoretical models and compare their results with the experimental data.

Since we are mostly concerned with thin films ($d \leq 2000$Å) the surface impedance can be approximated by its thin film limit. In the local limit the surface impedance can be written in terms of the complex conductivity :

$$\vec{J}_\omega = -i\,\omega\,(\sigma_1 - \sigma_2)\,\vec{A}_\omega \tag{3.14}$$

$$Z_s = R_s + X_s = R_n(d)\left[\frac{\sigma_1}{\sigma_n} - i\,\frac{\sigma_2}{\sigma_n}\right]^{-1} \tag{3.15}$$

where $R_n(d)$ is the surface resistance in the normal state, $\rho_n = 1/\sigma_n$, ρ_n and σ_n are respectively the normal state resistivity and conductivity of the film.

From the above eqn. we get, assuming $(\sigma_1/\sigma_n) << (\sigma_2/\sigma_n)$ as is usually the case :

$$\frac{\delta R_s}{R_s} = \frac{\delta\sigma_1}{\sigma_1} - 2\,\frac{\delta\sigma_2}{\sigma_2} \tag{3.16}$$

$$\frac{\delta X_s}{X_s} = -\frac{\delta\sigma_2}{\sigma_2} \tag{3.17}$$

We shall use these greatly simplified equations in the discussions that follow.

In the presence of a supercurrent the conductivities are changed and the above eqns. are used to calculate the effect on the measured quantity - R_s.

Conceptually the changes of σ_1 and σ_2 can be represented using eqn(3.2) as :

$$\delta\sigma_1 = \frac{1}{\omega}\left[\ \mathrm{Im}\ q_1 + \mathrm{Im}\ q_2\ \right] A_0^2$$

$$\delta\sigma_2 = \frac{-1}{\omega}\left[\ \mathrm{Re}\ q_1 + \mathrm{Re}\ q_2\ \right] A_0^2$$

The resultant changes in R_s are independent of the high frequency field and quadratic in the static field.

7. Temperatures near T_c (t > 0.9): Order Parameter Effects (Ginzburg - Landau Theory)

Near T_c a particularly simple formulation of superconductivity exists in the form of the Ginzburg-Landau (GL) theory (G4). In GL the superconducting state is described by a complex order parameter ψ and the free energy can be written:

$$f_s = f_{n0} - \alpha\,|\psi|^2 + \frac{\beta}{2}\,|\psi|^4 + \frac{1}{2m}\left|\left(\frac{\hbar}{i}\nabla - \frac{e\vec{A}}{c}\right)\psi\right|^2 \qquad (3.18)$$

where f_n = free energy of the normal state and α , β (> 0) are parameters. The effect of a vector potential which produces a current is included, the associated magnetic field being assumed negligible. $|\psi|^2$ can be associated with ρ_s the density of Cooper pairs.

In the presence of a current the kinetic energy associated with the current increases f_s (towards f_n). Consequently $|\psi|^2$ and ρ_s must decrease. As a result both the penetration depth λ increase and σ_2 decrease since $\lambda \propto 1/\sigma_2\ 1/\rho_s$. From eqn.(3.16) R_s has to increase. This can also be seen from the temperature dependence of $R_s(T)$ (Fig.2.6). The effect of the static current is as if to "push" the superconductor towards T_c thus increasing R_s.

The calculation of k(t) in this model yields (G5):

$$\frac{\delta R_s}{R_s} = -2\,\frac{\delta\sigma_2}{\sigma_2} = \left(\frac{\lambda}{d}\right)^2 \left(\frac{B_0}{B_{co}}\right)^2 \frac{1}{(1-t^2)^2\,(1-t^4)}$$

$$k_{GL}(t,d) = +\left(\frac{\lambda}{d}\right)^2 \frac{1}{B_{c0}^2}\,\frac{1}{(1-t^2)^2(1-t^4)} \qquad (3.19)$$

where $\lambda = \lambda_p(\xi_0/l)^{1/2}$ is the m.f.p. corrected penetration depth and B_{c0} is the bulk critical field at $T = 0$, λ_p is the penetration depth in the pure bulk material (= 510Å for Sn).

7.1. Comparison with experiment

Fig.3.10 is a plot of the experimental data for the various films studied along with $k_{GL}(T)$ calculated for the same films using the parameters listed in Table 3.1. We make the following comments :

(1) The experimental results are very well described by $k_{GL}(t)$ for $t > 0.9$ both as regards temperature and thickness dependence. This implies that at high temperatures the experimental results are consistent with the order parameter being depressed by the static current.

(2) The analytic solution $k_{GL}(t)$ was obtained in the limit $\kappa = \infty$ where $\kappa = \lambda/\xi$ is the GL parameter(G5). This corresponds to the dirty or type II limit. The other limit $\kappa = 0$ (type I) for which analytic solutions can be obtained has a weaker temperature dependence $(1-t^2)^{-2}\,(1-t^4)^{-1/2}$ and is not consistent with the data.

(3) Eqn.(3.19) is a manifestation of the first term in eqn.3.1. The second term in eqn.(3.1) leads to a subtler effect. If $\vec{A}_0 \parallel \vec{A}_\omega$ as is the case here, the instantaneous $\vec{A} = \vec{A}_0 + \vec{A}_\omega$. Because the change in pair density $\delta\rho_s \propto A^2 = A_0^2 + 2\vec{A}_0\cdot\vec{A}_\omega$ the density and hence the order parameter have a high frequency component. In the presence of the static current this leads to an additional contribution to the current $\vec{J}_\omega = \rho_s \vec{A}$ and hence to the conductivity σ_2. This contribution is absent if $\vec{A}_\omega \perp \vec{A}_0$.

In this simple picture (S8) then the net result representing both the q_1 and q_2 terms can be represented phenomenologically as :

$$\frac{\delta R_s}{R_s} = -2\,\frac{\delta\sigma_2}{\sigma_2} \propto 1 + \frac{2\cos^2(\vartheta)}{1-\omega\tau_R}$$

where ϑ is the angle between $\vec{A}_0$ and $\vec{A}_\omega$. Thus if $\vec{A}_0 \parallel \vec{A}_\omega$ *and* $\omega\tau_R << 1$ the result is 3 times larger than if $\omega\tau_R >> 1$ because the second term is proportional to $1/\omega\tau_R$ in the latter case. The pair density responds like a low pass filter.

This simple picture dominated the thinking in the early analysis (G5). It entirely ignores the fact that the superconductor is a two component system so that even if $\omega\tau_R >> 1$ the density of states can oscillate at the frequency ω so long as $\omega < 2\Delta$. This gives rise to an additional contribution which turns out to be of crucial importance in interpreting the data at low temperature (see Sec.9). (It is possible that this density of states oscillation is responsible for the discrepancy from the simple ideas described above in the experiments of Ref.P2).

The experimental data (Fig.3.10) seem to show that at high temperature such contributions are dominated by the direct static effect eqn.(3.19). From the discussion in Sec.3.4 the best way to determine such effects would be in the temperature dependence rather than in the absolute magnitude.

(4) The simple order parameter effect eqn.(3.19) predicts that $k_{GL}(t) \rightarrow$ const as $t \rightarrow 0$. Fig.3.10 shows that the experimental results deviate strongly from this prediction in two very interesting ways depending on thickness. We summarize these differences below.

7.2. Deviations from GL at low temperatures

(a) Thicker films $d \geq 800\text{Å}$

The experimental results for $t < 0.9$ for these films are greater than $k_{GL}(t)$. The most interesting aspect is that k(t) (note that it is +ve) increases with decreasing temperature.

(b) Thinner films $d \leq 500\text{Å}$

For $t < 0.9$ the data for thin films differs not merely in temperature dependence or magnitude but *most importantly in sign*. It was found that $\delta R/R < 0$ (hence $k(t) < 0$) - a *startling* result.

At low temperature changes in the the surface resistance are dominated by the number of quasiparticle ($\propto \exp(-\Delta/T)$) rather than the pair density. In the GL theory the quasiparticles are ignored. We now examine the effects of quasiparticles on R_s in the presence of a supercurrent. The dominant contribution is that of σ_1/σ_n which we have ignored so far.

8. Quasiparticle Effects in the "Clean" Limit

In the BCS theory in the absence of any external perturbations the quasiparticle energies and density of states are given by :(T1)

$$E = \left(\varepsilon_{\vec{k}}^2 + \Delta^2\right)^{1/2} \tag{3.20}$$

$$N(E) = \frac{|E|}{\left(E^2 - \Delta^2\right)^{1/2}} \Theta(E^2-\Delta^2) \tag{3.21}$$

where $\varepsilon_{\vec{k}} = \hbar^2/2m\,(\vec{k}^2 - \vec{k}_F^2)$ is the Bloch energy (relative to the Fermi level ε_F) and ϑ is the step function. We now examine changes that occur in this description in the presence of a static current and further describe how the conductivities are affected.

In a clean superconductor where scattering is negligible the current displaces the Fermi surface in $\vec{k}$ space by $m\vec{v}_0/\hbar = -(ec/\hbar)\vec{A}_0$ where $\vec{v}_0$ is the velocity of the pairs due to the supercurrent. The result of this is to shift the quasiparticle energies and make the density of states anisotropic :

$$E_v = E + \vec{p}_F\cdot\vec{v}_0 = E_0 - \vec{p}_F\cdot\vec{A}_0 \tag{3.22}$$

$$N(E) = \frac{|E_v|}{\left(E_v^2 - \Delta^2\right)} \Theta(E_v - \Delta) \tag{3.23}$$

The density of states is described pictorially in Fig.3.11(a). At a finite temperature the distribution of quasiparticles is anisotropic while the total number is increased (on averaging over the Fermi surface).

It should be noted that a current-carrying state in a superconductor is a state of thermodynamic equilibrium and can be formally obtained by minimising the total free energy of the system (Cooper pairs and quasiparticles) subject to the constraint $\vec{J}_0 = -\frac{c}{4\pi\lambda^2}\vec{A}_0 = ne\vec{v}_0$. The resultant distribution function is anisotropic and simply given by the equilibrium Fermi distribution function with shifted energies (B3,P5):

$$f(E) = \left[\exp(\beta(E-\vec{p}_F\cdot\vec{v}_0)) + 1\right]^{-1} \tag{3.24}$$

where $\beta = 1/kT$. Using this distribution function the conductivities σ_1 and σ_2 can be calculated. The well-known Mattis-Bardeen expressions for σ_1/σ_n and σ_2/σ_n (M1,T1,P4) are modified for this case by the use of eqns.(3.22) and (3.23). The resultant expressions are (see also G3,M1) :

$$\frac{\sigma_1(v_0)}{\sigma_n} = \frac{4}{\pi\omega}\int_0^{\pi} d\vartheta \cos^2(\vartheta+\gamma) \int_{\Delta}^{\infty} dE\, g(E)$$

$$\times \left[f(E - p_F v_0 \cos(\vartheta)) - f(E - p_F v_0 \cos(\vartheta) + \omega) \right]$$

$$\frac{\sigma_2(v_0)}{\sigma_n} = \frac{2}{\pi\omega}\int_0^{\pi} d\vartheta \cos^2(\vartheta+\gamma) \int_{\Delta-\omega}^{\Delta} dE\, h(E) \left[1 - 2f(E - p_F v_0 \cos(\vartheta) + \omega)\right]$$

where γ is the angle between $\vec{A}_0$ and $\vec{A}_\omega$ ($\gamma = 0$ in this experiment). Further we are interested only in effects to lowest order in v_0 (i.e.B_0) so that $p_F v_0 \ll \Delta, T$. In this limit :

$$\frac{\sigma_1(v_0)}{\sigma_n} = \frac{\sigma_1(0)}{\sigma_n}\left[1 + \frac{2 + \cos 2\gamma}{16}\left(\frac{p_F v_0}{kT}\right)^2 \frac{I_2 - I_0}{I_0}\right] \qquad (3.25(a))$$

$$\frac{\sigma_2(v_0)}{\sigma_n} = \frac{\sigma_2(0)}{\sigma_n}\left[1 - \frac{1 + \cos 2\gamma}{16}\left(\frac{p_F v_0}{kT}\right)^2 \frac{I_3}{I_4}\right] \qquad (3.25(b))$$

where I_0 , I_2 , I_3 , I_4 are integrals over E. Using the above equations and (3.16) $\delta R_s/R_s$ can be calculated. This can only be done numerically. However the low temperature limit is particularly interesting ($\gamma = 0$ and $p_F v_0 \ll \omega \ll T \ll \Delta$) :

$$\frac{\delta R_s}{R_s} = + \frac{3}{8}\left(\frac{p_F v_0}{kT}\right)^2 + O\left(e^{-\Delta/T}\right) \qquad (3.25(c))$$

This result has a particularly simple interpretation. The anisotropic distribution function leads to an increase in the number of quasiparticles proportional to $(p_F v_0/kT)^2 \exp(-\Delta/T)$. σ_1/σ_n is a frequency dependent measure of this number and the *fractional increase* leads to the first term. The *fractional decrease* in σ_2 (equivalently the increase of penetration depth) due to the quasiparticles is smaller by $O(\exp(-\Delta/T))$ and leads to the second term.

Now $v_0 = j_0/n_s e = (4\pi e/mc^2)\lambda^2(t)\, j_0$ where λ is the m.f.p. corrected penetration depth in the "dirty" material. For a thin film with a field applied on one side, $j_0 = (c/4\pi)\, B_0/d$. In addition we have that in the pure bulk case at T = 0, with $\lambda = \lambda_p(0)$ the pure bulk penetration depth and $B_0 = B_{c0}$ the bulk critical field at T = 0, then $\Delta(0) = p_F v_c(T=0) = (e/mc)\lambda_p(0)B_{c0}$. Hence :

$$p_F v_0 = \frac{\lambda(t)}{\lambda_p(0)} \frac{\lambda(t)}{d} \frac{B_0}{B_{co}} \Delta(0) \tag{3.26}$$

$$k_{q-eq}(t) = \frac{3}{8}\left[\lambda\frac{(0)}{\lambda_p(0)}\right]^2 \frac{1}{B_{co}{}^2}\left[\frac{\Delta(0)}{kT_c}\right]^2 \frac{1}{(1-t^4)^2}\frac{1}{t^2} \tag{3.27}$$

We use a correction factor $\zeta = 0.4$ for d = 2000 Å in evaluating eqn.(3.27).

8.1. Comparison with thick film results ($d \geq 800$Å)

In Fig.(3.12) we compare the experimental results with eqn.(3.27) calculated using the values listed in Table I. We make the following comments :

(a) For $d \geq 800$Å k_{q-cl} describes the temperature dependence of the data very well. In particular for $t \to 0$, $k_{q-cl}(t) \to 1/t^2$. This is in good agreement with the data and resolves the striking disagreement between the experimental results and the GL theory.

(b) From Ch.II the measurements of R_s as a function of thickness indicate that for thick pure films of Sn nonlocal effects enter into R_s. This means that the $\vec{q}$ large part of the kernel $Q(\vec{q},\omega,\vec{A}_0=0)$ used in Ch.II contributes significantly to R_s. In the calculation leading to eqn.(3.27) we assumed that the wavevector dependence in the presence of a static current would be the same as in its absence. In other words in the absence of current the Mattis-Bardeen conductivity ratios σ_1/σ_n and σ_2/σ_n are both independent of $\vec{q}$. This is because for small $\vec{q}$ σ_1 , σ_2 , σ_n are independent of $\vec{q}$ and for large $\vec{q}$ they are all proportional to $1/q$. We assume that the same holds in the presence of current. A microscopic calculation by Maki (M2) for the case of large $\vec{q}$ seems to bear this out since he gets the same expression. (Maki gets a negative sign for δR_s at $\Delta < T$ which we believe is due to an error).

(c) The above analysis yields positive quadratic dependence for δR_s at all temperatures. It does not predict the observed low temperature negative quadratic behaviour for thin films.

These calculations have been carried out in the "clean" limit $\tau_{imp} T_c \gg 1$ ($l \gg \xi_0$) where $\tau_{imp} = l/v_F$ is the impurity or elastic scattering time. In this limit each quasiparticle remains in its momentum state but changes its energy according to (3.22). If $\omega\tau_{imp} \ll 1$, then this holds for the 2nd. term in eq.(3.2) also, i.e. the distribution function follows the high frequency field and the quasiparticle number changes accordingly even though $\omega\tau_{in} \gg 1$ (τ_{in} is the inelastic electron-phonon scattering time).

The clean limit should not be expected to apply to these films since the m.f.p. is smaller than ξ_0. Consequently we view the apparent agreement of the experimental results with this "clean" limit theory as being coincidental. As discussed in Sec.10 it is possible that the spatial variation of the current across the film needs to be incorporated into the calculations in a nontrivial way i.e. the distribution function at a point is affected by the current over a spatial region of order ξ and the local relation assumed in eqn.(3.22) does not hold.

9. Proposed Explanation of the observed decrease in surface resistance

Since the low temperature results for $d \leq 500$Å *differs in the important aspect of sign* from the predictions of the above model we examine why the latter seems to be inapplicable to the thin film case.

When the film is made thinner scattering at the surface and also due to the increased presence of inhomogeneities becomes important. This of course manifests itself in the decrease of m.f.p. with thickness (see Table 3.1). The electrodynamics is consequently modified (Ch.I and II).

Increased scattering also leads to a randomization of the quasiparticle momentum. Under these conditions the "clean" picture for the density of states used above (Fig.3.11(a)) is no longer valid. Rather the anisotropy is washed out and the density of states becomes as shown in Fig.3.11 (b).

Neither or both of these modifications are adequate to explain why the surface resistance decreases at low temperature in the thin films. They merely

modify the quantitative details and do not yield the observed change in sign.

Rather the most important aspect is the assumption regarding the second term, that it is present if either the pair density or the quasiparticle number are allowed to oscillate with the field, and that it is absent if the frequency is so high that they cannot do so. This is a simple picture of a relaxation process and we find that it is inadequate to describe the experimental results since it merely modifies the magnitude by a factor of 3 depending on whether it is presumed to be present or absent and does not affect the sign.

Consider what happens if the condition $\omega\tau >> 1$ is satisfied, as is the case here.(see Ch.I), where τ is the quasiparticle scattering time. Unlike the static term A_0^2 the high frequency pairbreaking term $\vec{A}_0 \cdot \vec{A}_\omega$ will not be able to change the quasiparticle number since $\omega\tau \gg 1$. However the density of states and gap can follow the high frequency field since their fundamental frequency is $\Delta \gg \omega$. Both these effects would for $\omega < 1/\tau$ tend to increase the quasiparticle number. At high frequencies $\omega > 1/\tau$ and in order to counteract this increase the quasiparticle distribution function has to respond in an opposite way. Thus the quasiparticle distribution function has a high frequency component f_ω which leads to an additional current which we call $J_{q\omega}^{ne} \propto (\vec{A}_0 \cdot \vec{A}_\omega)\vec{A}_0$ that is exactly out of phase with the electric field. Because this current is out of phase with the electric field it leads to a *-ve sign for this contribution* to the conductivity with a resultant decrease in the absorption. Similarly there is a supercurrent component called $J_{s\omega}^{ne}$ which *adds* to the usual supercurrent $J_{s\omega}$ (present in the absence of static field see Ch.I).This implies that the penetration depth *decreases* at the same time. These currents and their phase relationships are depicted in Fig.3.14. The superscript "eq" refers to the contributions considered in the previous sections (due to the first term $(\vec{A}_0 \cdot \vec{A}_0)\vec{A}_\omega$ in eqn.(3.2)) which increase the surface resistance while the superscript "ne" refers to the nonequlibrium contribution just discussed.

Calculations in which the above considerations are included are described next.

9.1. Calculation of k(t) for "dirty" limit *and* $\vec{q} \to 0$

These calculations are based upon the high frequency response calculations of Ovchinnikov (O1) and Ovchinnikov and Schon (O2). They assume the "dirty limit" and local electrodynamics.

In the presence of a current the density of states is no longer anisotropic as in the "clean" case discussed above. We now have "pairbreaking" effects entering into the picture leading to states in the gap. Thus the minimum energy of excitations $\Omega_G < \Delta(\vec{A}_0=0)$, the value of the gap in the absence of current. The density of states now looks as in Fig.3.11(b). These effects are described in terms of a pairbreaking parameter Γ given by :

$$\Gamma = 2 D e^2 A_0^2 = \frac{2}{3} (\vec{p}_F \cdot \vec{v}_0)^2 \tau_{el} \qquad (3.28)$$

where $D = 1/3\, v_F^2\, \tau_{el}$ is the diffusion coefficient and $\tau_{el} = l/v_F$ is the elastic scattering time.

The calculation of the high frequency response in the presence of a static current is a formidable one requiring elaborate Green's function techniques. This has been carried out by Ovchinnikov(O1) and Ovchinnikov and Schon(O2). Since the particular case of this experiment was not analysed though general results were given, the details and specializations to cases of interest had to be carried out (S3). Here we quote the final results and give a description of the relevant processes.

The equivalent of eq.(3.1) for this case is:(the convention $\sigma_s = \sigma_1 + i\,\sigma_2$ is used here following (O1) and (O2)).

$$\frac{\vec{J}_\omega}{\sigma_n} = - \left[Q_1(\omega,t,\Gamma)\, \vec{A}_\omega + \frac{1}{\omega} Q_2(\omega,t,\Gamma)\, 2e^2 D\, \vec{A}_0\, (\vec{A}_0 \cdot \vec{A}_\omega) \right] \qquad (3.29)$$

In this experiment we have $\vec{A}_0 \,||\, \vec{A}_\omega$. Further $\Gamma = 2e^2 D\, A_0^2 << \omega, T, \Delta$. We are also only interested in effects linear in Γ ($\propto A_0^2$). Hence :

$$\frac{\vec{J}_\omega}{\sigma_n} = - \left[Q_1(\omega,t,\Gamma) + \frac{\Gamma}{\omega} Q_2(\omega,t,0) \right] \vec{A}_\omega \qquad (3.30)$$

Since we are interested in low temperatures, the dominant effect is due to σ_1/σ_n

which is simply proportional to the imaginary part of the kernel $Q_1 + (\Gamma/\omega)Q_2$.

$$\frac{\sigma_1(\Gamma)}{\sigma_n} = \frac{\sigma_{1,1}}{\sigma_n} + \frac{\sigma_{1,2}}{\sigma_n} = -\frac{1}{\omega}\,\mathrm{Im}\,Q_1(\Gamma) - \frac{\Gamma}{\omega^2}\,\mathrm{Im}\,Q_2(\Gamma=0) \qquad (3.31)$$

$$\frac{\delta R_s}{R_s} = \frac{\delta\sigma_1(\Gamma)}{\sigma_1} = -\frac{\delta\,\mathrm{Im}\,Q_1(\Gamma)}{\mathrm{Im}\,Q_1(0)} - \frac{\Gamma}{\omega}\frac{\mathrm{Im}\,Q_2(0)}{\mathrm{Im}\,Q_1(0)} \qquad (3.32)$$

where $\sigma_1(0)$ is the Mattis Bardeen result. The contribution Q_1 arises from the direct action of the static current on the quasiparticle energy spectrum. The microwaves act as probe (the first term in eqn.(3.2)). The Q_2 term arises from the modification of the pairbreaking by the high frequency probe field (second term in (3.2)).

The contribution $\sigma_{1,1}$ due to Im Q_1 can only be evaluated numerically. We have carried out the computations in some detail. The main result of interest here is that for small $\Gamma \ll \omega$, T , Δ and at low temperature ($\Delta \gg T$), $\sigma_{1,1}$ increases linearly with Γ and hence A_0^2, implying that R_s increases due to this channel. This is due to the slight reduction in the gap which increases the number of quasiparticles. For large $\Gamma^{2/3} \gg \omega$, $\sigma_{1,1} < \sigma_1$ so that R_s could decrease. This is an interesting effect but not of relevance here since in this case $\Gamma \approx 10^{-2}\,\omega$. (This decrease is similar to the decreases computed by Garfunkel (G3) at high fields $\vec{p}_F\cdot\vec{v}_0 > \omega$. For $\vec{p}_F\cdot\vec{v}_0 < \omega$ the results of (G3) are equivalent to those of eqns.(3.25)).

We conclude once again that the equilibrium effect of the static current alone in modifying the quasiparticle spectrum is not adequate to explain the observed decrease of R_s.

The origin of the second term $\sigma_{1,2}$ due to Q_2 arises from the modification of the static pairbreaking by the high frequency probe field. Conceptually this is described by the following diagram :

$$\vec{A}_0\cdot\vec{A}_\omega \propto \Gamma_\omega$$

$$\Delta_\omega \qquad f_\omega$$

The high frequency component $\vec{A}_0 \cdot \vec{A}_\omega \propto \Gamma_\omega$ leads to pairbreaking effects at the frequency ω. This means that both the quasiparticle distribution function and the gap parameter Δ have a high frequency component f_ω and Δ_ω. The presence of these components in turn alters Γ_ω. Thus these quantities have to be calculated selfconsistently. Fortunately this task has been carried out in Ref.(01,02) quoted above. In the low temperature limit :

$$\frac{\delta R_s}{R_s} = \frac{\sigma_{1,2}}{\sigma_1} = -\left[\frac{\Gamma}{\Delta}\right]\left[\frac{\pi/\sqrt{2}}{\ln(4T/\omega)-\gamma}\right]\left[\frac{\Delta}{\omega}\right]^{3/2} - \pi\left[\frac{\Gamma}{\Delta}\right]$$

We have simplified the expressions using the low temperature limit of interest $\Gamma \ll \omega \ll T \ll \Delta$. Using eq.(3.28) and (3.26) we get in the low temperature limit :

$$k_{q-ne}(t) = -\frac{2}{3}\frac{1}{B_{co}^2}\left[\frac{\lambda}{d}\right]^2\left[\frac{\pi\sqrt{2}}{\ln(4T/\omega)-\gamma} + \pi\right] \qquad (3.33)$$

This term was found to numerically dominate the +ve effect due to Im Q_1.

Note that this gives a decrease for δR_s ($k(t) < 0$). In Fig.3.13 we compare this result with the experimental results for d = 500Å and 260Å. Considering the approximations (particularly in regard to relating Γ to B_0) in the calculations we consider the agreement to be satisfactory at low temperature.

10. Discussion of results for Sn films

A summary of the conclusions arrived at from the analysis described above is:

(a) For $d \geq 800$Å the experimental results can be described in terms of equilibrium concepts. At high temperature the dominant effect is due to the fractional decrease of the order parameter while at low temperature the fractional increase of the quasiparticle number dominates. These equilibrium effects describe very well the experimental results in sign (+ve), magnitude and temperature dependence. The analysis also seems to imply that the order parameter does not oscillate with the field while the quasiparticle number "follows" the field.

(b) For $d \leq 500$Å the high temperature results are describable in terms of the order parameter decrease. At low temperature ($t < 0.9$) the results are that

the surface resistance R_s decreases with static applied current. This cannot be explained by the equilibrium increase of the quasiparticle number due to the static current alone. Rather a non-equilibrium modification of the static pair-breaking by the high frequency field has to be considered. This leads to a quasiparticle current that is out of phase with the electric field and gives rise to a decrease of the surface resistance. Calculations of this backflow current show that it is the dominant effect and agrees with the experimental results as far as sign and approximate magnitude and temperature dependence to within the experimental and calculational uncertainties.

These results imply that there exists a critical thickness d_c ($500\text{Å} < d_c < 800\text{Å}$) above which the non-equilibrium backflow contribution becomes unimportant. One is tempted to say that with increasing thickness d, the inelastic scattering time becomes shorter and the opposite condition $\omega \tau \ll 1$ is valid. There is no other experimental evidence to support this - rather with decreasing m.f.p. as d increases τ_{in} should get longer (see Ch.IV).

As we have mentioned earlier in this chapter and discussed in detail in Ch.II the nature of the electrodynamic response changes with the m.f.p. The parameter $l/\lambda = ql$ determines this response. For $ql << 1$ the electrodynamics is local (London type) and the response is determined by the $q \to 0$ part of the kernel. For $ql >> 1$ the electrodynamics is nonlocal (Pippard type) and the response is determined by the large q part of the kernel. From Table 3.1 we see that l/λ is increasing rapidly with thickness. It seems reasonable to ask whether the observed difference between thin and thick films is a consequence of the difference in their electromagnetic response.

The concept of local vs. nonlocal is a purely equilibrium one. Similar considerations hold true for the normal state also. In other words the concepts of locality and nonlocality have only to do with J - A relationship and not with the quasiparticle distribution. The proposed explanation of the low temperature decrease is based upon a disequilibrium of the quasiparticle and is intimately determined by the coupling to the condensate. It seems unlikely that the equilibrium electrodynamics could account for the apparent absence of this mechanism as the thickness increases.

An examination of the parameter $\lambda/\xi = \kappa$ reveals a more plausible answer. ξ and λ are the m.f.p. corrected Ginzburg-Landau (not Pippard) coherence length and penetration depth respectively and κ is the well-known G-L parameter. From Table 3.1 it is seen that this parameter crosses 1 when $d \approx 800$ Å. λ determines the spatial size of variations of electromagnetic fields in the superconductor and ξ sets the scale of variations of the order parameter. The quasiparticle distribution function is tied to the order parameter. When $\lambda \gg \xi$ the ideas we have discussed apply. When $\lambda < \xi$ the quasiparticles are affected by the order parameter over a wider region and the non-equilibrium effect could be suppressed. It is possible that the non-equilibrium current discussed above is counteracted (rather than suppressed) by an additonal quasiparticle current in phase with the electric field. This could explain why the thickest film seems to show a greater +ve k(t) than the equilibrium ideas imply. (See also the discussion in Sec.10).

A more complete comparison of experimental results with the above theory requires extensive numerical computations of all the contributions considered by (O1) and (O2). Thus the theory could be extended to all temperatures. In the temperature range of interest here ($0.38 < t < 0.9$), we have estimated that the result will still be the same but with a slightly smaller magnitude (we have considered only one term). Near T_c the calculations should agree with the G-L theory. We intend to carry out the detailed computations in the near future.

Two further points of interest are mentioned below :

(a) In the above approach the system (superconductor + field) is considered translationally invariant, i.e. there are no spatial dependences either in the electromagnetic response or in the response of the density of states, order parameter and quasiparticle systems.

Thus only the temporal aspect of the response enters and results in current contributions that are either in phase or out of phase with the driving fields at every point in space. This holds true when $\lambda \gg \xi$. In the other limit $\lambda \ll \xi$ space and time effects are mixed in and the situation is much more complicated. A complete non-equilibrium analysis of this case does not yet exist.

(b) Since the static current decreases the absorption, the result is like a "cooling" of the superconductor. From simple thermodynamic considerations, $(\partial S/\partial H)_T = (\partial M/\partial T)_H$ where S is the entropy and M the magnetic moment. Since $(\partial M/\partial T)_H > 0$, $(\partial S/\partial H)_T > 0$ implies that on application of the field, the thermodynamic requirement that the entropy should increase means that the system should respond in such a way as to apparently increase its temperature i.e. "heating". This was just the increase of absorption discussed in Sec.7.

"Cooling" effects then would appear to be in violation of this equilibrium thermodynamic reasoning. The present explanation in terms of dynamic processes yields a novel perspective on this concept. Since $\omega > 1/\tau$ the system does not respond along equilibrium thermodynamic lines. The dynamic "cooling" occurs only because we are examining the response at very short time scales. In non-equilibrium dynamic situations the Maxwell relation used above is not expected to hold and more sophisticated considerations regarding entropy production enter (1,2). It would be interesting to analyse the present situation in terms of irreversible thermodynamics.

Discussion of In film results

Only one film d = 500 Å was studied for which the results for k(t) are:(see Fig.3.15)

$$\frac{\delta R_s}{R_s} = k(t)\, B_0^2$$

$k(t) > 0$ $\quad t > 0.65$

$k(t) < 0$ $\quad t < 0.58$

Thus the results are similar to those of the thinner Sn films except that $0.58 < t_{cr} < 0.60$

With d = 500 Å at t = 0.60 (i.e. $\approx t_{cr}$) clear oscillations were observed with a period of approx. 0.3 G. It was observed that in the temperature region 0.58 - 0.65 the dependence of R_s on B_0 was not monotonic.

We make the following comments :

(1) The results are similar to those for thin Sn films and the interpretation is the same. For high temperature the GL order parameter depression mechanism agrees with the results in sign (+ve), magnitude and temperature-dependence. Better agreement was found with the $\kappa = 0$ limit for which the temperature dependence is $(1 - t^2)^2 (1 - t^4)^{-\frac{1}{2}}$. For very low temperature ($0.4 < t < 0.65$) k(t) is negative. The non-equilibrium effect (eqn.(3.33)) gives the correct sign (- ve) and approx. magnitude.

However an important difference between these results and the Sn results is the reduced temperature called t_{cr} below which $\delta R_s < 0$. For this In film $0.58 < t_{cr} < 0.65$. while for the Sn films $0.88 < t_{cr} < 0.90$. The uncertainty is due the fact that k(t) is very small and the resultant signal is far from quadratic. In fact it is not even monotonic but seems oscillatory. We believe that this is an underlying effect whose understanding is beyond the present analysis.

However from Fig.3.15 it is apparent that the experimental results are significantly below the GL theory at a slightly higher temperature (~ 0.7). It would seem that the -ve effect is present at least up to $t = 0.7$.

Thus it would seem that the non-equilibrium effect is significant in this thin In film for $t \leq 0.7$ while for the thin Sn film it is significant for $t \leq 0.9$. Our analysis of the non-equilibrium effect was restricted to $\Delta >> T$ whereas $\Delta = T$ at $t = 0.9$ and $\Delta = 2T$ at $t = 0.72$. From a preliminary examination it seems unlikely that an extension of the calculations to general temperature would explain this difference (see also next Sec.).

11. Comparison with Previous Experiments on Bulk Superconductors

A number of experimenters have studied the magnetic field dependence of the surface impedance of superconductors over the past 25 years (see G3,J1,R2 for a list of references). For the case of parallel static and microwave fields the results have complicated dependence on frequency, material parameters and crystal orientation. To date no satisfactory explanation has been proposed which accounts for the results. Even the qualitative aspects of the data remain to be explained. (For the case of perpendicular fields the results of Raynes (R2) indicate agreement with the theory).

In making a comparison of the results of this experiment with previous experiments the following notable differences should be borne in mind (see also the discussion at the begginning of this chapter).

(1) The previous experiments were done at high fields ($B_0 \lesssim B_c$) where $\vec{p}_F \cdot \vec{v}_0 \gg \omega$ and even T. Our calculations (S3, see also G3) show that at high fields results could get very complicated and R_s could decrease (Sec.9). Indeed the results of (R2) confirm this. In this experiment $B_0 \sim 10^{-2} B_c$ because of the great sensitivity.

(2) The previous experiments were all on bulk and almost all pure superconductors where the limit is $\lambda / \xi \gg 1$. As we have earlier mentioned this could complicate the analysis considerably. Further the spatial dependence of the fields could cause further complications which are absent in the thin films studied here.

(3) The intrinsic anisotropy of single crystalline bulk specimens would introduce another complication.

Despite these considerably different experimental situations the experiments do fall into a similar class. There are striking qualitative similarities and differences. Quantitative comparisons are harder to make because

(1) the earlier investigators quote $\delta R_s(B_0)$ not k(t)

(2) the quadratic coefficient cannot be inferred from their data because the experiments were unable to measure the absolute value of R_s as we have done in Ch.II.

The main feature of all the experiments is the sign of δR_s and its temperature dependence (i.e. of the sign). Generally δR_s seems to have one sign in one temperature range and the opposite one in another. Thus there exists a reduced temperature at which δR_s is zero (to within experimental uncertainty). We confine our remarks to this crossover temperature and the sign of δR_s.

(1) *The crossover temperature* t_{cr}

A precise definition and measurement of t_{cr} is complicated by two features. In this experiment we are directly examining the quadratic coefficient so that the definition is $k(t_{cr}) = 0$. In the previous experiments only δR_s is quoted and

the definition is $\delta R_s(t_{cr}) = 0$. The other complication arises from the additive nature of the effects that determine δR_s and that these could be differently affected by scattering.

Despite these technical difficulties one interesting feature can be observed concerning t_{cr} between the bulk data and the present thin film results. In the present experiment the results for Sn and In gives :

Sn $0.88 < t_{cr} < 0.90$

In $0.58 < t_{cr} < 0.65$

We note our earlier discussion that for In the actual estimate could be higher if the GL term were accounted for.

Glosser(G2) has given a list of the crossover temperatures observed in bulk by various experimenters. There is a high temperature crossover $t \sim 0.98 \pm 0.1$ which is not of relevance here. Interestingly the low temperature crossover seems to be in either of two narrow ranges 0.85 - 0.91 and 0.68 - 0.70 for a wide range of materials (Sn, Ta, In?), crystal orientation and frequency (1-24 GHz). The similarity between Glosser's and the present results is fairly striking.

At $t = 0.9$ $\Delta = kT$ and it seems reasonable that below this temperature quasiparticle effects would come into their own. It is not apparent why the temperature 0.7 should be significant. We can only note that at $t = 0.72$, $\Delta = 2kT$ but it is not clear whether this has any implications.

(2) *Sign of* δR_s

Having noted the similarity in t_{cr} we now point out a striking difference in the sign of δR_s above and below t_{cr}.

Previous Bulk Experiments

$t > t_{cr}$ (≈ 0.9 or 0.7) $\delta R_s < 0$

$t < t_{cr}$ $\delta R_s > 0$

The sign of δR_s is exactly opposite to the present experiment ! We examine possible reasons for this surprising feature.

(1) The different field configurations : In this experiment the static and high frequency fields are applied on opposite sides of film whereas in bulk they are of necessity on the same side. In other words the *magnetic field* (not

current) *gradients* are exactly opposite in the two cases. Since it is the induced current that is the fundamental quantity this possibility seems unlikely.

(2) The bulk results could be consequences of the high fields used while the present results are at low fields (see earlier discussion). This can only be checked by repeating the bulk experiments with greater sensitivity. In this experiment comparable fields are not reached due to flux entering the thin films (see Sec.3.5 and Ch.IV).

(3) The most plausible reason is the wide difference in the ratio λ/ξ between the present experiment and the bulk experiments. In pure bulk Sn $\lambda/\xi \sim 0.22$ at low temperature while in the present experiment (Table I) λ/ξ varies from 2.28 to 0.89. We see a low temperature decrease of δR_s for $\lambda/\xi > 1$ and for $1 > \lambda/\xi$ $\delta R_s > 0$ for all temperature. In other words the difference in sign could be ascribed to the different values of this ratio .

This receives partial confirmation from the experiments of Richards (R1) on bulk Sn and Sn doped with In. Starting from pure bulk Sn he doped the samples with In in order to reduce the m.f.p. He found that the high temperature ($t > 0.9$) decrease became positive with increasing In concentration. Very interestingly his results for the doped samples are similar to the present results for thicker films with $\lambda/\xi < 1$. (His data still remain unexplained.) From his list of parameters it seems that λ/ξ is always < 1 which could explain why he did not see the low temperature negative sign in this experiment. (Richards has surmised in (R1) that l/λ rather than λ/ξ is the relevant parameter).

This picture is summarized in Fig.3.16 which is a sketch of the qualitative features in all the experiments carried out to date. Curve (a) is for the thinnest films studied in this work for which $\lambda/\xi >> 1$. Curve (b) represents the results for the thicker films ($800\text{Å} \leq d \leq 2000\text{Å}$). This curve is similar to Richards' curve for bulk Sn samples with In concentrations between 0.2% and 1% and seems to be characteristic of samples with $\lambda/\xi \lesssim 1$. Curve (c) is the typical result obtained with pure bulk specimens for which $\lambda/\xi << 1$.

SUMMARY OF COMPARISON BETWEEN PREVIOUS BULK AND PRESENT THIN FILM RESULTS

This analysis implies that δR_s has a temperature dependent sign which reverses *almost* exactly in going from the limit $\lambda/\xi >> 1$ (Type II) to $\lambda/\xi << 1$ (Type I). We use the word almost because t_{cr} seems to have more than one value (in the vicinity of 0.9 and 0.7). For the case $\lambda/\xi >> 1$ we have associated the low temperature negative sign with a non-equilibrium quasiparticle contribution. For the case $\lambda/\xi << 1$ we can only speculate if a contribution of opposite sign arises due to space-time effects associated with the spatial variation of fields.

12. CONCLUSIONS

We have measured the effect of an induced static current on the microwave surface resistance of Sn films. Except for a narrow region of temperature ($0.88 < t < 0.9$) for the thinnest films the surface resistance changes have a quadratic dependence on the current. The quadratic coefficient was measured and compared with calculations using the microscopic theory.

At high temperatures ($t > 0.9$) and for all thicknesses the results can be described by the the effects of the current in modifying the superconductor to a new equilibrium state with new parameters. This new equilibrium state is characterised by a depressed order parameter leading to an increased penetration depth and hence increased R_s (absorption). Calculations of this effect based on the Ginzburg-Landau theory agree in sign (+ve), magnitude and temperature dependence with the experimental results.

For the thinnest films ($d \leq 500\text{Å}$) and at low temperature ($t < 0.9$) the surface resistance was found to *decrease* with applied static current. For this surprising "cooling" effect, we propose a novel explanation in terms of an additional quasiparticle current which is out-of-phase by π with the applied microwave electric field. Estimates of this process based upon the microscopic theory agree in sign (-ve) and approximate magnitude with the experimental results. This is a non-equilibrium effect and has been proposed for the first time in the context of these measurements. The central idea behind this effect is that in the combined presence of both static and high frequency currents the

quasiparticle distribution function counter-oscillates (with respect to the high frequency current) in order to satisfy the requirement that the total quasiparticle number cannot change when $\omega > 1/\tau$. This distribution function counteroscillation leads to the quasiparticle current mentioned above and hence to a decreased R_s.

Further tests of these ideas could be carried out with regard to frequency dependence, material and scattering (i.e. effects of impurities).

For thicker films ($d \geq 800\text{Å}$) the surface resistance was found to *increase* with applied static current *at low temperature* ($t < 0.9$). The experimental results apparently agree with calculations in the "clean" limit ($l >> \xi_0$) even though the material parameters do not satisfy this limit. Despite the fact that $\omega \gg 1/\tau$ still holds, because the current profile is not uniform across the film for thicker films, the non-equilibrium calculation discussed above (last paragraph) is not expected to apply since it assumes uniform currents and local response.

Examination of the material parameters indicates that due to space-time effects the non-equilibrium contribution apparently decreases in importance as the parameter λ/ξ becomes smaller than 1. A comparison with previous bulk results (for which $\lambda/\xi << 1$) indicates that this contribution either changes sign in the limit $\lambda/\xi << 1$ or is counteracted by an additional contribution of opposite sign.

List of Figures Ch.III

Fig.3.6 - $\delta V \propto \delta R_s$ for $t > 0.9$ and large applied field showing effects of induced flux. (a) Applied magnetic field (b) Resulting $-\delta V \propto \delta R_s$ (see Fig.3.7 and Sec.5 for discussion)

Fig.3.7 Proposed explanation of high field effects resulting in induced flux (see Sec.4.3).

(a) Applied "large" magnetic field

(b) Resulting δR_s

(c) Induced current density J in the presence of flux

(d) Magnetic Moment of film

δR_s is varying quadratically with J when J is changing and $\propto |M|$ when M is changing. M is measure of the flux induced in the film.

Fig.3.8 Experimental results for k(t) for thicker ($d \geq 800$Å) films.

Fig.3.9 Experimental results for *absolute value* of k(t) for thinner films ($d \leq 500$Å)

Fig.3.10 Experimental results of k(t,d) for Sn films. Solid lines are the results of calculating $k_{GL}(t,d)$ arising from the order parameter depression by the static current.

Fig.3.11 Influence of scattering on the density of states in the presence of static current

(a) Weak scattering or "clean" case. Note the anisotropy due to the direction of the current.

(b) "Dirty" case. Pair-breaking effects lead to a smearing of the BCS singularity and introduce states in the gap. The anisotropy is almost absent. Dashed curve represents the BCS density of states in the absence of current.

Fig.3.12 Comparison of experimental results for thicker Sn films of k(t,d) with $k_{q-eq}(t,d)$ arising from the increase of quasiparticle number (solid lines)

Fig.3.13 Comparison of experimental results for *abs. value* of k(t,d) for thinner Sn films ($d \leq 500$Å) with $k_{q-ne}(t,d)$ arising from the non-equilibrium contribution discussed in Sec.6). Note that both data and calculation are actually *negative* (for $t < 0.9$). Solid lines represent $k_{GL}(t,d)$.

Fig.3.14 Current and field configurations in the presence of static and high frequency fields. Shown are the non-equilibrium and equilibrium contributions discussed in Ch.III.

Fig.3.15 Experimental results for ***abs. value*** of k(t) for an In film d = 500Å thick. The data for $t \leq 0.58$ are ***negative***. Also shown are k_{GL} (solid line) and k_{q-ne} (dashed-dotted line).

Fig.3.16 Qualitative features of data obtained for bulk (previous experiments) and thin films (present work). We have associated the parameter λ/ξ with the results. The present results have been obtained for $\lambda/\xi >> 1$ (thinnest films, curve (a)) and for $\lambda/\xi \lesssim 1$ (thicker films $d \geq 800$ Å, curve (b)) while the bulk experiments were with pure superconductors with $\lambda/\xi << 1$ (curve(c)). Richards' work with bulk Sn doped with In seems to cover the range $\lambda/\xi \gtrsim 1$ to $>> 1$. His results for the "dirtier" samples $\lambda/\xi \gtrsim 1$ are qualitatively similar to the present results for thicker films ($d \geq 800$Å $\delta R_s > 0$ at all temp.).

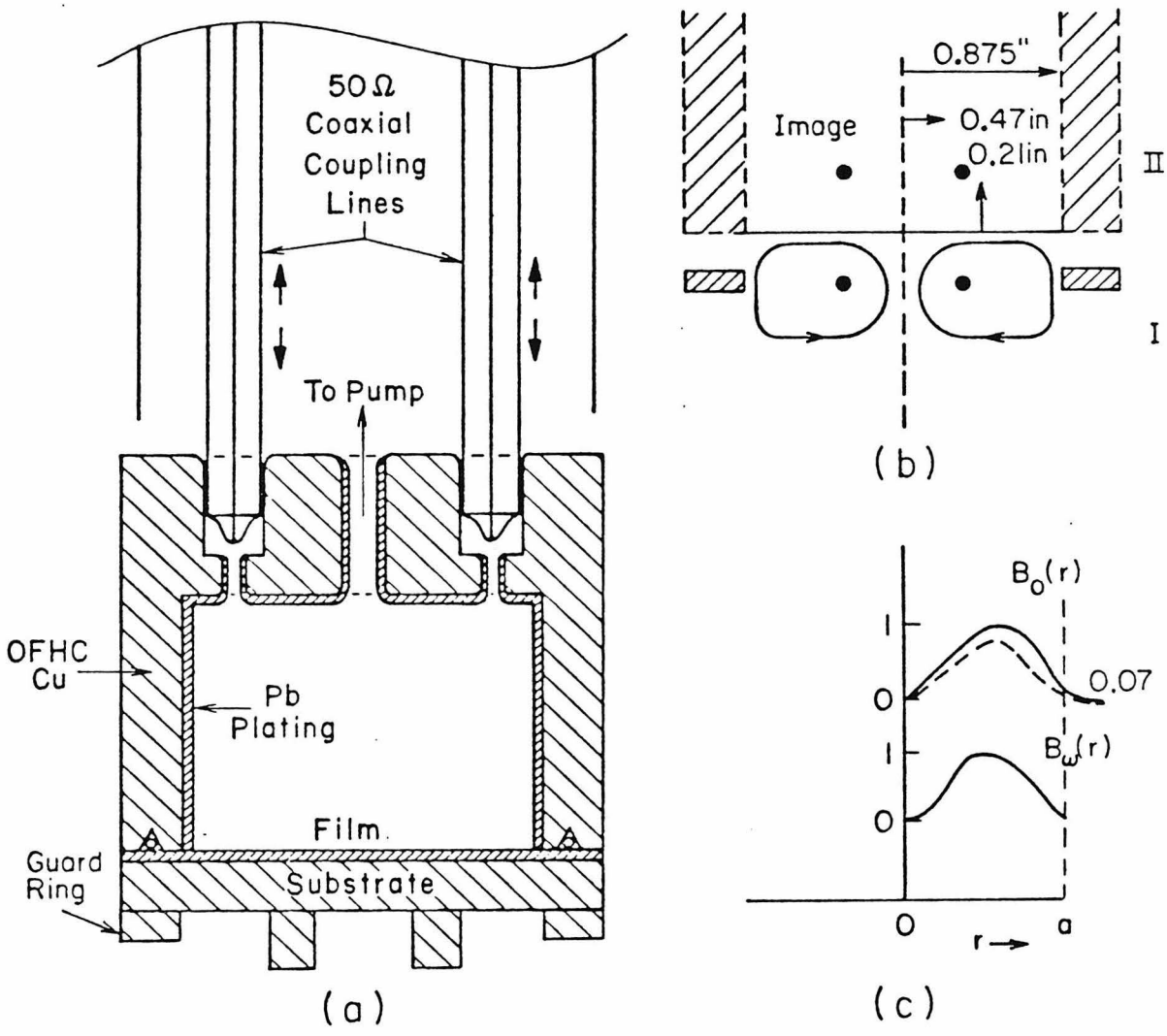
50 Ω
Coaxial
Coupling
Lines
To Pump
OFHC
Cu
Pb
Plating
Film
Guard
Ring
Substrate
(a)
0.875"
Image
0.47in
0.2lin
II
I
(b)
$B_0(r)$
1
0
0.07
1
0
$B_\omega(r)$
0
r
a
(c)

FIG.3.1

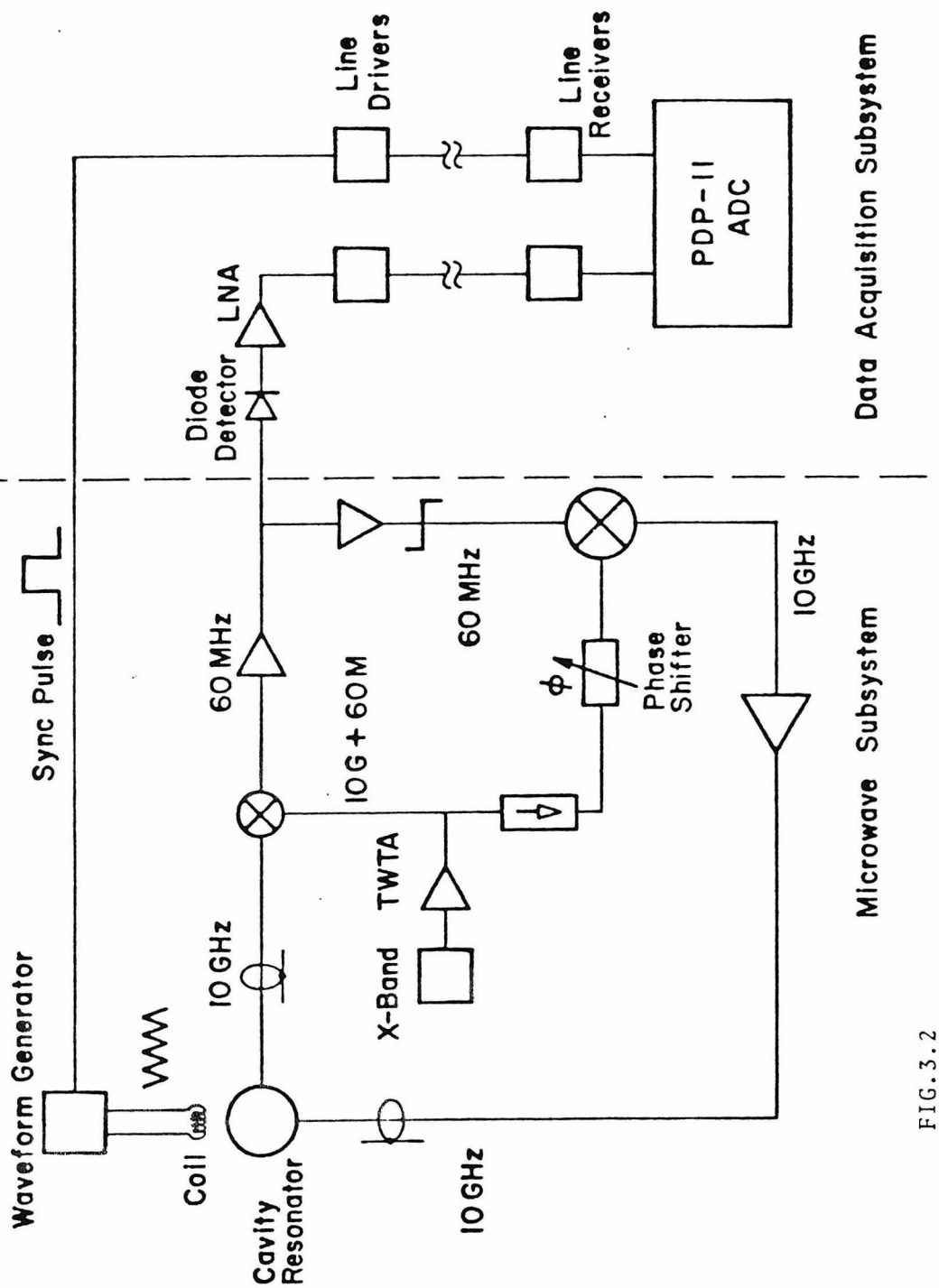

FIG.3.2

Microwave Circuitry and Data Acquisition System used to Measure $\frac{\delta R}{R}$

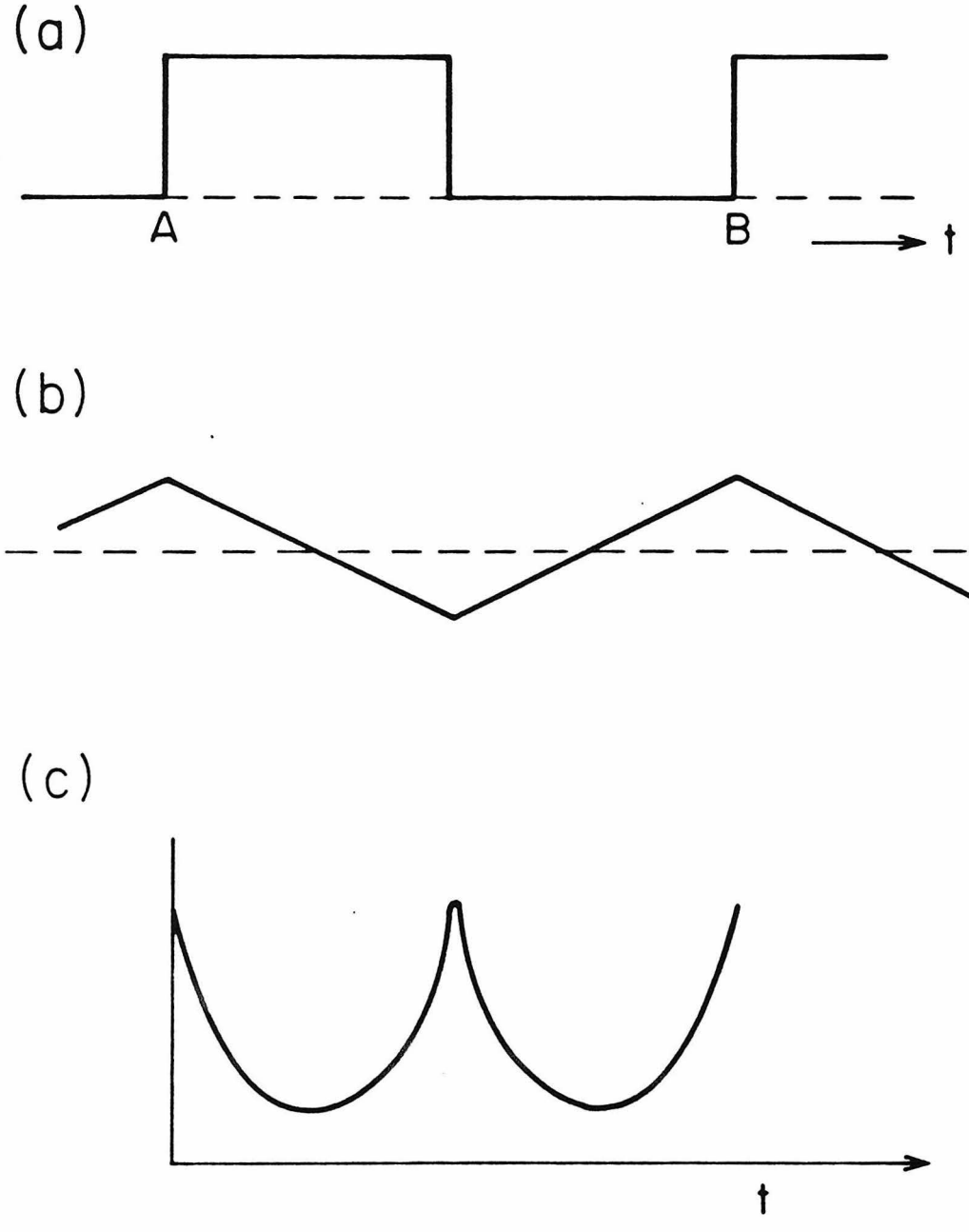

FIG.3.3

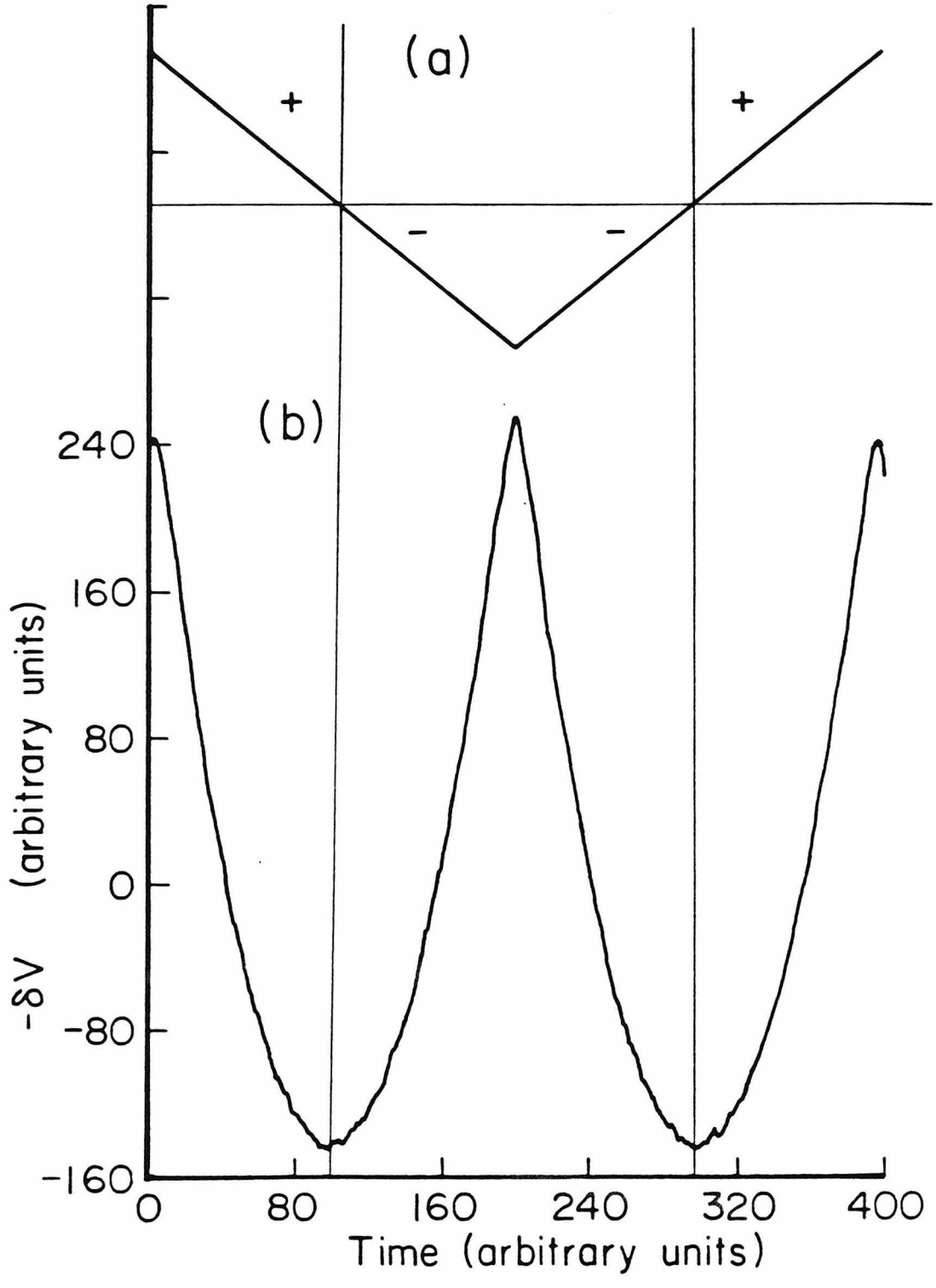
(a)
+
+
-
-
(b)
240
160
80
0
-80
-160
-δV (arbitrary units)
0
80
160
240
320
400
Time (arbitrary units)

FIG.3.4

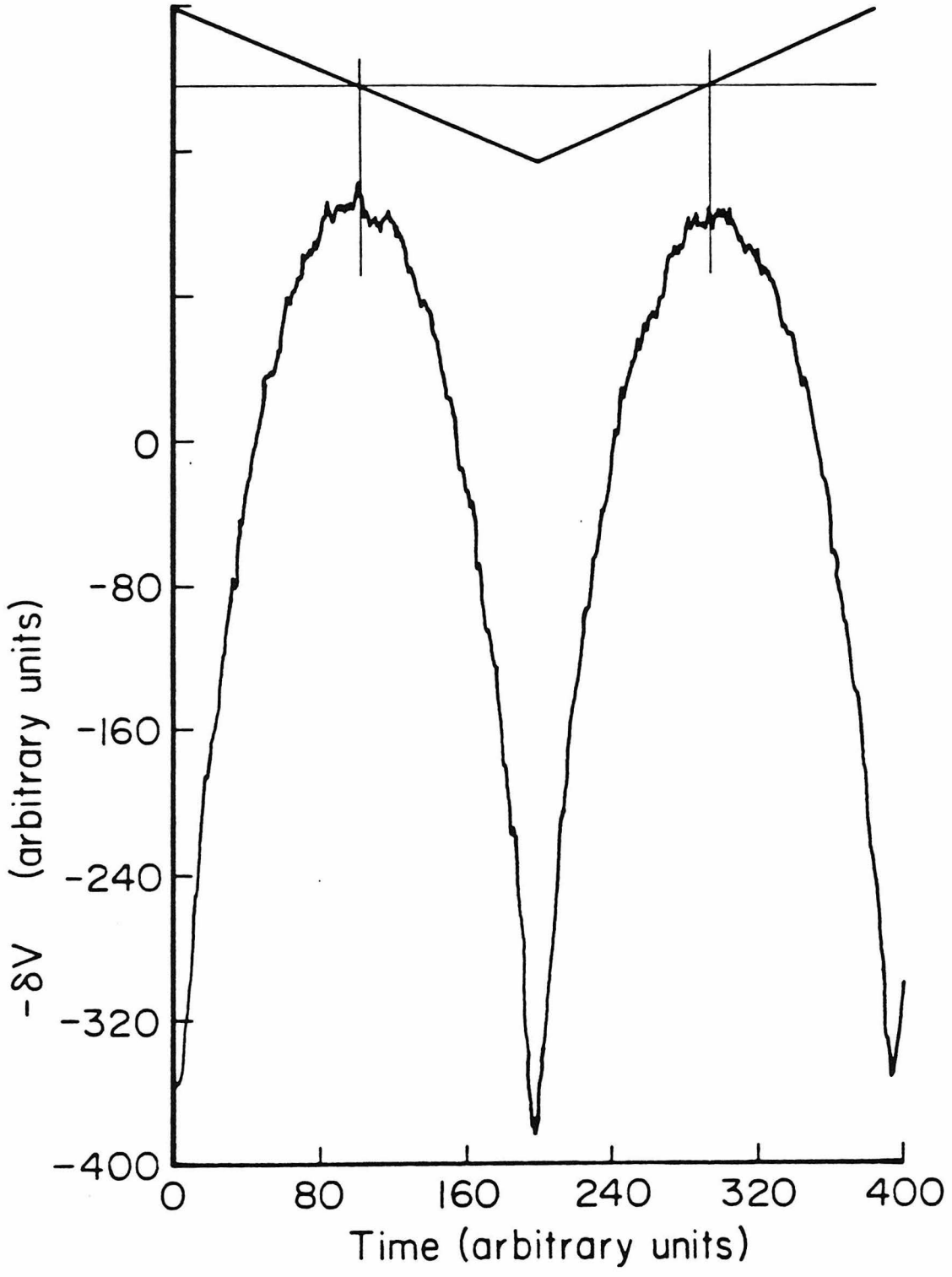
0
-80
-160
-240
-320
-400
-δV (arbitrary units)
0
80
160
240
320
400
Time (arbitrary units)

FIG.3.5

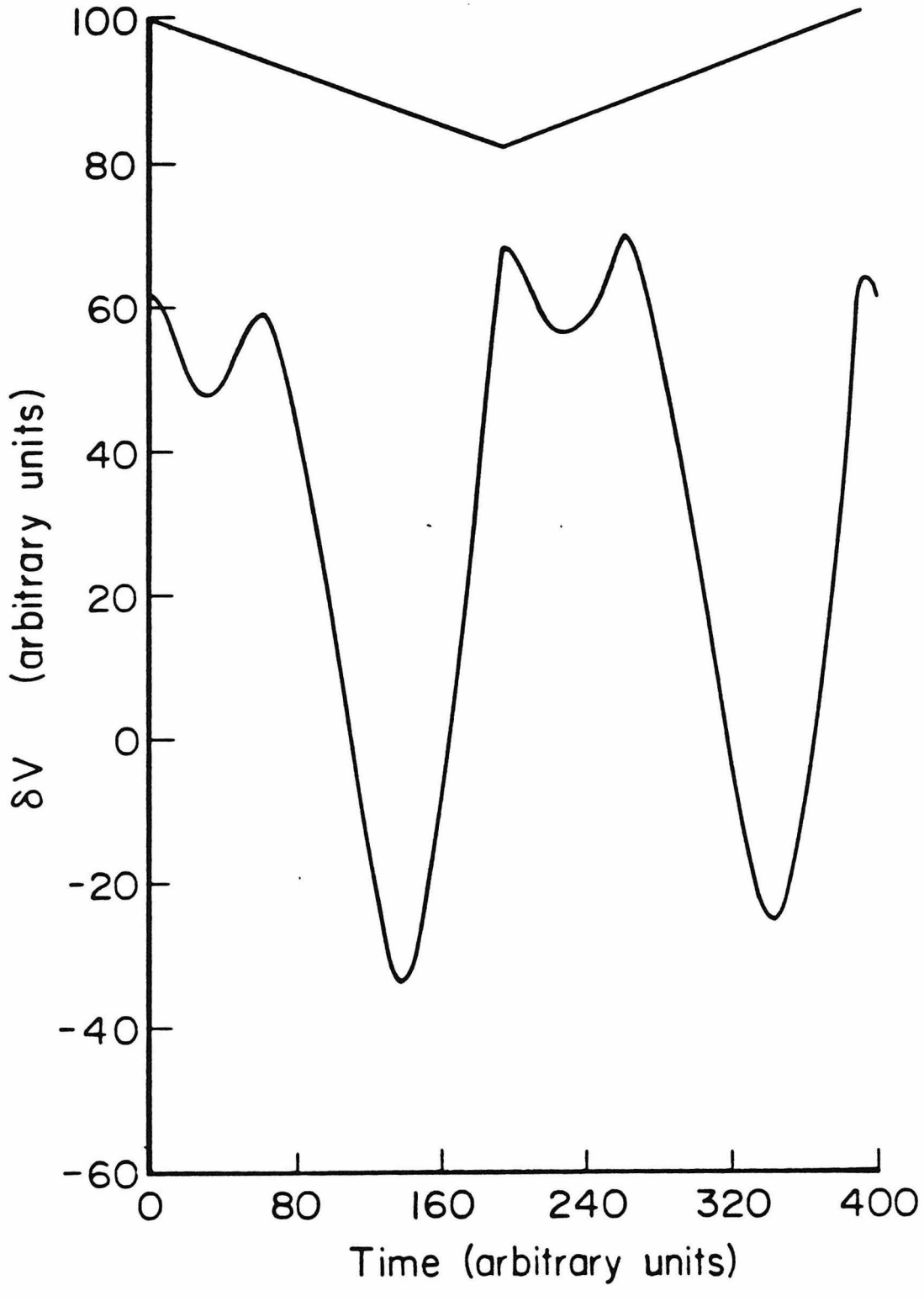
100
80
60
40
20
0
-20
-40
-60
δV (arbitrary units)
0
80
160
240
320
400
Time (arbitrary units)

FIG.3.6

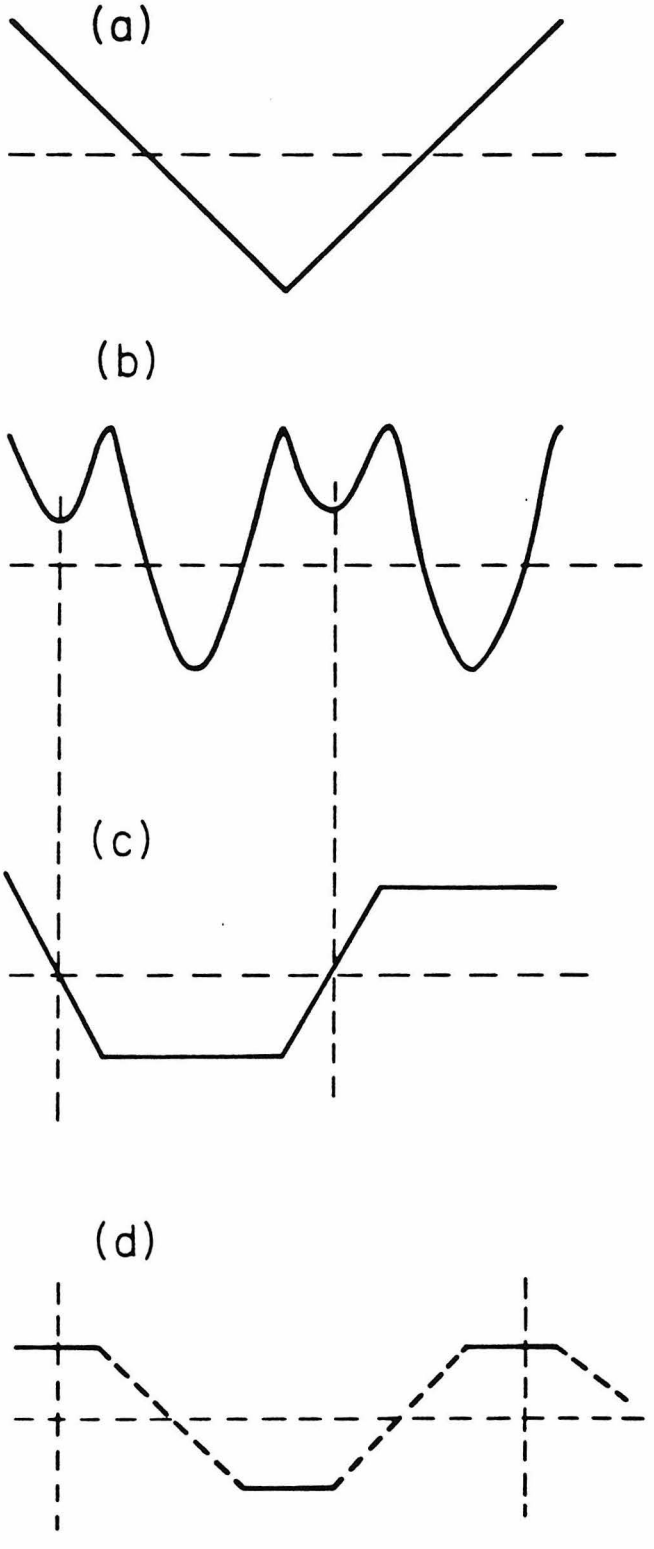

FIG.3.7

FIG.3.8 THICKER SN FILMS

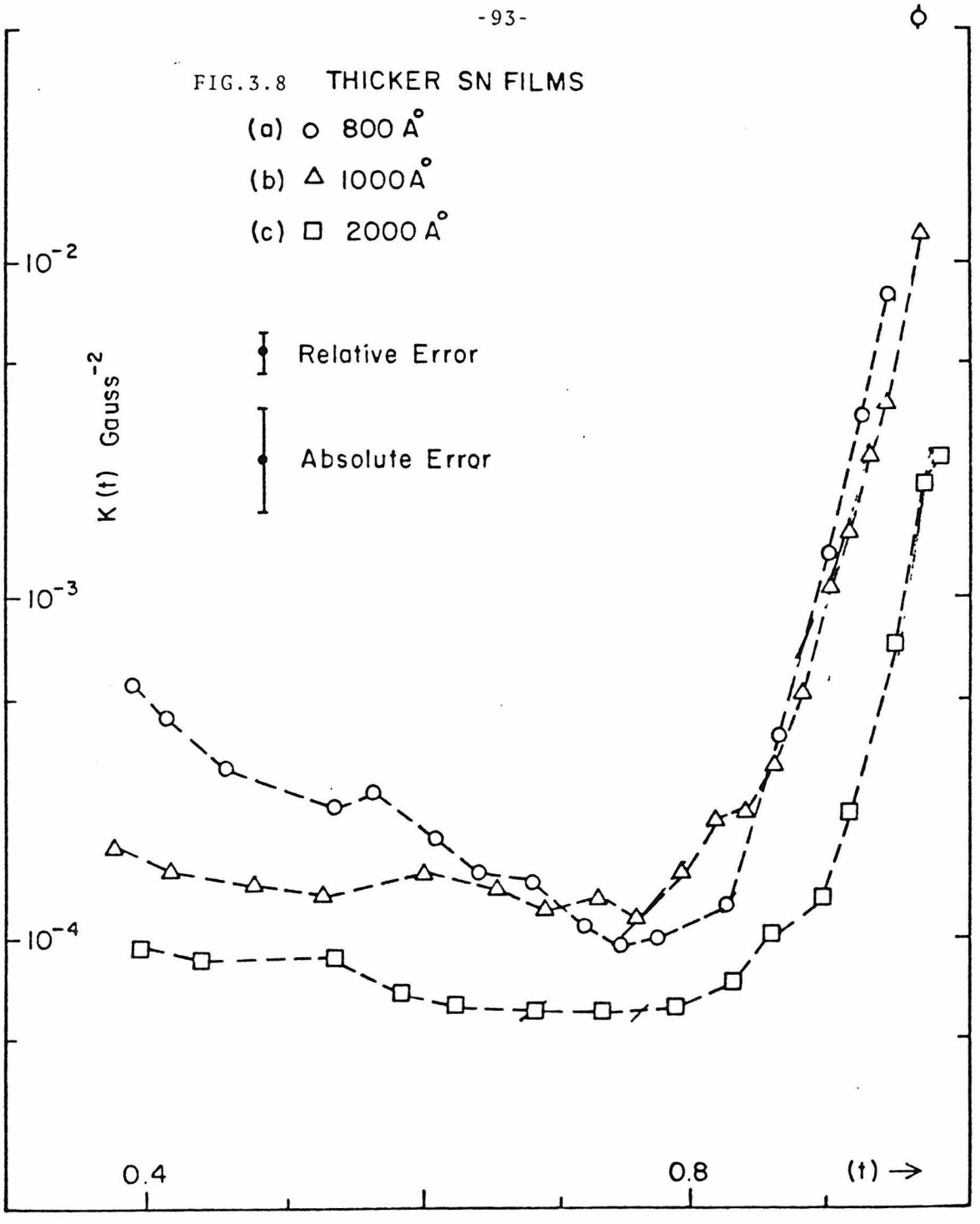

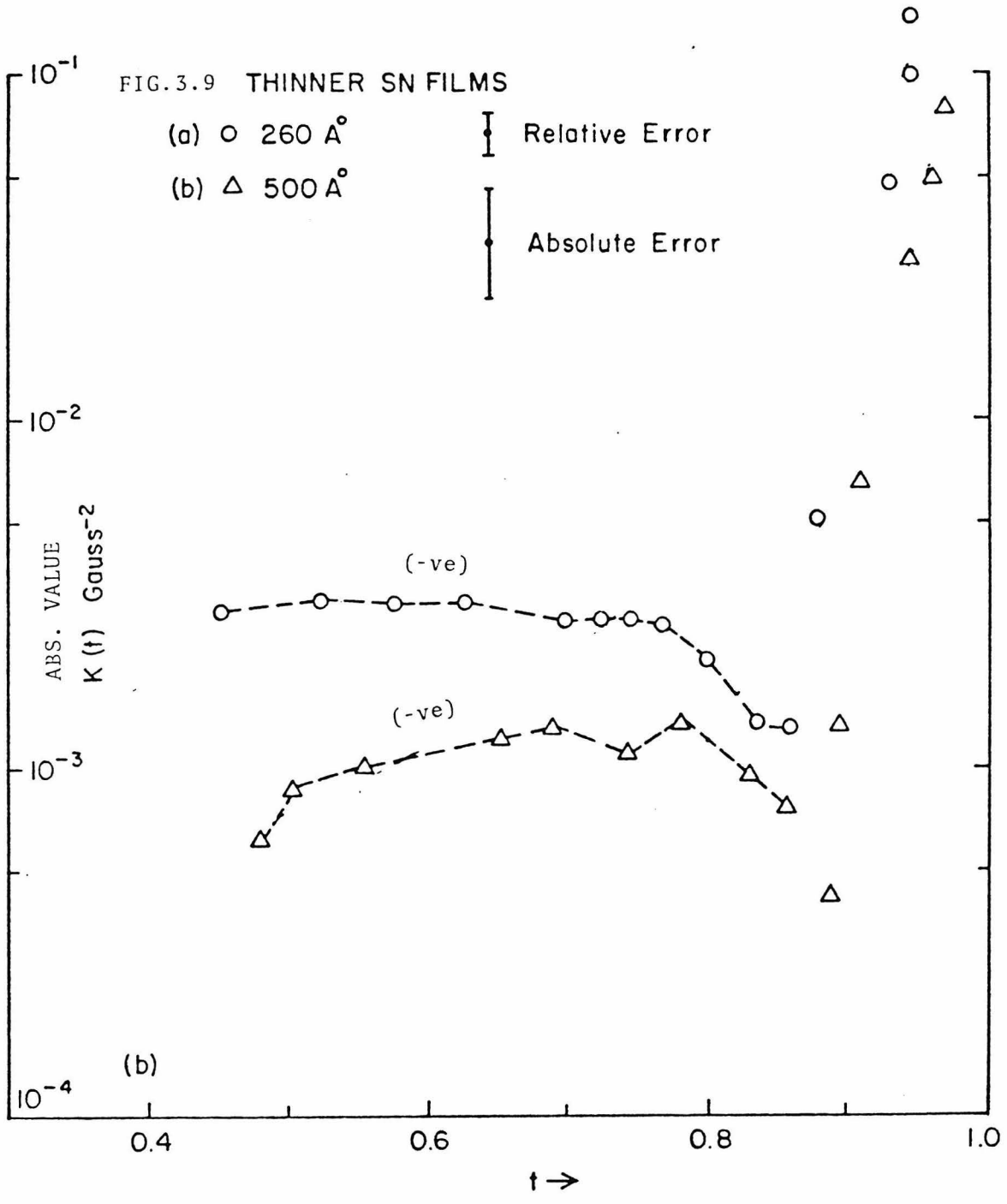
FIG. 3.9 THINNER SN FILMS
(a) ○ 260 Å°
(b) △ 500 Å°
Relative Error
Absolute Error
ABS. VALUE K (t) Gauss^{-2}
(-ve)
(-ve)
(b)
10^{-1}
10^{-2}
10^{-3}
10^{-4}
0.4
0.6
0.8
1.0
t →

FIG.3.10 THICKER SN FILMS

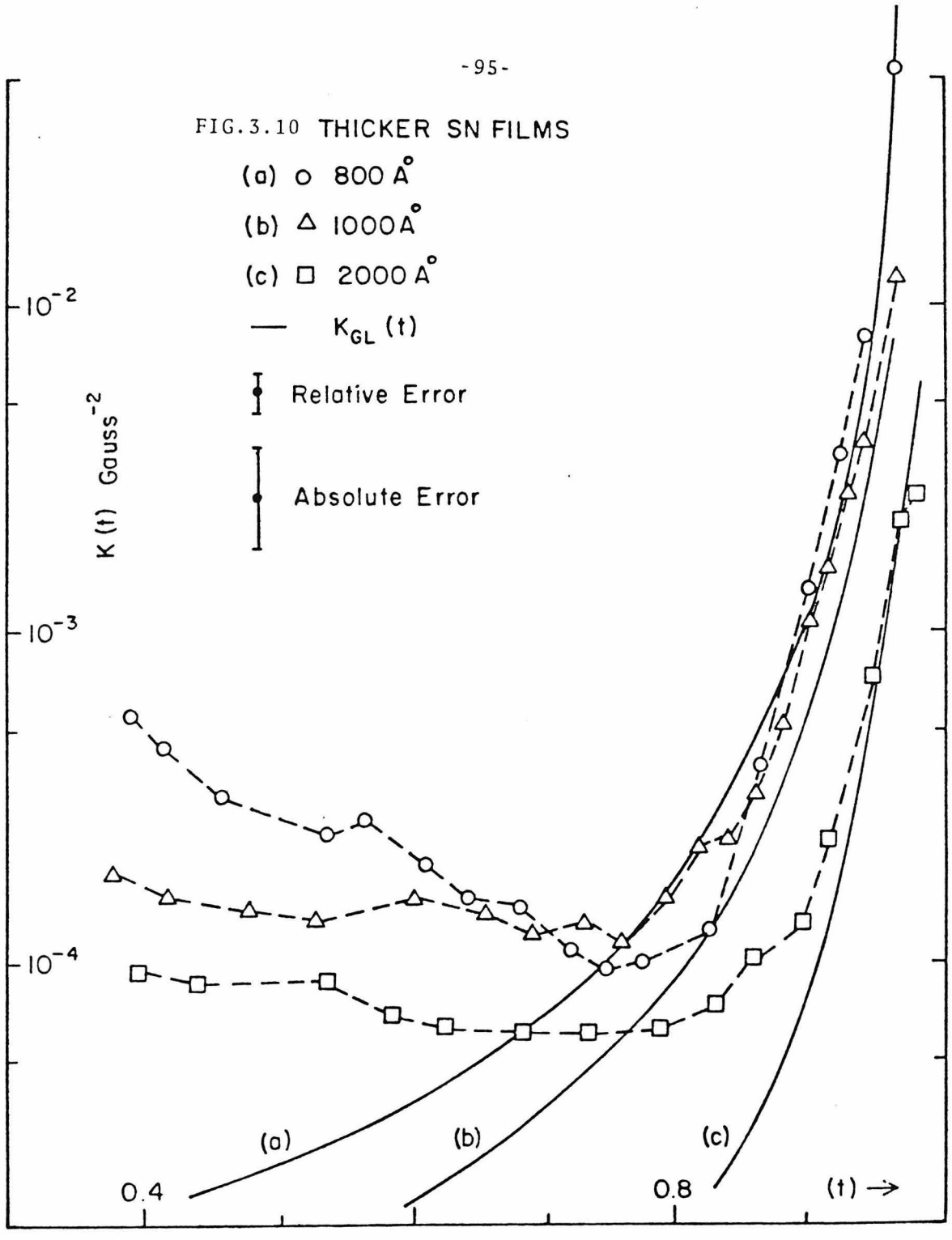

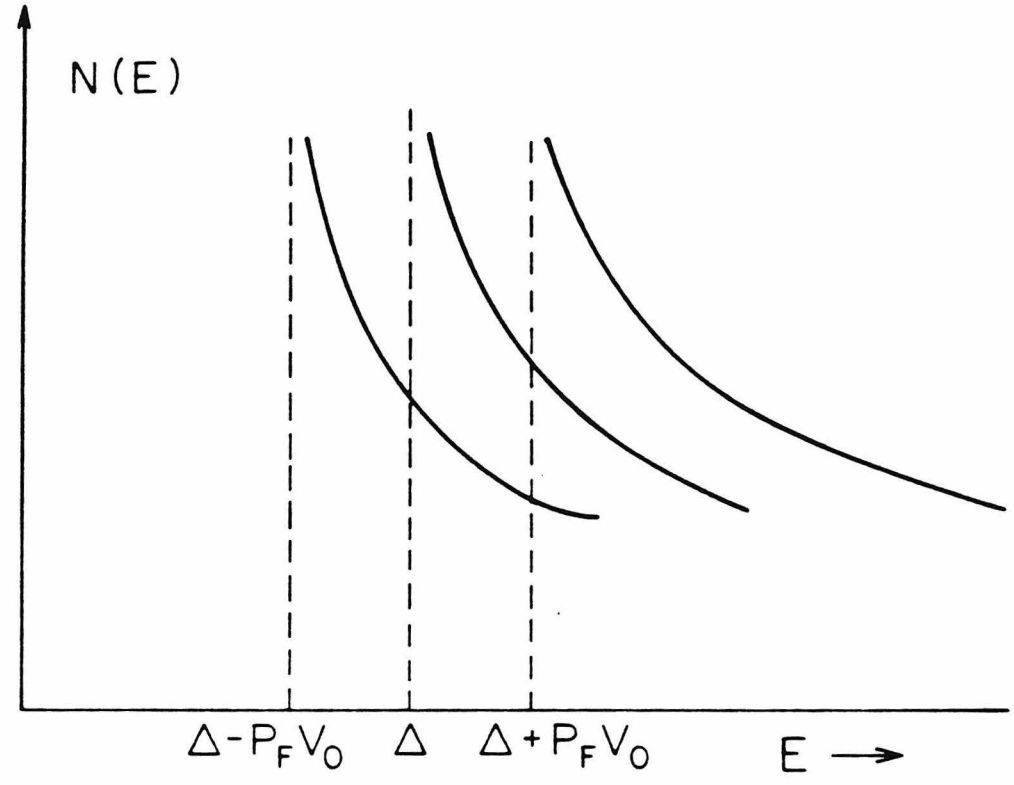

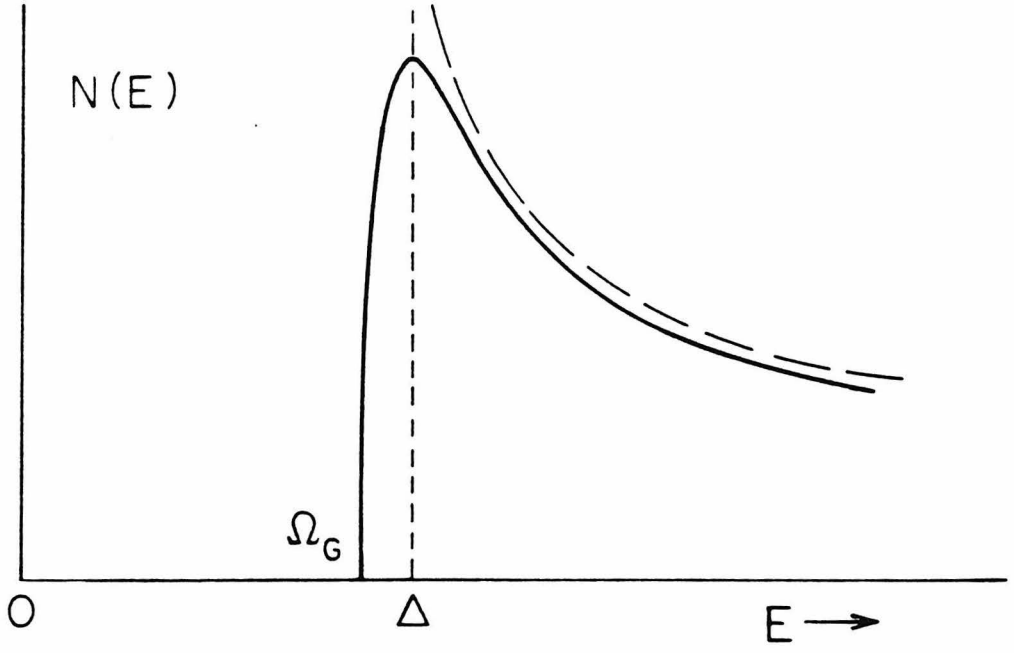

FIg.3.11

FIG.3.12 THICKER SN FILMS

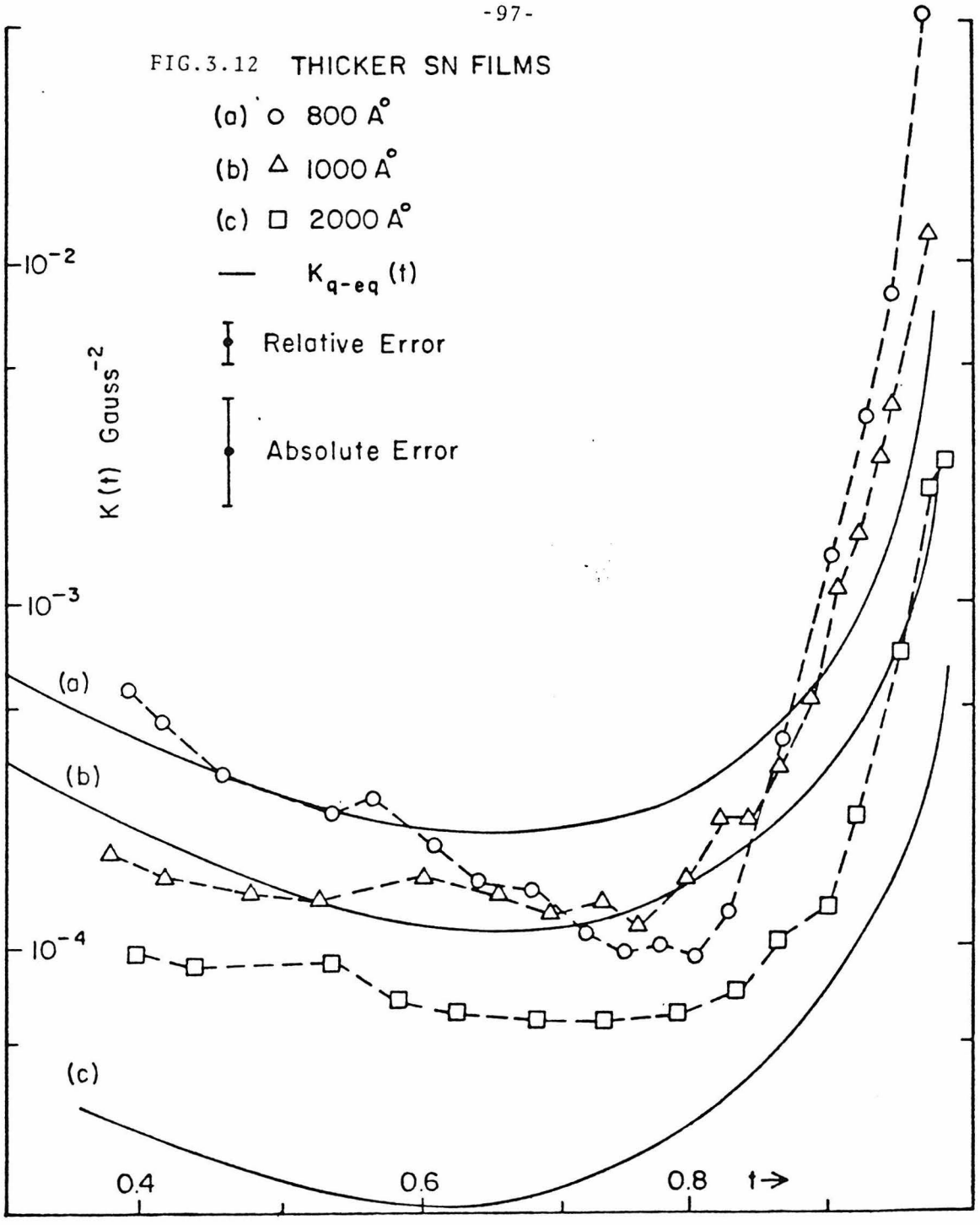

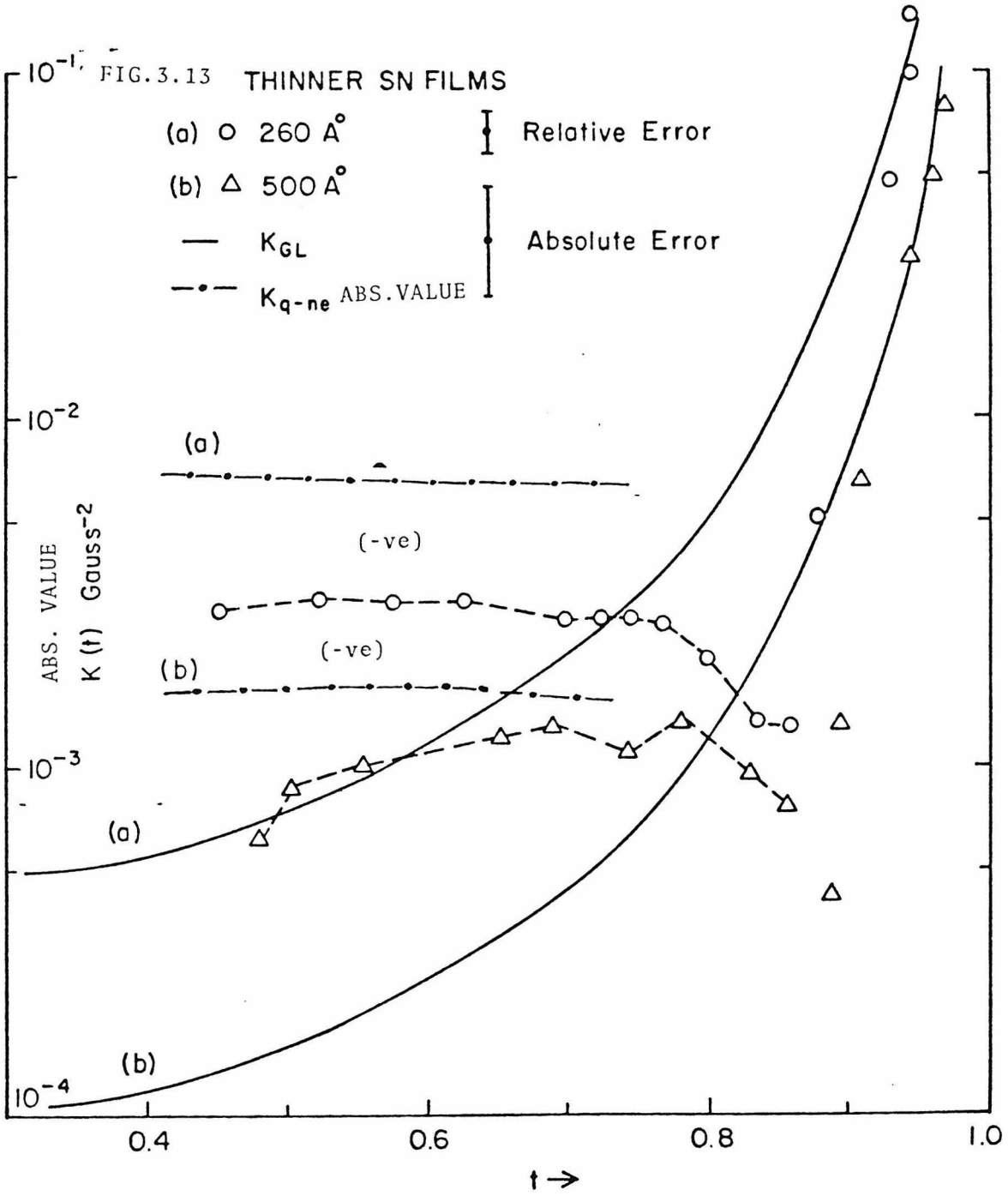
FIG.3.13 THINNER SN FILMS
(a) O 260 A°
(b) Δ 500 A°
Relative Error
Absolute Error
K_{GL}
K_{q-ne} ABS.VALUE
10^{-1}
10^{-2}
10^{-3}
10^{-4}
ABS. VALUE K (t) Gauss^{-2}
(a)
(b)
(-ve)
(-ve)
0.4
0.6
0.8
1.0
t →

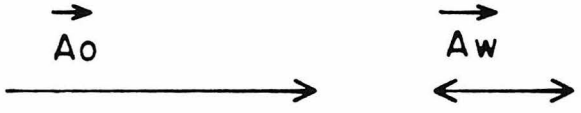

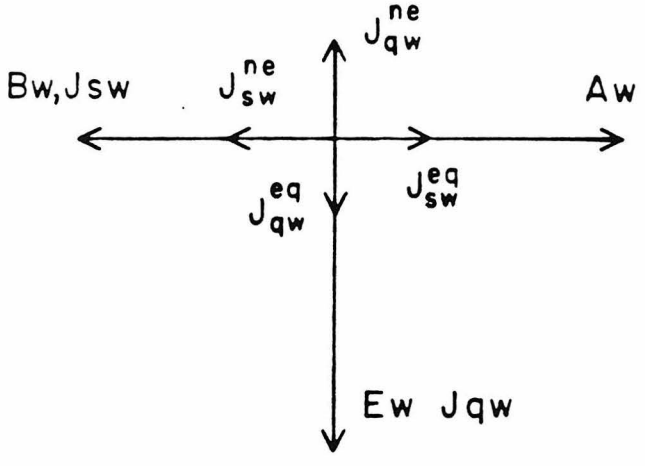

FIG.3.14

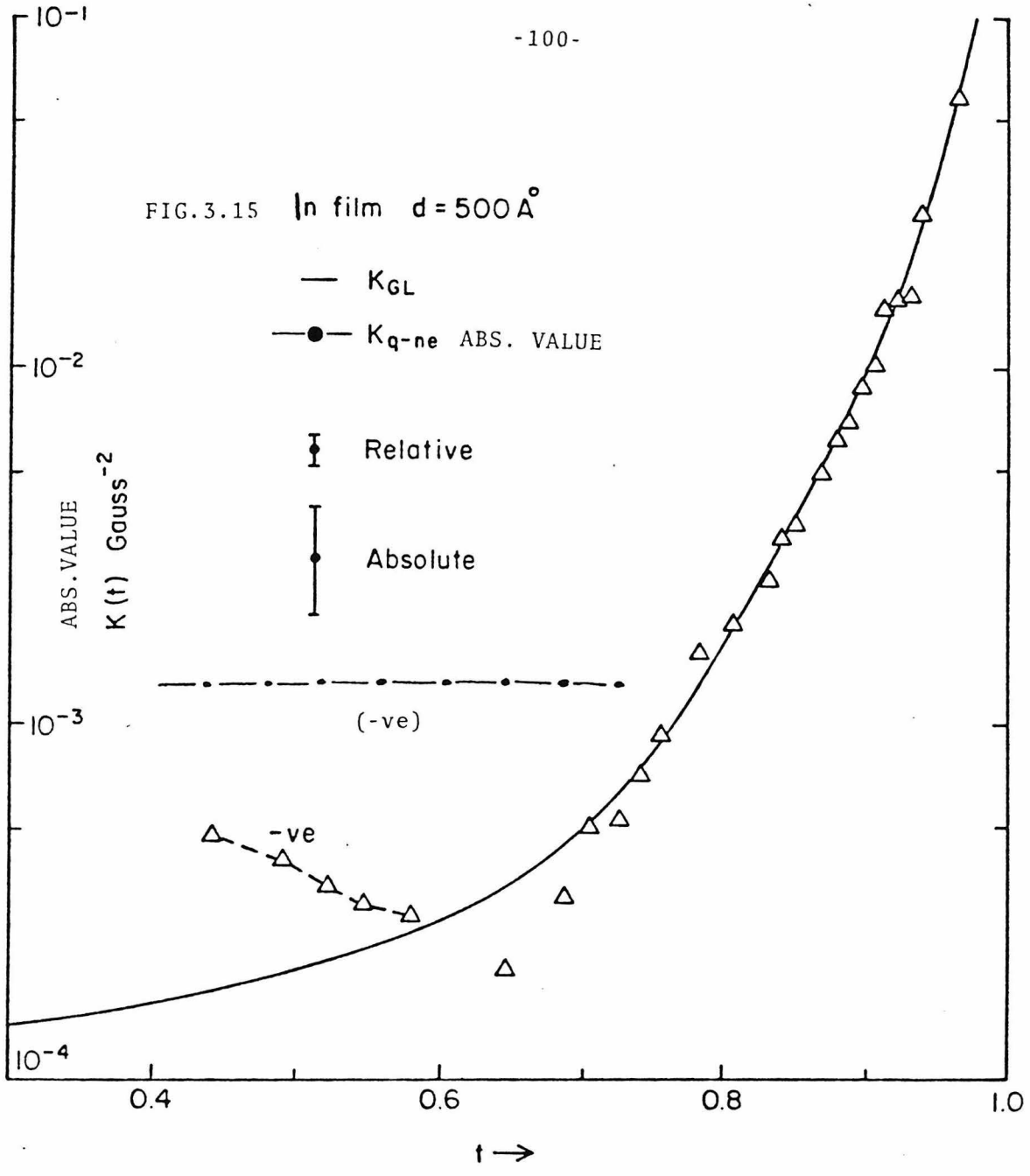
10⁻¹
10⁻²
10⁻³
10⁻⁴
0.4
0.6
0.8
1.0
t →
ABS. VALUE
K(t) Gauss⁻²
In film d = 500 Å°
K_GL
K_q-ne ABS. VALUE
Relative
Absolute
(-ve)
-ve

FIG.3.15

FIG.3.16

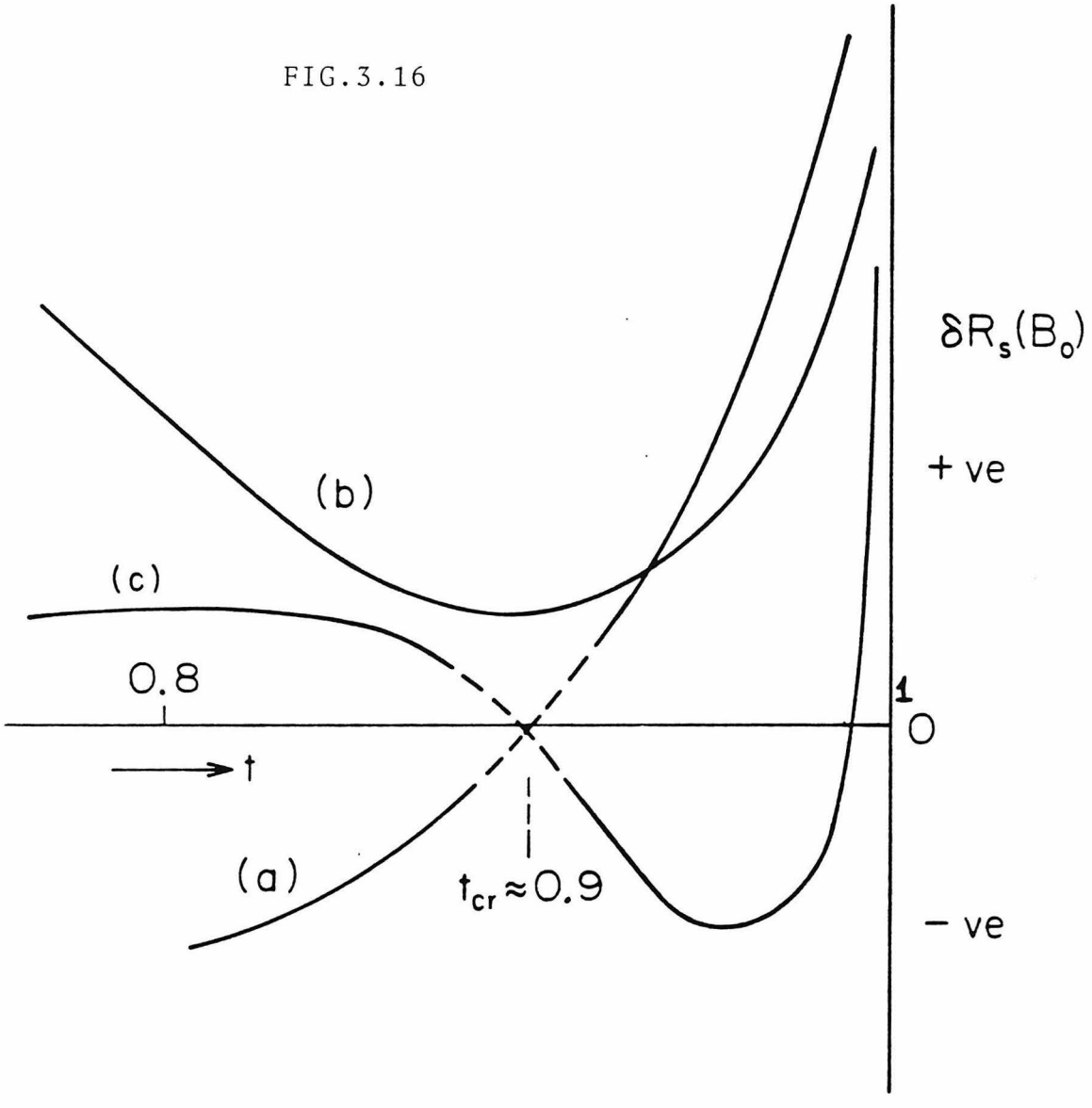

TABLE 3.1 Material Characteristics of Sn Films studied in $\delta R_s(B_c)$ experiment

Thickness	m.f.p.[a]	Pen.depth[b]	d/λ	l/λ	coh.length	λ/ξ
d (Å)	l (Å)	λ (Å)			ξ(Å)	
260	240	1460	0.18	0.16	640	2.28
500	300	1326	0.38	0.23	714	1.86
800	450	1122	0.71	0.40	875	1.28
1000	510	1069	0.94	0.48	931	1.15
2000	680	960	2.1	0.71	1075	0.89

(a) Measured from the normal state surface resistance R_n (see Ch.II)

(b) $\lambda = \lambda_p(0)\,(1 + \xi_0/1.33\,l)^{1/2}$, $\lambda_p(0) = 510$Å, $\xi_0 = 2300$Å

(c) $\xi = 0.85\,(\xi_0\,l)^{1/2}$

Ch.IV High Frequency Critical Fields of Thin Superconducting Films

When a transport measurement is carried out on a system by measuring its response to an external perturbation, the response is usually linear for small values of the perturbations. For larger values the results of the measurement often depend on the magnitude of the applied perturbation fields. In this chapter we discuss the results of analysing such a situation experimentally and theoretically in superconducting films when microwaves are used to measure the impedance of the film and the results are expected to be dependent on the microwave field strength.

The concept of the experiment that is analysed here is that the film forming part of a resonator is irradiated by microwaves at the cavity resonant frequency (10.12 GHz). The film surface resistance R_s can be measured from the cavity Q. There is no static current flowing in the film (Ch.III discusses such a case). The experimental configuration is identical to that of Ch.II.

In Ch.II results were reported for these quantities when the microwave surface field was low and the film impedance was *independent of the microwave field strength*. The measured quantities were characteristic of the equilibrium state since the perturbing fields were low. As discussed in Ch.II, the experimentally measured surface impedance agreed with the thin film BCS calculated values with no adjustable parameters. This result means that the films studied were well characterised in their equilibrium state . This provides a firm baseline for the high-field results reported in this chapter.

As the applied microwave field strength B_ω is raised, we might expect that the measured quantities R_s and X_s would depend on B_ω. Here the film itself is modified by the perturbation and the situation corresponds to the nonequilibrium steady state (Ch.I, Sec.2 and Fig.1.1 region II).The superconductor-microwave interaction is now nonlinear. The purpose of the work reported in this chapter is to examine this nonlinear interaction.

A quantitative consideration of this interaction requires the absolute specification of the microwave surface magnetic field B_ω or the power P_{abs} absorbed in the film. In this experiment we exploit the precise geometry of the microwave resonator; because of this geometry the microwave-film coupling is well defined. This enables us to specify B_ω and P_{abs} in absolute units. The change of the resonator Q as B_ω is raised yields information regarding the dependence of R_s on B_ω or P_{abs}.

Experimentally, an unexpected phenomenon was observed as the microwave magnetic field B_ω incident on thin Sn films was raised by increasing the power incident to the resonator. The resonator Q did not change, to within experimental accuracy, until a field $B_\omega = B_{\omega c}(t,d)$, which was well below the thermodynamic critical field for a thin film, was reached. When the incident power was raised further, the film reacted to prevent the surface field from increasing further. The resonator Q decreased steeply and the power absorbed increased - both happening in such a way as to keep the field constant.

This abrupt onset of increased absorption is indicative of a critical phenomenon and requires concepts beyond those discussed thus far in this thesis. Hitherto the perturbations of the BCS state were homogeneous and the resulting perturbed state was considered stable. Here in examining this dynamic (high frequency) phenomenon we find that we have to go a bit further and include the notions of inhomogeneity and instability.

The observed critical phenomenon of increased absorption was shown experimentally to be associated with the increased penetration of applied field by measuring the transmitted power (as described in Ch.II.). A new mechanism is proposed for such a penetration via the formation of a vortex-anti vortex pair (S9). An equilibrium energy balance shows that this formation can occur at fields B_v well below the thermodynamic critical field. The observed values of $B_{\omega c}$ are smaller than the calculated values B_v, indicating that the equilibrium considerations for the pair formation may be inadequate due to the finite frequency of the applied field. Experimentally we have demonstrated that the thinner films ($d < 1000\text{Å}$) are definitely thermally stable while the results for thicker films indicate that due to larger powers involved thermal effects cannot be ignored.

1. Principles and procedures of measurement of $Q(B_{max})$

The basic principle of the measurement of impedance as a function of B_ω are as follows :

The experimental configuration was identical to that of Ch.II. At low incident power the resonator Q was measured (Ch.II) and verified to be independent of incident power.

The maximum surface magnetic field B_{max} (which occurs on a circle of radius 0.411 in) and the power absorbed P_{abs} were calibrated as described in the next section. The incident power was raised thus increasing B_ω and P_{abs}. The instantaneous Q was measured and from it the instantaneous R_s could in principle be determined. Below we describe the principle and procedures of the measurement.

For the TE_{011} mode (see Fig.1.1), the microwave magnetic field B_ω at the bottom plate,has a Bessel function $J_0(r)$ dependence on the radial distance outward from the center (H5,J2). The maximum field B_{max} is reached at 0.411 ins from the center. Note that there are no normal electric fields at the superconductor surface - a situation which was deliberately chosen in order to minimise possible dielectric losses.

The absolute magnitude of B_{max} can be determined from the relation for the TE_{011} mode :

$$B_{max} = 8.95 \times 10^{-3} \ (Q_0 \, P_{abs})^{1/2} \text{ Gauss} \qquad (4.1)$$

where Q_0 is the unloaded Q of the resonator and P_{abs} is the power absorbed in watts.

The experimental procedure used to measure B_{max} and Q as a function of B_{max} is described below.

1.1. Measurement of B_{max}

(1) The intrinsic unloaded Q of the resonator Q_0 was measured first under the condition of weak coupling of both input probes as described in Ch.II. Q_0 was verified to be independent of probe position and input power.

(2) The pickup probe was kept fixed at the same position, say h_0. The input or drive probe was then moved towards stronger coupling until it was critically coupled. Critical coupling (Ch.II) was verified by observing the point at which the reflected power reduced to zero. Since spurious reflection could give a wrong indication of critical coupling it was necessary to cross check. At critical coupling the loaded Q must be $Q_{c/c} = Q_0/2$. This was verified to within 10%, demonstrating that there were no spurious reflections.

(3) At critical coupling, all the power incident at the cavity is absorbed, i.e. $P_i = P_{abs}$. P_i was measured by sampling the incident power using a directional coupler with a coupling of 22 db. The sampled power was measured with a power meter to an accuracy of 5%. Since there was some attenuation due to the remainder of the system from the sampled port of the directional coupler to the cavity input, this had to be accounted for. Including the losses of the coupler (0.5db) and the coax line(2.5db), this attenuation amounted to 3 db.

Q_0 and P_{abs} being thus determined, B_{max} was calculated from eq.(4.5).

(4) Since the output port was weakly coupled, the heterodyned signal at steady state $S_{o/p} = \alpha P_{o/p} = \beta\alpha k_{o/p} B_{max}^2$, where α is the constant of proportionality asssociated with the heterodyning system and $k_{o/p}$ is determined by the coupling and mode geometry. β is the attenuation introduced by the attenuator included before the heterodyning system (see Fig.1.3). If the output probe is kept fixed, the coupling, and hence $k_{o/p}$, is uniquely determined. Thus $S_{o/p} \propto B_{max}^2$ independent of Q_0 , P_{abs} or the coupling of the input probe. This means that once B_{max} was determined by procedures (1) to (3), $S_{o/p}$ was directly calibrated in Gauss. Changes in B_{max} caused by changing Q_0 , P_{abs} or P_{inc} could be monitored through $S_{o/p}$.

Since the heterodyning system was susceptible to possible nonlinearities (i.e. α dependent on $P_{o/p}$), a slight modification of the above technique was employed. $S_{o/p}$ was always kept fixed at 60 mv. p-p and changes in B_{max} were determined by changing β, since $B_{max} = (k_{o/p}\alpha S_{o/p})^{1/2} \frac{1}{\beta^{1/2}}$. The attenuator was found to be linear to 5% over a wide range of powers. Nonlinearities in the heterodyning system were thus eliminated once the power input to the system was kept fixed.

1.2. Measurement of $Q(B_{max})$

The intrinsic unloaded Q called Q_0 of a resonator whose energy content is U is a measure of the rate of energy decay in the resonator :(see Ch.II)

$$\frac{1}{Q_0} = -\frac{1}{\omega U}\frac{dU}{dt} \tag{4.2}$$

If Q_0 is independent of U (and hence B_ω), this leads to the well known exponential decay $U = U_0\exp(-t/\tau)$, where $\tau = Q_0/\omega$ is the time constant for energy decay. Determining τ then yields Q_0 as was done in Ch.II.

When Q_0 is dependent on B_ω, then we assume that eqn.(4.2) is still valid instantaneously and we use it to determine Q_0 from the energy decay envelope. The time constant $\tau(B_\omega)$ was determined from the scope display of the energy content as obtained by heterodyning the pick-up probe output. Under conditions of weak coupling,

$$\frac{1}{\tau(B_{max})} = \frac{1}{S_{o/p}}\frac{dS_{o/p}}{dt} \tag{4.3}$$

$$Q_0(B_{max}) = \pi f \tau (B_{max}) \tag{4.4}$$

The determination of the field dependence of R_s from the measured Q is not straightforward because of the spatial variation of the field for the given mode configuration. A quantitative determination requires an assumption of the dependence computation of the resultant Q values and then comparison with the measured results. We do not go into the details of the procedure here since for the discussion that follows it is not of importance.

In accordance with the procedures described in the last section, B_{max} was first measured and $S_{o/p}$ correspondingly determined. From the scope display, the decay time was also measured and $Q(B_{max})$ determined. For low levels of B_{max}, it was verified that Q_0 was independent of B_{max} and equal to the intrinsic unloaded Q of the resonator.

B_{max} was then increased by increasing the incident power. $S_{o/p}$ was kept fixed by changing the attenuation β - the new value of β being used to determine the new B_{max}. The logarithmic decay rate $\tau(B_{max})$ was measured from the scope.

It is sufficient to measure the decay rate just when the incident pulse is switched off (t = 0) as this gives the decay rate at B_{max}. By changing B_{max} and repeating the entire procedure $\tau(B_{max})$ and hence $Q(B_{max})$ was determined.

We estimate that the errors in determining B_{max} amount to ±25 % while the errors in Q are ± 1%.

2. Results for $Q(B_{max})$

Measurements of the resonator Q as a function of B_{max} were carried out for all the samples described in CH.II. The experimental configuration of the sample was identical to that in the low field experiments - the sample formed the entire bottom plate while the remainder of the resonator was Pb plated onto Cu.

(a) Full Pb/Cu resonator

First it was necessary to establish to what extent the presence of the Pb/Cu part would contribute to the results. In order to test this, an experiment was carried out with the bottom plate also 5μ Pb plated on Cu.

In Fig.4.1. typical results for 1/Q vs. B_{max} are displayed at T = 1.5 K. The resonator Q was field independent until approximately 80 G and decreased by a factor of approx. 3 at the highest field (which was 260 Gauss) reached with the maximum power available. Furthermore, as pointed out in Ch.II the contribution of the Pb part to the surface resistance was always well below 5%. Since the results on the Sn samples (to be presented next) showed field dependent effects at fields well below 20 Gauss we conclude that the Pb plated part of the resonator did not contribute to the results for Sn.

(b) Sn/Sapphire results

Fig.4.2 presents typical results for the Q of a resonator when the bottom plate consisted of the Sn films deposited on Sapphire discussed in Ch.II. $Q(B_{max} \rightarrow 0)$ corresponds excellently with the value expected from the BCS theory incorporating thin film electrodynamics.

Consider the results for the thinnest film with d = 190 Å at T = 1.5 K. As the surface magnetic field B_{max} was raised by increasing the power, the resonator Q was *unchanged* to within the experimental accuracy (5%) until a field of 1.4 (±

0.35) Gauss was reached. Upon raising the input power further the Q began to decrease rapidly; however, it was found that the magnetic field could not be raised further. Thus there exists a threshold field which we call $B_{\omega c}$ above which the surface magnetic field cannot be raised. Further increase of input power decreases the Q keeping the product $QP_{abs} \propto B_{\omega c}^2$ constant and hence the field is kept constant at $B_{max} = B_{\omega c}$. Corresponding to $B_{\omega c}$ there exists a critical threshold power which we call P_c.

These results indicate that for $B_{max} < B_{\omega c}$ the film could be described in terms of a uniform BCS superconductor. When $B_{max} = B_{\omega c}$ (and $P_{abs} = P_c$), a new process seems to turn on which makes such a description invalid. The superconductor responds to further increases in incident power by maintaining a constant surface magnetic field B_{ons}. This forces the resonator to follow the load line determined by QP_{abs}= const.

As Fig.4.2 shows these features are true for all thicknesses that were studied, though for the thicker films there was a slight decrease in Q before $B_{\omega c}$ was reached. This decrease may be attributed to a small increase in temperature which became important for thick films where the values of P_c were fairly large.

To summarize the results - there exists a threshold field $B_{\omega c}$ (T,d) (and correspondingly a threshold power P_c(T,d)) which demarcates two different types of behaviour. Above the threshold values the film responds quite unlike a uniform BCS superconductor. As discussed later it was found that the measured values of $B_{\omega c}$ were well below the thermodynamic critical field at which superconductivity is destroyed. It was decided to explore why this apparently critical behaviour appeared unexpectedly at such low fields.

2.1. Comparison of theory and experiment for Sn films

We briefly compare the experimental results with the analysis which predicts that R_s should decrease with increasing microwave field. The details of the analysis are not discussed here (we refer to S2) but only the final results.

The parameter A that describes the perturbing effect of the microwaves on the distribution function determines the magnitude of the expected decrease in the surface resistance (Sec.4.1). For a given material $A \propto \tau B_\omega^2$. For all the films

studied the surface magnetic field could not be raised above a threshold field $B_{\omega c}(T,d)$ and correspondingly the absorbed power had an upper limiting value $P_c(T,d)$. Consequently A could not be raised above a maximum value A_c :

$$A_c = \frac{\tau\ P_c}{2\ N(0)\ (\hbar\omega)^2\ (\sigma_1/\sigma_n)\ \eta\ A\ d} \qquad (4.3)$$

For the Sn films for which systematic data as a function of thickness was obtained we have : $N(0) = 8 \times 10^{21}$ /eV, $\sigma_1/\sigma_n = 0.527$ at $\omega = 2\pi\ 10.12 \times 10^{10}$ rad/sec and $t = 0.5$. $\eta = 0.48$ is the correction factor due to the spatial inhomogeneity of the fields. τ is the quasiparticle scattering time.

Using the calculated values from the literature (Ch.I) for τ, the calculated results for A_c at T = 1.5 K is plotted as a function of thickness in Fig.4.3 (a). It is interesting that $A_c \approx 0.3$ approximately independent of thickness. This is because experimentally $P_c \propto d$ up to $d \leq 3600$ Å . It should be pointed out that eq.(4.3) is strictly true for small $d < \lambda$, l_{in} in order that corrections due to spatial decay of fields and quasiparticle diffusion are ignored.

In Fig.4.3(b) the results of the calculation for the expected maximum decrease in the surface resistance, $\Delta R_s(A_c)/R_s(0) = (R_s(A_c) - R_s(0))/R_s(0)$, which is obtained for the maximum value $A = A_c$, is plotted as function of d for t = 0.5. The experimental results for the same quantity are also shown in the same figure. To within the experimental accuracy of 5% the predicted decrease was not observed in the Sn films studied up to the maximum rf fields $B_{\omega c}$ attainable.

In eqn.4.3 all the quantities except τ are experimentally determined or have reliable values taken from the literature. τ was based upon a calculated estimate for the electron-phonon coupling and there are no direct experimental values available. In fact an observation of the effects predicted by ref.(S2) would lead to a measurement of τ.

If τ were shorter than predicted by theory then the magnitude of the decrease from the analysis would be smaller, since $\Delta R_s \propto A \propto \tau$. In order for the calculated values to be less than 5% (the accuracy of the experiment) τ would have to be smaller by a factor of 4 for d= 200Å and by a factor less than 2 for d = 3600 Å from the value $\tau = 2 \times 10^{-9}$ sec (Ch.I) at t = 0.5.

In other experiments (C2) it is reported that the scattering time τ_E (the same as τ_0 in Ch.I except for a numerical factor) was reduced due to impurity elastic scattering in dirty Al films. This is qualitatively consistent with theoretical predictions (B2,Z1). If the material parameter τ_0 is reduced, then the times τ_R and τ_s and hence τ (Ch.I) would also be reduced.

However a reduced scattering time is not the only reason that the predicted decrease might not be observed. In the analysis of ref. (S2) the phonon system was assumed to be in equilibrium with the bath. The thermal impedance (see section on heating effects) between film and substrate was ignored. The finite value of this impedance would lead to a non-equilibrium phonon distribution (usually called phonon trapping (K1)) which would counteract the predicted decrease. This particularly affects τ_R (K1). Unfortunately the question can only be settled by detailed numerical calculations and we have not pursued the matter any further.

2.2. "Dirty" Al films

It was earlier mentioned that one "dirty" Al film did show a decrease of surface resistance with increasing power. Since Al has the longest τ it would be the most suitable material to study. This apparently promising result was not pursued for two reasons :

(a) The low field R_s was higher than the predicted BCS value by a factor approx. 10 (Fig.4.6). R_s did not have the BCS temperature dependence either.

"Dirty " Al films are well known to be granular. Josephson coupling between the grains is known to dominate the superconducting aspects of such films and the absorption mechanism according to BCS is likely to be inadequate. Because of this aspect, the interpretation of this decrease in R_s in terms of the model in ref.(S2) based on the BCS model seemed dubious.

(b) Other films prepared under apparently identical conditions showed no change in R_s to within 5% until the onset field was reached . However B_{ons} was the same (0.5G) . Thus the observed decrease seemed likely to be sensitive to morphological details of the film.

2.3. Suggestions for further experiments

In light of the above analysis we make several suggestions toward the possible observation of the predicted effects of ref.(S2).

(a) Since Al has the longest τ ($\approx 10^{-7}$ sec) among common materials it would be the most suitable material to study in pure form. In fact, gap enhancement has been observed only in Al. However we need to go to lower temperatures (< 1.3 K) which was not easily feasible.

(b) The sensitivity of the measurement could be greatly enhanced by employing more than one frequency. One frequency could be used to excite the superconductor and another to measure its response. This could be done by employing a multimoded cavity. Care would have to be taken to avoid spurious nonlinearities. Such an experiment would be more complicated than the one described here, particularly if one were to be able to measure the power absorbed in the cavity.

3. The High-Frequency or Dynamic Critical Field

Earlier in this chapter, mention was made of an unexpected limitation on the maximum microwave field that could be applied to the superconducting films. When this field level was reached, the absorption increased abruptly (Fig.4.2). This sudden or critical phenomenon cannot be understood in terms of a gradual departure from the homogeneous BCS ground state, but is rather indicative of a threshold, whence a radically new process comes into play. The remainder of this chapter is devoted to an elucidation and identification of this process.

Associated with the critical field $B_{\omega c}$ is a critical absorbed power P_c. The two are related by eqn.(4.1). Despite this interrelation it is possible to associate effects due to either $B_{\omega c}$ or P_c, e.g.thermal heating associated with absorbed power. We examine both cases in the subsequent discussion.

4. Thermal Effects : Experimental and analytical investigations

First we consider effects associated with the absorbed power - particularly the question of thermal stability. Next we consider magnetic field effects.

4.1. Steady State Temperature increase

Since microwaves are absorbed it is natural to ask whether the increased absorption is due to a temperature rise caused by heating of the film. The energy absorbed by the film from the microwaves is transmitted to the substrate and then to bath. There are, however, thermal boundary resistances at both the Sn/Sapphire and Sapphire/liq. He interfaces which could result in an increase in temperature of the film above the ambient given by the expression :

$$\Delta T = R_k(T) \frac{P_{abs}}{\eta A} \tag{4.6}$$

where R_k is the thermal boundary resistance, P_{abs} is the power absorbed, A is the area of the film and η=0.48 is a geometric factor arising out of the spatial inhomogeneity of the microwave fields in the TE_{011} mode. The values of R_k reported in the literature are (T5):

$$R_{Sn/Sapphire}(T) = \frac{29}{T^3} \text{ cm}^2\text{K/Watt} \tag{4.7}$$

$$R_{Sapphire/liq.He}(T) = \frac{44}{T^3} \text{ cm}^2\text{K/watt} \tag{4.8}$$

For the 650 Å film at T= 1.5 K the temperature rise at $P_{abs} = P_c$ is ΔT = 5mK in the steady state. The change in R_s caused by a temperature rise of this magnitude is well below the accuracy of the measurement (5%). Clearly the steady state temp. increase is inadequate to explain the onset behaviour described earlier. We have experimentally verified this steady state temperature rise (see later in this section).

4.2. Dynamic Thermal Instability

The above consideration was limited to the steady state which was assumed to be stable. We turn now to the question of stability and show that there exists a threshold power absorption level above which the assumption of stability breaks down and compare this power level with the observed values of $P_{ons}(T,d)$.

Consider the situation depicted in the accompanying figure.

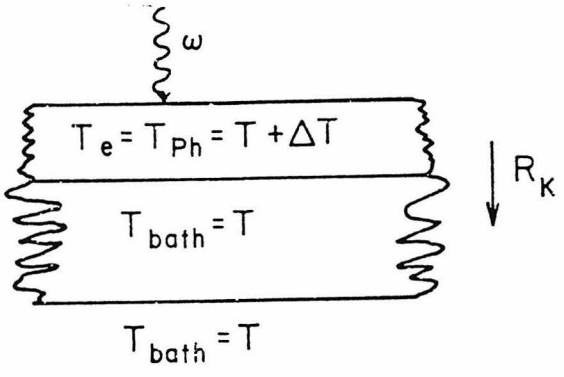

The instantaneous temperature difference ΔT between film and substrate is determined by the rate equation :

$$C \frac{d}{dt}(\Delta T) = P_{abs}(T+\Delta T) - \frac{A}{R_k}\Delta T$$

where C is the specific heat of the film material. Using the assumptions valid at $T \ll T_c$:

$$P_{abs} \propto R_s H^2 \propto e^{-\Delta/T}$$

$$P(T+\Delta T) = P + \frac{dP}{dT} \Delta T$$

we get :

$$C\frac{d(\Delta T)}{dt} = P_{abs} + (P_{abs}\frac{\Delta}{kT^2} - \frac{A}{R_k})\ \Delta T$$

The solution to this eqn is :

$$\Delta T = (\Delta T)_0 + A\, e^{Dt} \qquad (4.9)$$

$$(\Delta T)_0 = \frac{P_{abs}}{C}\frac{1}{D}$$

$$C\,D = P_{abs}\frac{\Delta}{kT^2} - \frac{\eta A}{R_k}$$

From the above eqns. it is clear that $\Delta T \to (\Delta T)_0$ as $t \to \infty$ and hence the steady state is stable for $D < 0$. When $D > 0$, $\Delta T \to \infty$ at $t \to \infty$ and the temperature difference is unstable. Thus $D = 0$ defines a threshold power absorption level :

$$P_{th} = \frac{kT^2}{\Delta}\frac{\eta A}{R_k} \qquad (4.10)$$

Using eqn.(4.7) for R_k and A = 15 cm^2, eqn.(4.10) becomes, with T in K :

$$P_c(T) = 0.038\,T^5 \text{ watts} \qquad (4.11)$$

Of course ΔT does not rise indefinitely when P_{abs} is above the critical value. One expects that when the temperature has risen to T_c superconductivity is destroyed. When that happens the above analysis has to be modified. However eqn.(4.11) correctly predicts a threshold power level for the occurrence of such a process.

Eq. (4.11) is compared with the experimental values of P_c at T = 1.5 K in Fig.4.4. It is immediately apparent that the values predicted by eqn (4.11) are larger than P_c by a factor between 10^1-10^2 depending on thickness. Furthermore, whereas $P_{ons} \propto d$ approx., eqn (4.11) predicts that P_c is independent of thickness. The reason is that thermal transport across the interface is only determined by the area (the films were thin enough that temp. gradients across the films were expected to be negligible) and is independent of the amount of material behind the interface. (Note further that the thicknesses d > 200 Å are greater than the wavelength of thermal phonons which is approx < 100 Å.)

The above considerations clearly rule out the possibility that the observed onset phenomenon was due to thermal heating of the film.

We have also analysed the case of an unstable electron temperature. The analysis is similar to that above with the electron - phonon volume resistance

(determined by the electron - phonon scattering time τ) replacing R_K. Because the process is a volume effect, the resulting critical power d $P_{e-p} \propto$ d, as are the experimental results. However, if this process were relevant, τ would have to be longer (by $\sim$ 50) than predicted by theory. Since there is no other evidence to support this possibility, we feel that this process is unlikely to be applicable to the present situation.

4.3. Experimental examination of thermal heating effects

Despite the indications of the analysis that thermal heating effects are unimportant, it is necessary to establish this as an experimental fact. Several experimental observations and checks carried out that reinforce this conclusion are described below.

(a) The steady state temperature rise of the substrate was measured with an Aquadag thermometer. A strip of Aquadag was deposited on the substrate and its temperature coefficient of resistance(TCR) measured between 1.5 - 4.2 K. With microwave power incident on the film the instantaneous temperature rise of the thermometer was observed as a change in resistance This change in resistance when converted into a temperature change from the measured TCR was never greater than 2 mK, an entirely negligible change.

(b) It was observed that $B_{\omega c}$ was independent of pulse length, especially for thin films and low temperatures. Heating effects have a characteristic signature in being dependent on pulse length. In this observation we are using the film itself as its own thermometer since the surface resistance rises with temperature. For the thicker films the results were pulse length dependent and consequently we have concentrated on the thin films.

(c) In all the analysis carried out so far the assumption has been made that the boundary resistance between the superconductor and substrate was fairly well known. This assumption is very well justified . For the solid-solid interface, experiment and theory agree very well for the thermal boundary resistance (Ch.I,G1). There does exist a well known disagreement with theory for the solid - liq. He interface. Even there the experimental picture is well documented (T5).

Despite the confidence one can attach to the heat transport across the interface, it was necessary to verify that there did not exist pathological problems associated with the films that were used in this study. This possibility was examined by measuring B_{ons} in the following situations :

(1) First $B_{\omega c}$ was measured with the resonator evacuated (usual configuration). Then liq. He was condensed into the resonator at 4.2 K so as to entirely fill the resonator. The apparatus was then cooled down and $B_{\omega c}$ measured again.

Because of bubbling in the liq. He , coupling to the cavity was difficult above the lambda point. Below 2.1 K when liq. He becomes superfluid this problem did not exist and measurements were made as before.

The meaured values for $B_{\omega c}$ and P_c for the two cases were identical to within the experimental accuracy. Since the thermal conductivity of superfluid He is infinite below 2.1 K, this result clearly demonstrated that the thermal conductivity of the material in contact with the film was not a limiting factor. Furthermore the dynamic response for $P_{inc} > P_{ons}$ was the same in both cases. In other words the two configurations were indistinguishable in their consequences on R_s , $B_{\omega c}$ and P_c. Nucleate pool boiling, which might arise if a localized area suddenly increased in temperature, would give a clear signature of instability. This was not observed.

(2) The above experiment still did not eliminate possible substrate effects on the results, since the heat conduction could take place via two channels - film - substrate - He and film - liq . He. In order to eliminate entirely the effects of the first channel an experiment was carried out with identical films evaporated on sapphire and an optically polished glass disc.

Since the glass substrate had a thermal conductivity $\approx 10^3$ times smaller than sapphire it was impossible to carry out measurements unless the film was in direct contact with liq. He . Once again below the lambda point measurements of $B_{\omega c}$ and P_c were carried out. The results for the glass substrate were identical to those of the sapphire substrate to within the experimental accuracy.

These two sets of experiments demonstrated that the measured values of $B_{\omega c}$ and P_c were the same to within the experimental accuracy of $\pm$ 35 % for the

three configurations -- vacuum-film-sapphire, liq. He - film-sapphire and liq.He - film-glass. These results clearly demonstrated that the observed critical phenomenon was not due to possible thermal heating effects associated with the absorption of microwaves.

From the experiments described above we conclude that the film is apparently stable at the absorbed critical power, especially for thin films. Thermal instability as a possible cause for the observed critical behaviour can be categorically ruled out.

We now examine effects associated with the magnetic field.

5. Thermodynamic Critical Field

We now turn to the examination of magnetic field effects as possible mechanisms for the observed critical phenomenon.

It is well known that there exists a critical field at which the homogeneous superconducting state is destroyed. The details of the magnitude of the critical field and the response of the superconductor when this field is applied depend on the nature of the superconductor i.e. whether Type-I or Type-II. In either case one would expect that when this field is reached the superconductor would show an abrupt increase in absorption, largely because of the appearance of normal inclusions.

For a thin film with a field applied on one side and zero field on the other (Fig.4.6 a), a current is induced in the film. (Ch.II & Ch.III). When the current reaches the Ginzburg-Landau critical current,depairing sets in and the film makes a transition to the normal state. Douglass (D1) has derived an expression for the critical field under such conditions for a thin local film with $d << \lambda$:

$$B_c(d) = \sqrt{(8/27)}\,\frac{d}{\lambda}\,B_{co} \qquad (4.12)$$

where B_{co} is the bulk critical field. As $d >> \lambda$ then $B_c = B_{co}$.

In Fig.4.5(a) we plot the experimental results for $B_{\omega c}$ for d = 190 Å along with the values calculated from eqn.(4.12). It is evident that the experimental values lie well below the calculated values indicating that homogeneous

destruction of the superconductor was not responsible for the observed critical phenomenon.

6. Vortex Pair Generation

We now turn to the possibility of inhomogeneous destruction of superconductivity.

In bulk superconductors the nature of field penetration into the superconductor on the sample at large applied fields is dependent on the type of superconductor (H1). In type I superconductors normal sheets or laminae develop. In type II it is favourable for the field to penetrate into the sample in the form of quantized vortex lines.

Thin films in perpendicular fields also exhibit Type II behaviour (H1) forming vortices perpendicular to the film plane. However in the present configuration the magnetic field is parallel to the film and applied on one side only - surprisingly a rather uncommon configuration. Consequently we have had to develop a new idea regarding penetration by formation of vortices. (This was first reported in (S10)).

For the thin films under consideration, $d < \xi$ and it is energetically unfavourable to form a vortex line parallel to the film plane.

Consider the situation depicted in Fig.4.6(a) and (b). Starting from Fig.4.6(a) which depicts the Meissner state, let a small normal "bubble" form as in (b). We consider this bubble to be in the form of two vortices of opposite sign almost superposed on each other. The current induced in the film by the magnetic field tends to push this vortex-antivortex pair apart. At the same time the vortices tend to attract each other (P3). The attractive interaction energy can be written as :

$$U_{vv}(r) = \frac{{\varphi_0}^2}{8\pi^2\Lambda} \ln\left(\frac{r}{\xi}\right) \qquad r \ll \Lambda \tag{4.13}$$

$$U_{vv}(r) = \frac{{\varphi_0}^2}{8\pi^2\Lambda} \exp(-r/\Lambda) \qquad r \gg \Lambda$$

where $\Lambda = \lambda^2/d$ is called the transverse penetration depth and ξ is the core

radius (taken to be the coherence length). The repulsive potential due to the field(current) is just $U = -\varphi_0 H / 4\pi r$. The configuration of Fig.4.6(c) will be energetically stable at a maximum field which is obtained for a separation $r \approx \Lambda$, since the interaction falls off exponentially at larger distances. From an energy balance at this distance we get for the critical field at which the pair is just stable :

$$B_v = \frac{\varphi_0}{\pi \Lambda^2} \ln\left(\frac{\Lambda}{\xi}\right) \tag{4.14}$$

to within a numerical coefficient of order unity.

Eq.4.14 represents a threshold field above which the vortex pair dissociates under the action of the external field. We now show that under certain conditions $B_v(d)$from eq.4.15 can be smaller than the critical field $B_c(d)$ from eqn.(4.12).

Using the Ginzburg-Landau value for the bulk critical field (T1) :

$$B_{c0} = \frac{\varphi_0}{2\sqrt{2}\pi\xi(T)\lambda(T)}$$

$$B_v(d) = 2\sqrt{2}\,\frac{\xi}{\Lambda} \ln\left(\frac{\Lambda}{\xi}\right) B_c(d)$$

Thus this mechanism predicts a critical field smaller than the thermodynamic value by a factor of order

$$\frac{\xi}{\Lambda} \ln\left(\frac{\Lambda}{\xi}\right)$$

This factor is << 1 if $\xi \ll \Lambda$. This is basically equivalent to the statement that the size of the vortex core ξ has to be much smaller than the range of interaction Λ. This factor is proportional to $l^{3/2}$ and so the vortex pair dissociation field is well below the thermodynamic value when the m.f.p. is reduced (which also happens if the thickness is reduced).

We compare the experimental values for $B_{\omega c}$ with the calculated values in Fig.4.5(a) and (b) along with the G-L critical field. Two comments are appropriate :

(1) Fig.4.5 displays the fact that B_v is smaller than B_c the thermodynamic critical field as the thickness is decreased - this was demonstrated earlier.

(2) Experiment and the theory for B_v approach each other as the thickness decreases. Using the parameters of Table 2.1 we have for the films studied here:

d(Å)	ℓ(Å)	Λ (Å)	ξ(Å)	ξ/Λ
190	160	16164	520	0.03
650	280	2871	690	0.24
1100	725	800	1100	1.4

The calculation of B_v is strictly valid in the limit $d, \xi \ll \Lambda$ and so is more applicable to thinner films. Note further our comments that thermal effects may impact on the results for thicker films.

We regard these results as indicative that the proposed vortex-pair generation mechanism is responsible for the observed critical behaviour at least for the thicker films.

We have further attempted to experimentally test these ideas in the following ways:

(1) EXCESS TRANSMISSION

In Fig.4.6(c) the microwave field has penetrated to the other side of the film. If this actually occurs then it should manifest itself as excess transmission through the film.

This was verified by measuring the transmitted power P_{xmitt} as described in Ch.II. For $B_\omega < B_{\omega c}$ and $P_{abs} < P_c$, P_{xmitt} was linearly proportional to the power incident to the resonator. When $B_\omega = B_{\omega c}$ and the incident power was raised further, P_{xmitt} began to rise steeply (faster than linear), as is to be expected if the field begins to penetrate.

(2) SUPPRESSION BY MODIFICATION OF BOUNDARY CONDITIONS

A process like the vortex-pair generation should be sensitive to the electromagnetic boundary conditions. This is because in Fig.4.5 the field penetrates from vaccum on one side of the film to vacuum on the other. We have tested to see if the generation process could be suppressed by employing the configuration of Fig.4.5(d).

First a 500 Å film of Al was evaporated onto the sapphire substrate. It was exposed to air for 20 mins. whence it forms a dielectric oxide layer on the surface. Then 600 Å Sn was evaporated onto this configuration. The experimental observations were :

(a) The T_c of the Sn was unchanged, showing that the oxide suppressed the proximity effect as desired.

(b) the measured resonator Q as a function of B_{max} is shown in Fig.4.7. Also shown for comparison is the result for the usual configuration with d = 650 Å for Sn. Fig.4.7 indicates that the Al ground plane apparently suppressed the critical behaviour.

The decrease of Q at high fields is associated with the large absorption in the *normal* Al film resulting in heating since it was pulse length dependent.

(c) If the critical phenomenon were thermal then this configuration should enhance not suppress it since we have introduced two additional interfaces.

In this configuration the vortex pair generation is suppressed because of the normal Al film acting as a "ground plane". Motion of the vortices is hindered by eddy currents generated in the Al film - the ground plane effectively pins the vortices. In other words the vortices are not free to move - in this picture, their motion gives rise to the sharp increase in absorption observed in Fig.4.2.

6.1. Static and High Frequency fields

Hitherto we have used static concepts to understand the action of a high frequency field. Preliminary experiments have been carried out to see if these ideas apply to the static case.

For the measurement of a static critical field applied to one side of the film (not a usual configuration) the experimental setup used was identical to that of Ch.III. It was observed that at low temperature ($t < 0.9$) flux was irreversibly trapped into the film at a field level $B_0 = B_{fl}$.

Measured values for $B_{fl}(T,d)$ for $d = 190$ Å are shown in Fig.4.8 along with $B_{\omega c}$, B_v and Bc. We make the following comments:

(a) The measured static field $B_{fl}(t,d)$ was larger than the high frequency critical field $B_{\omega c}$, though still smaller than the thermodynamic critical field.

(b) B_{fl} is comparable to the vortex pair generation field B_v which is reasonable since B_v was derived using static concepts.

(c) Interestingly, the static transition at B_{fl} was irreversible - when the field was removed the resonator Q was irreversibly reduced implying that vortices or flux lines were irreversibly trapped either at pinning sites or at the edges.

(d) The critical current corresponding to B_{fl} agrees with the results reported in the literature for wide, flat samples (T7).

For the high frequency case the transition (Fig.4.2) at $B_{\omega c}$ was completely reversible.

Comments (a),(b) and (c) are consistent with relating the high frequency field $B_{\omega c}$ with Fig.4.6(b) and the static field B_{fl} with Fig.4.6(c). In Fig.4.6(c) we are implicitly assuming that the constituents of the pair have had all the time to reach full maturity as macroscopic objects with quantized angular momentum. In Fig.4.6(b) the bubble (" surface roton" ?) merely oscillates and does not have time to dissociate.

We might ask how far a vortex travels in 10^{-10} secs. Using purely classical (i.e. Maxwell's) eqns. it can be shown that a normal front propagates one normal state skin depth λ_n corresponding to the frequency ω. For these materials $\lambda_n \approx 1\mu$ at 10 GHz and this is expected to be the bubble size. Joule heating which has been ignored tends to increase this estimate.

COMMENT ON QUASIPARTICLE DYNAMICS

The analysis used thus far involved macrosopic considerations of quantized vortices. In Ch.III we considered the microscopic quasiparticle dynamics. Interesting questions arise when one considers the action of rapidly varying large fields applied to a superconductor and the consequent quasiparticle response. Using the ideas of Ch.III, the density of states, order parameter and quasiparticle distribution oscillate at the applied frequency. When the fields are large one has to consider if the distribution function is dynamically stable. This aspect is particularly interesting in the context of the stability of non-equilibrium states (T6). We have considered the case of instability of the electron temperature (Sec.4). It would be interesting to examine the microscopic distribution function response in this case in order to see if the observed onset is related to an instability of the distribution function.

7. Conclusions

A dynamic or high frequency critical field was observed experimentally as an abrupt onset of increased microwave absorption of thin superconducting films at the critical field level. This field level was well below the thermodynamic field level. Experimental and theoretical analyses unequivocally demonstrate that this onset is not associated with thermal heating effects. A model for the inhomogeneous destruction of superconductivity via formation of a vortex-antivortex pair is proposed. The formation of the vortex pair leads to penetration of the field through the film and hence to increased absorption. Calculations of this pair-generation critical field for thin dirty films agree with the experimental results for the thinnest films. Further experimental support for this model was obtained by observing that the transmission through the film increased when the critical field was reached and that this process was suppressed by a metallic ground plane.

Figures for Ch.IV

Fig.4.1 $1/Q(B_{max})$ vs. B_{max} for homogeneous Pb/Cu resonator.

Fig.4.2 $Q(B_{max})/Q(0)$ vs. B_{max} for Sn on Sapphire films.

Fig.4.3 Comparison of experimental results for Sn films with the calculations of ref.(S2).

(a) Maximum value of parameter $A = A_c$ (eq.4.3) for $B_{max} = B_{\omega c}$

(b) Experimental and expected changes in R_s at $B_{max} = B_{\omega c}$ for different thicknesses.

Fig.4.4 Experimental values for the critical power P_c compared with eq.(4.11) based on a dynamic thermal instability (solid line). ○ 200Å, x 440Å, ▫ 650Å, ✱ 3600Å.

Fig.4.5 Experimental values for $B_{\omega c}(T,d)$, vortex pair generation field $B_v(T,d)$ (eq.4.14) and thermodynamic critical field $B_c(T,d)$ (eq.4.12).

(a) vs. temperature for d = 190Å.

(b) vs. thickness for T = 1.5K.

Curves (a) B_c (b) $B_{\omega c}$

Fig.4.6 Expected sequence of events illustrating the penetration of magnetic field (Fig.a - c) via the formation of a pair of vortices. Fig.(d) is the configuration used to suppress the formation of the pair.

Fig.4.7 Comparison of the results for a bare 650Å Sn film and that of Fig.4.6 (d). Note that the ground plane has suppressed the critical behaviour.

Fig.4.8 Comparison of experimental values for static critical field B_{fl} (Δ), dynamic critical field $B_{\omega c}$ (O), vortex pair generation field B_v (curve (b)) and thermodynamic critical field B_c (curve (a)).

FIG.4.1

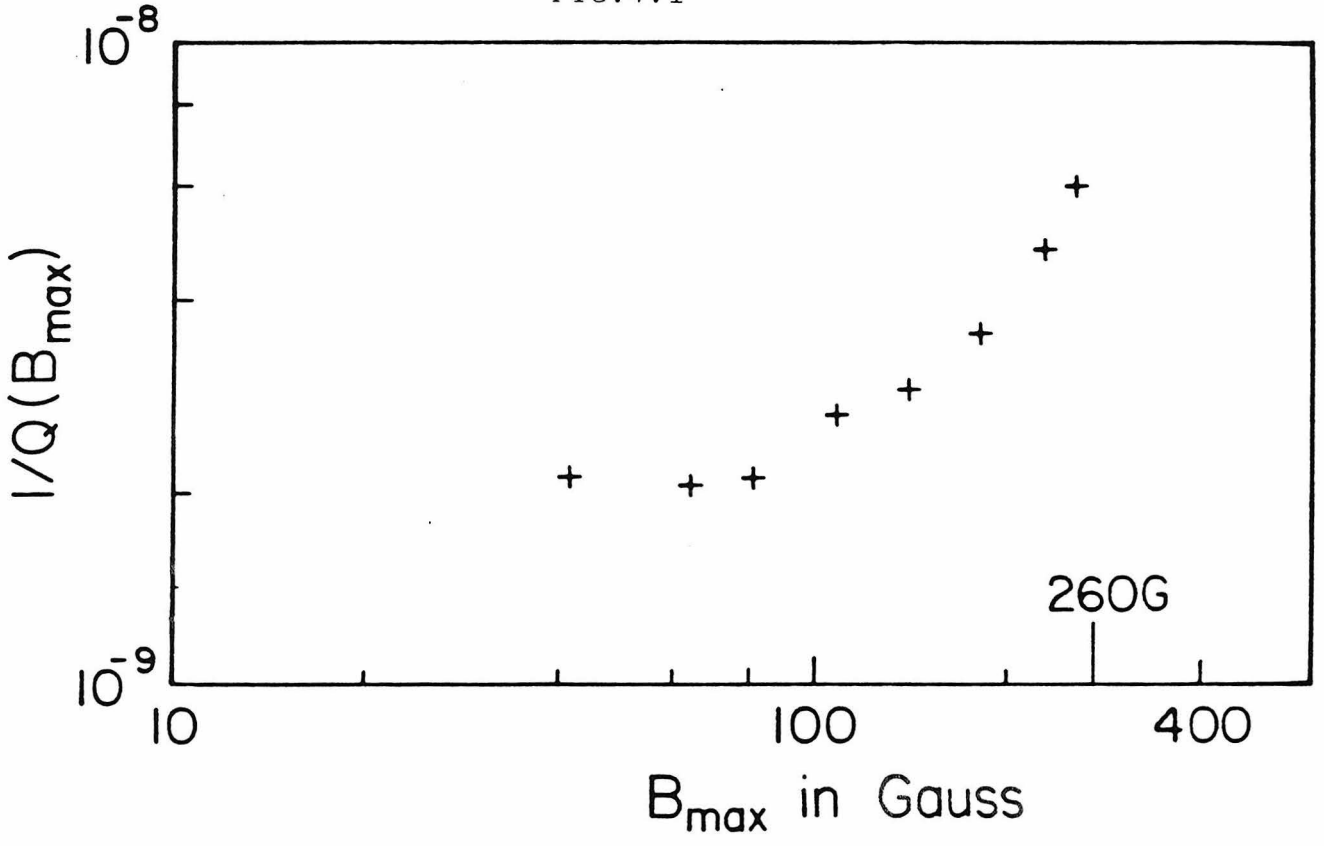

FIG. 4.2

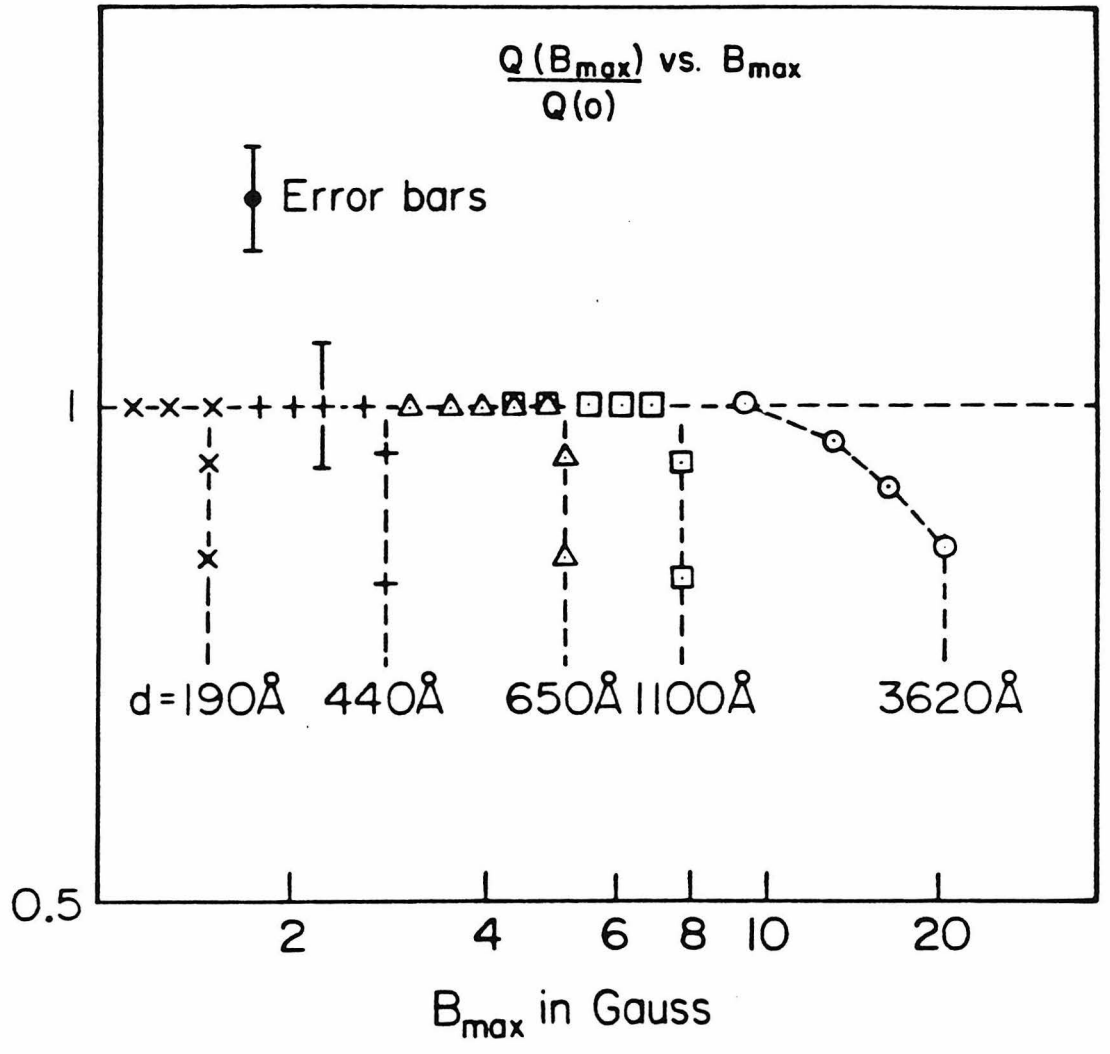
Q(Bmax) vs. Bmax
Q(o)
Error bars
1
0.5
d=190Å
440Å
650Å
1100Å
3620Å
2
4
6
8
10
20
Bmax in Gauss

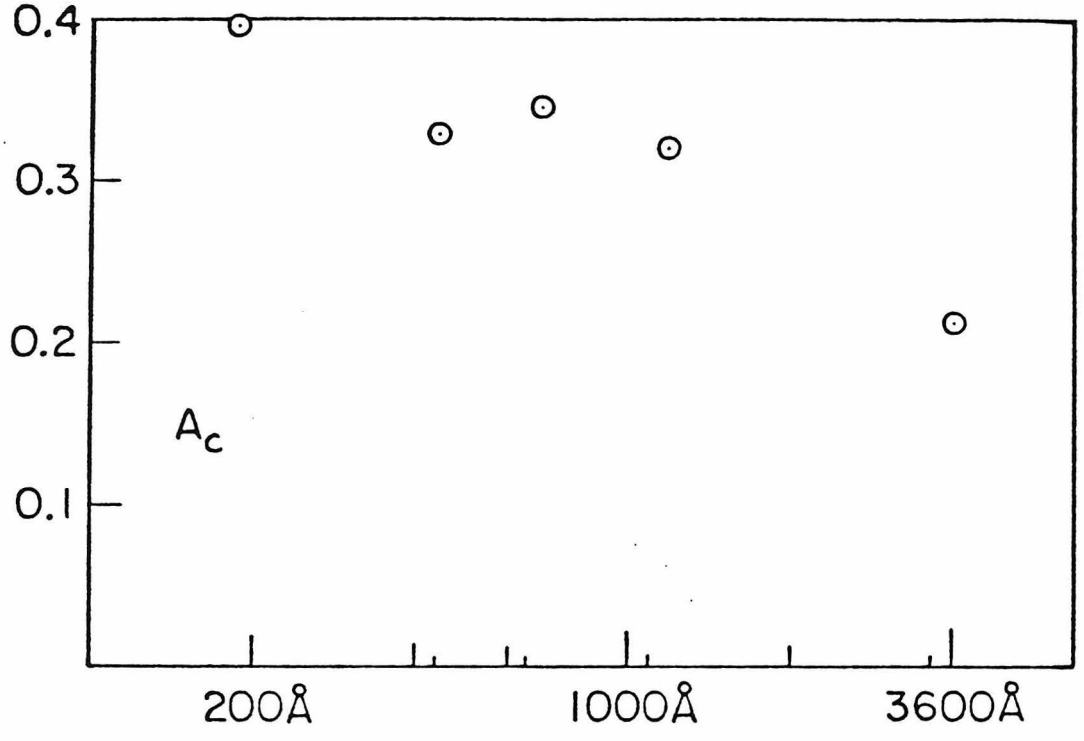
0.4
0.3
0.2
0.1
A_c
200Å
1000Å
3600Å

FIG.4.3

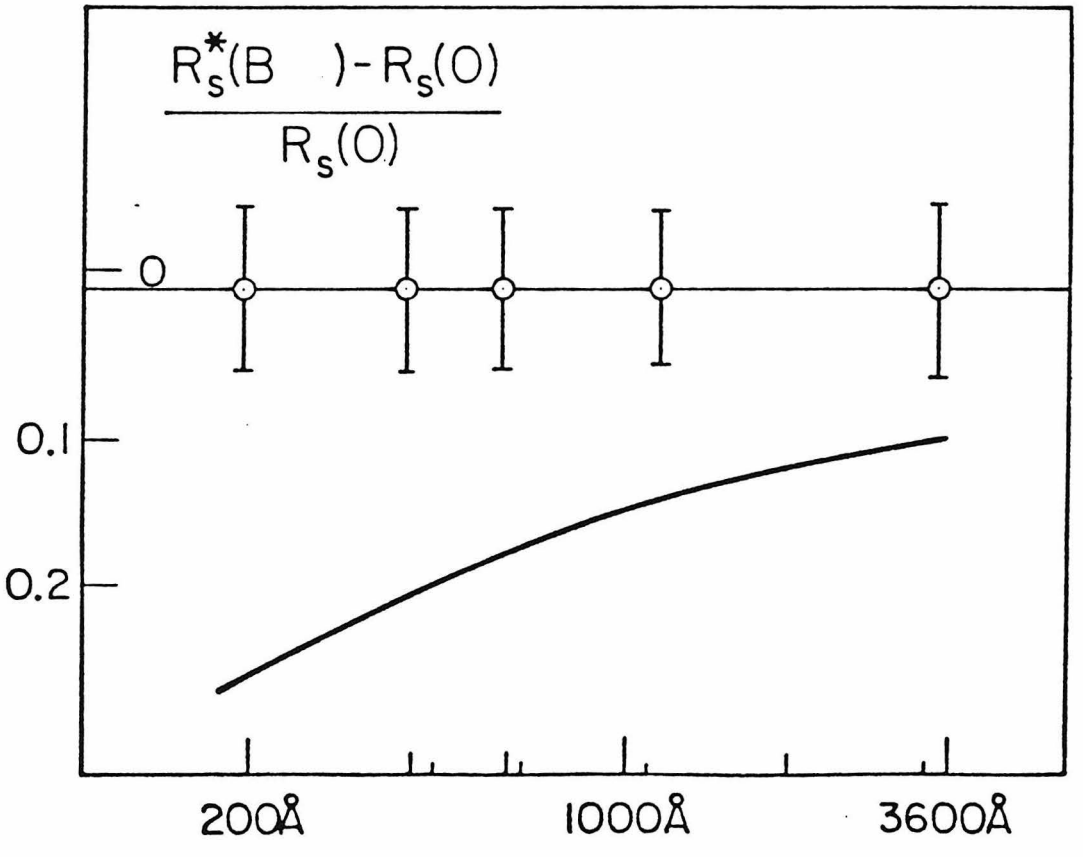
$\frac{R_s^*(B\ \ ) - R_s(0)}{R_s(0)}$
0
0.1
0.2
200Å
1000Å
3600Å

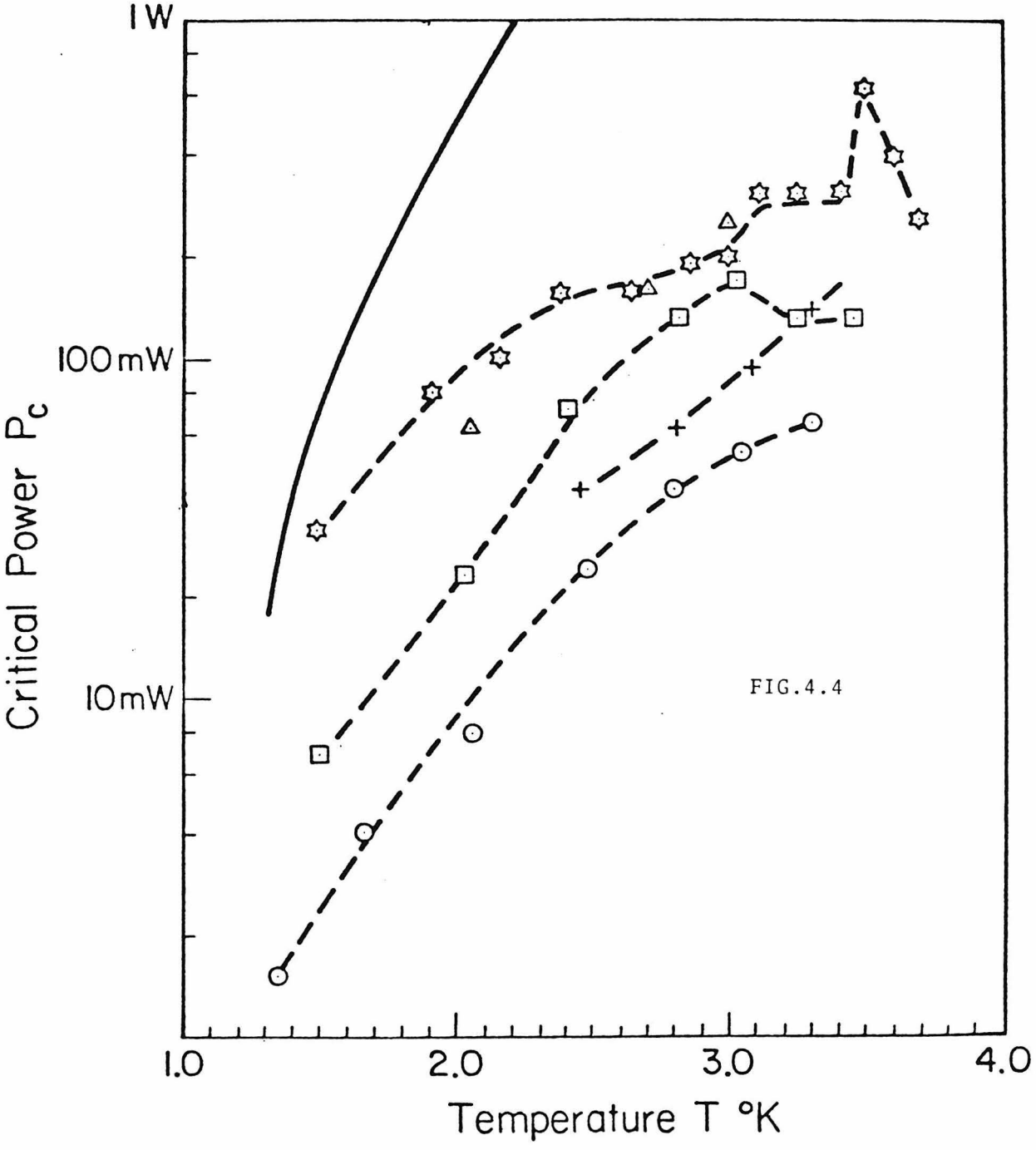

FIG.4.4

FIG.4.5(a)

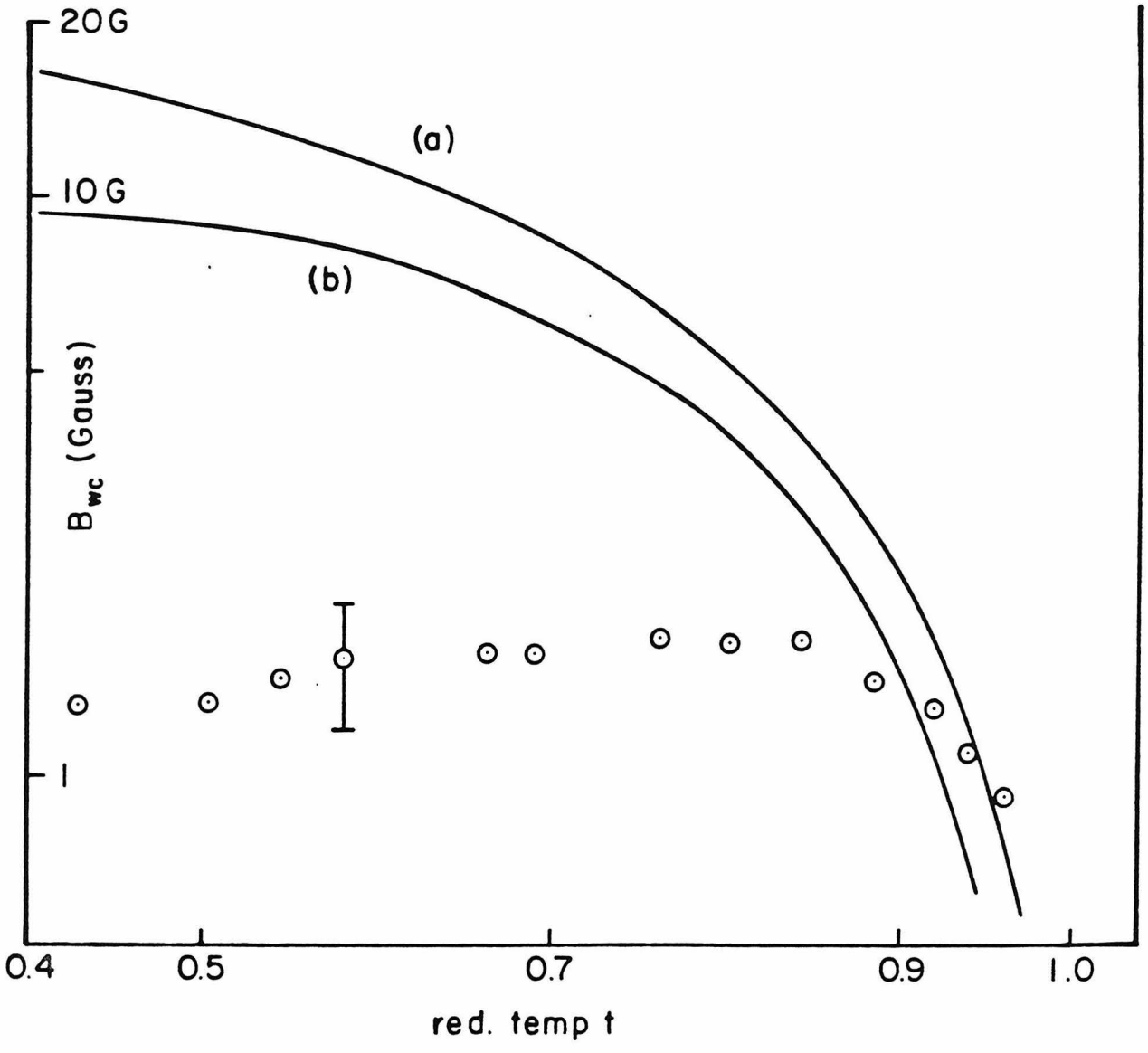

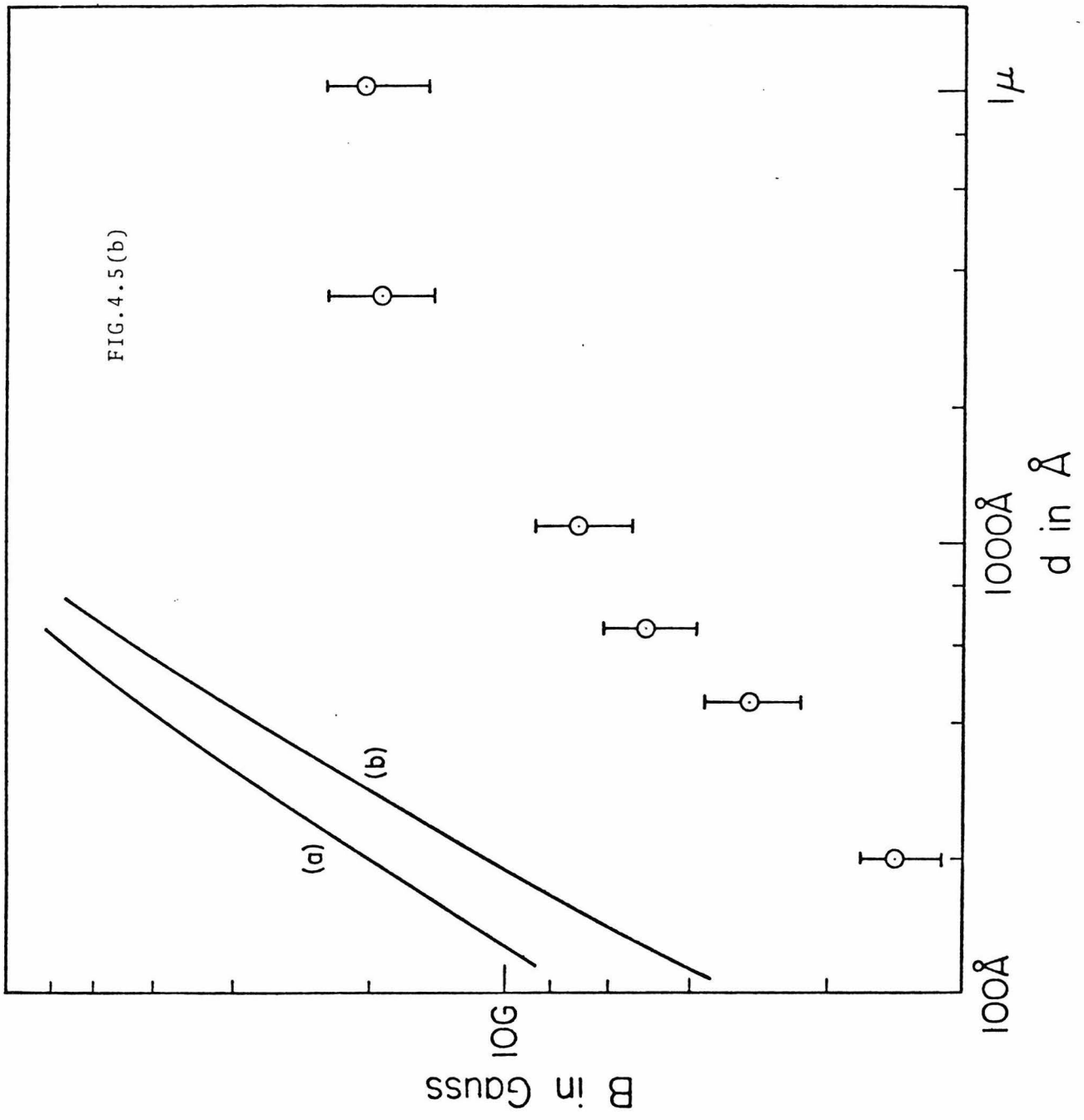

FIG.4.5(b)

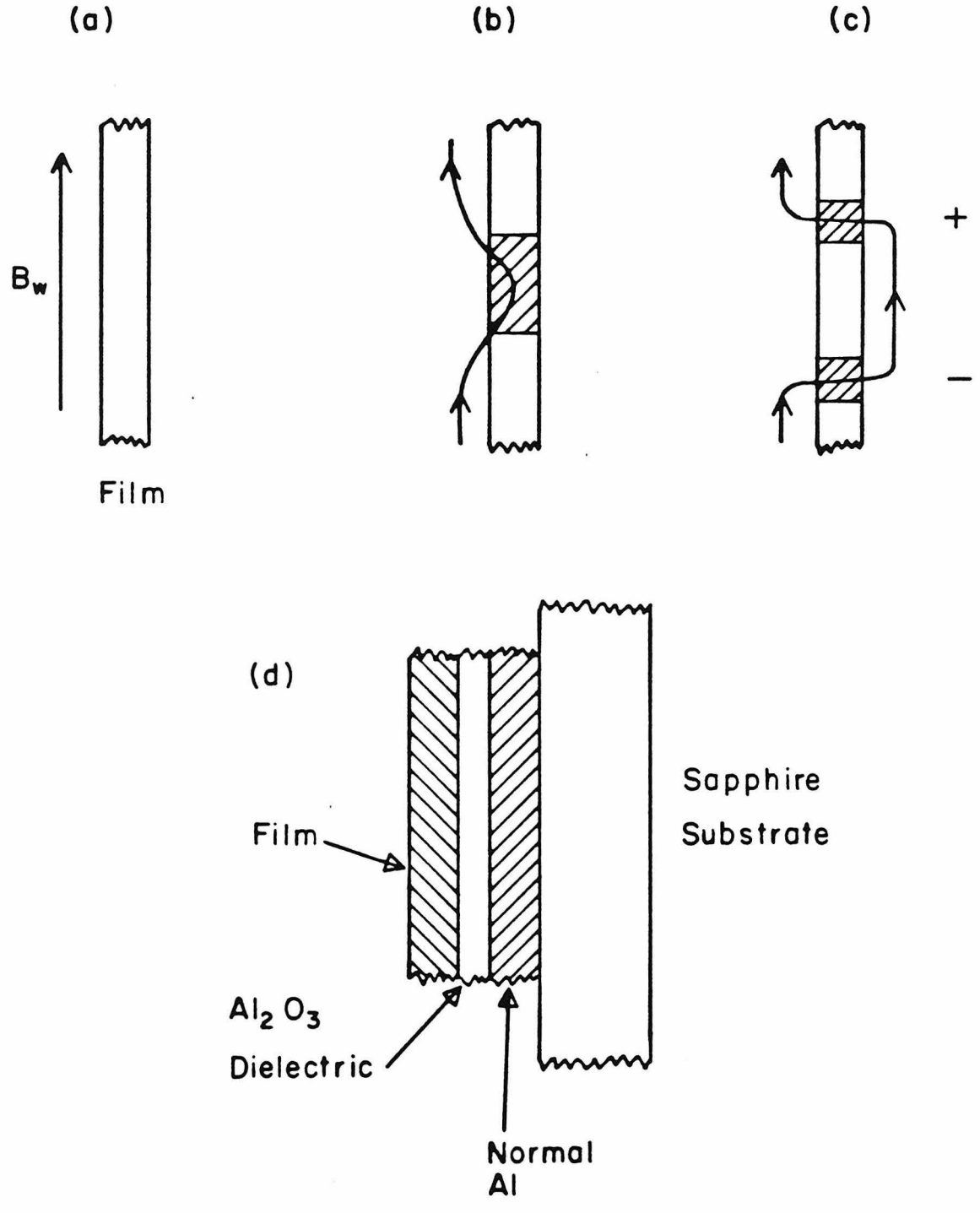
(a)
(b)
(c)
B_w
Film
+
−
(d)
Film
Sapphire
Substrate
Al_2O_3
Dielectric
Normal
Al

FIG.4.6

FIG. 4.7

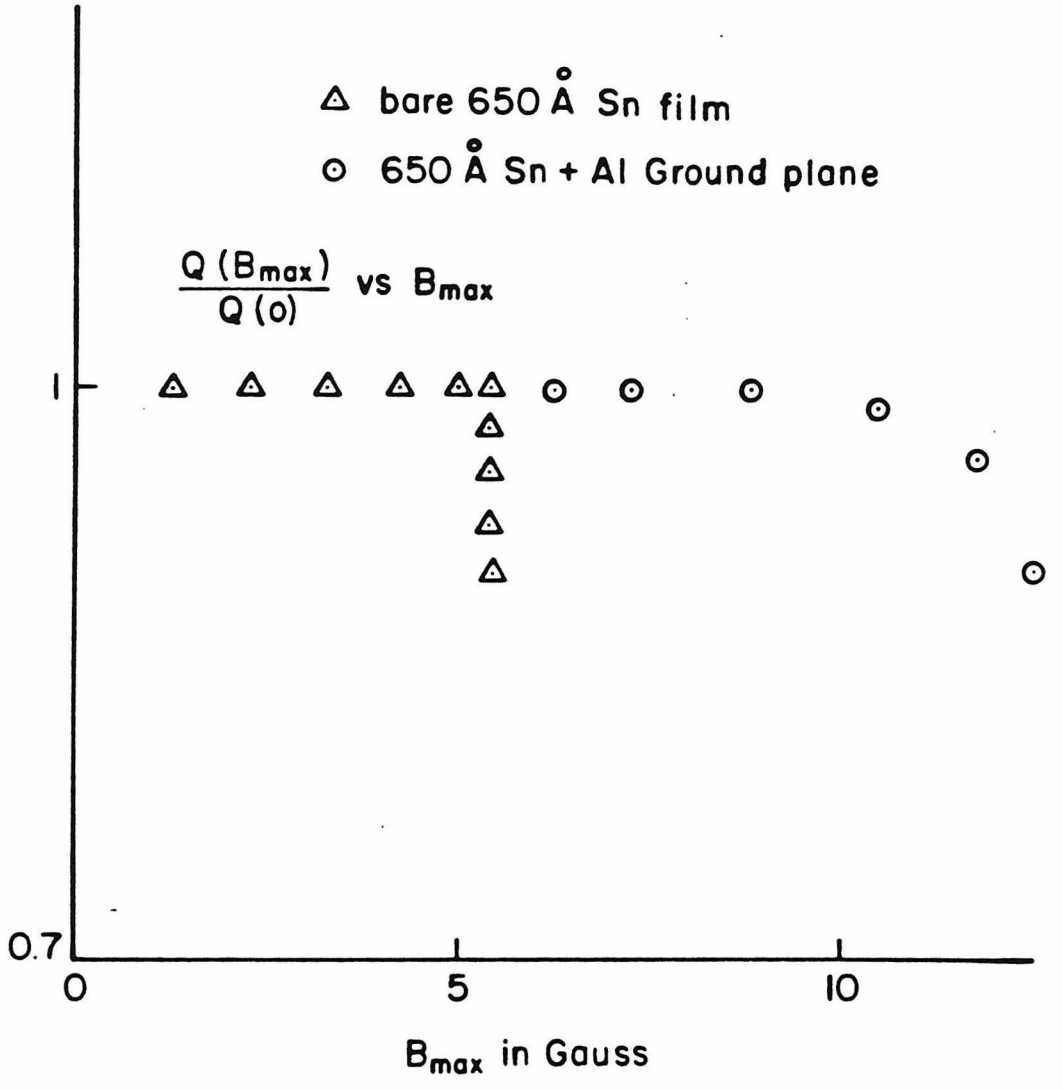
△ bare 650 Å Sn film
⊙ 650 Å Sn + Al Ground plane
Q (Bmax) / Q (o) vs Bmax
1
0.7
0
5
10
Bmax in Gauss

FIG.4.8

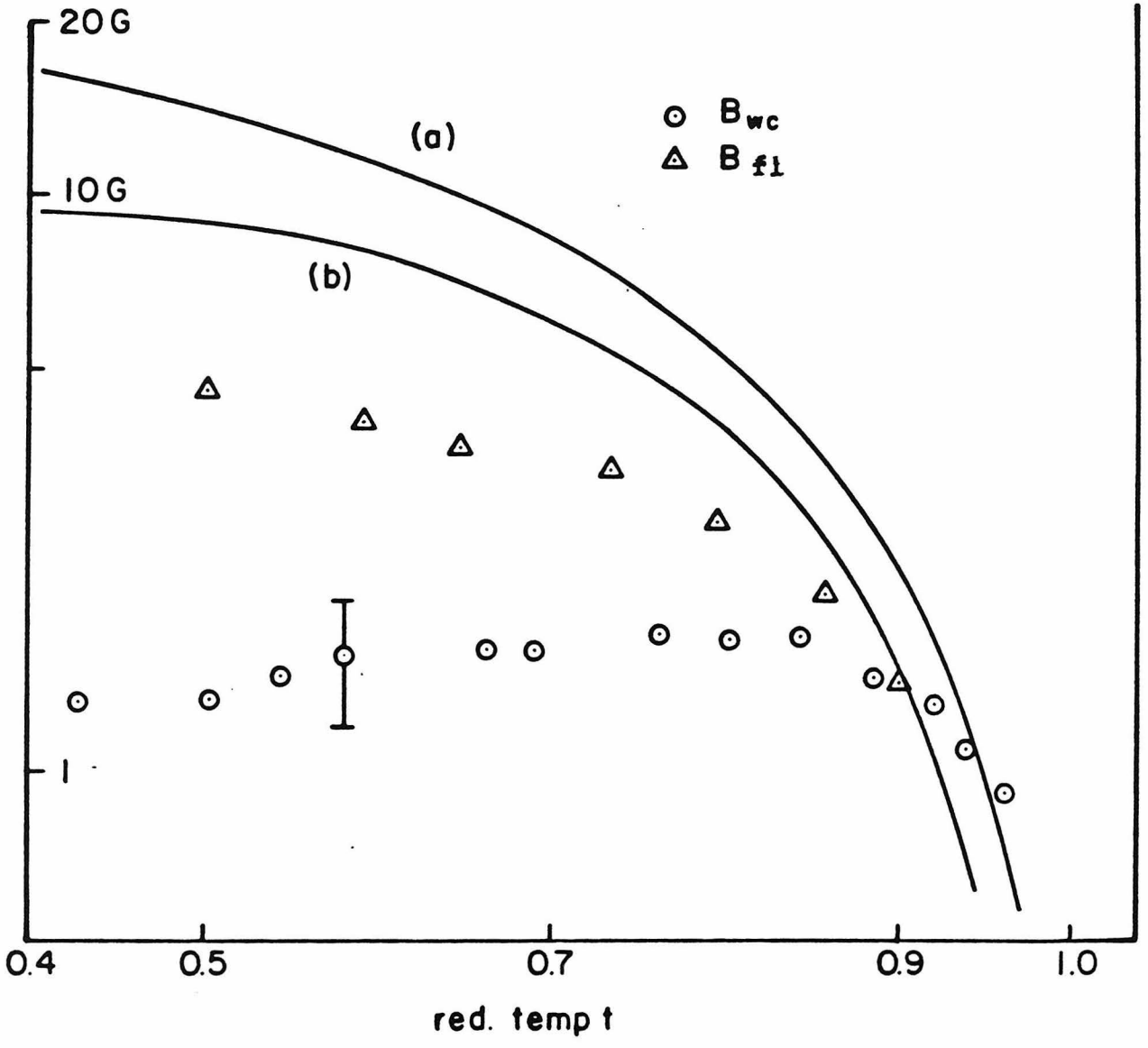

References

A1: Anderson,P.W., J.Phys.Chem.Sol.,**11**,26,(1959)

B1: Bardeen,J.,L.N.Cooper & J.R.Scrieffer, Phys.Rev. **108**,1175,(1957)

B2: Bergmann,G., Phys.Rev.B **3**,3797(1971)

B3: Bardeen,J., Phys. Rev. Lett. **1**, 399 (1958)

C1: Chambers,R.G., Proc. Roy. Soc. **A 215**, 481 (1952)

C2: Clarke,John ,Ch.13 in Ref.(G1)

C3: Chopra,K.L. "Thin Film Phenomena",McGraw-Hill,N.Y.(1969)

D1: Douglass,D.H., Phys.Rev., **124**, 735(1961)

D2: Dick,G.J., J.R.Delayen & H.C.Yen, Proc. IEEE, Trans. Nucl. Sci. **NS-24**, 1130 (1977), *see also* G.J.Dick & J.R.Delayen, Proc. Appl. Superconductivity Conf., Knoxville, Tenn.,U.S.A. (1982, to be published)

E1: Eliashberg,G.M., Sov. Phys. JETP Lett. **11**, 186 (1970)

G1: Gray,K.E. (ed.), "Nonequilibrium Superconductivity,Phonons, and Kapitza Boundaries", Plenum Press, N.Y.(1981)

G2: Glosser,R., Phys.Rev., **156**,500 (1967)

G3: Garfunkel,M.P., Phys.Rev., **173**, 516(1968)

G4: Ginzburg,V.L. & L.D.Landau, Sov.Phys.JETP **10**, *1064 (1950)*

G5 Gittleman,J.I. and Rosenblum,B.R., Phys. Rev. **137**, A527 (1967)

G6: Graham,A.K. (ed) : "Electroplating Engineering Handbook", Reinhold Book Corp., N.Y. (1968)

H1: Huebener,R.P. "Magnetic Flux Structures in Superconductors", Springer Verlag, Berlin (1979)

H2: Halbritter,J.,Externer Berichte, Kernforschungzertrum Karlsruhe, (June 1970)

H3: Halbritter,J.,Z.Physik, **266**, 209 (1974)

H4: Hook,J.R., J. Low Temp. Phys.,**23**, 645 (1976)

H5: Harvey,A.F. : "Microwave Engineering ", Academic Press, London (1963)

J1: Josephson,B.D., J.Phys.F, Metal Physics, **4**, *751,(1974)*

J2: Jackson,J.D. :"Classical Electrodynamics", John Wiley, N.Y. (1975)

K1: Kaplan,S.B. et.al., Phys.Rev.B, **14**, 4854(1977)

K2: Khalatnikov,I.M. & A.A.Abrikosov, Adv. Phys.**8**,45 (1958)

K3: Koch,J.F. & C.C.Kuo, Phys.Rev., **164**, 618 (1967)

K4: Knorr,K., and N.Barth, Sol.St.Comm. **8**, 1085, (1970)

L1: Larson,D.C. in "Physics of Thin Films", Vol.6, Academic Press,(1971)

L2: Lavenda,B. "Thermodynamics of Irreversible Processes", Macmillan, New York (1978)

M1: Mattis,D.C. & J.Bardeen, Phys.Rev., **111**, 41 (1958)

M2: Maki,K., Phys.Rev.Lett.,**14**,98,(1965)

M3: Mooij,J.E., Ch.7 in Ref.(G1)

O1: Ovchinnikov,Yu.N., Sov.Phys.JETP, **32**,72 (1971)

O2: Ovchinnikov,Yu.N. & G.Schon, "Low Temperature Response of Superconductors" (Preprint)

P1: Pippard,A.B., Inaugural Lecture in B.B.Schwartz ed. "SQUIDS" NATO Adv. Study Inst., Plenum Press (1975)

P2: Peters,R. & H.Meissner, Phys.Rev.Lett.,**30**,965 (1973)

P3: Pearl,J.D., Ph.D. Thesis, Polytechnic Inst. of Brooklyn, (1965),unpublished

P4: Parks,R.D. (ed) : "Superconductivity", Vols.I and II, Marcel Dekker (1969)

P5: Parmenter,R.D., RCA Review, **23**, 323, (1962)

R1: Richards, P.L., Phys. Rev., **126**, 912 (1962)

R2: Raynes,E.P., Ph.D. Thesis, Cambridge Univ. (1971, unpublished)

S1: Sridhar,S. & J.E.Mercereau,Bull.Am.Phys.Soc. **26**,412 (1980)

S2: Sridhar,S. & J.E.Mercereau,Phys.Lett. **75A**,392,(1980)

S3: Sridhar,S.unpublished

S4: Schmid,A. & G.Schon, J. of Low Temp. Phys. **20**,207, (1975)

S5: Schon,G: Proc. of LT 16, **I**, 171 (1981)

S7: Sherman,R.D., Ph.D. Thesis, Calif. Inst. of Tech., (1971, unpublished)

S8: Schmid,A., Phys. Rev., **186**, 420 (1969)

S9: Sridhar,S. and J.E. Mercereau, Bull. Am. Phys. Soc.,**27**, 254 (1982)

S10:Sridhar,S. and J.E. Mercerau, Bull. Am. Phys. Soc. **26**, 243 (1981)

T1: Tinkham,M.,"Introduction to Superconductivity", McGraw-Hill, New York (1975)

T2: Tinkham,M., in "Festkorperprobleme",Adv. in Solid State Physics, Vieweg, Braunschweig

T3: Turneaure,J.P. Ph.D.Thesis,Stanford Univ.(1967)

T4: Turkevich,L.N. & S.J.Putterman,Proc. of LT 16,**I**,491 (1981)

T5: Taborek,P. , Ph.D. Thesis, Calif. Inst. of Tech. (1981)

T6: Tremblay,A.-M.S., Ch.10 in Ref.(G1)

T7: Tholfssen,Paul and Hans Meissner,Phys.Rev. **185**, 653 (1969)

Y1: Yogi,T. Ph.D. Thesis, Calif. Inst. of Tech (1977), unpublished

Y2: Yogi,T.,G.J.Dick & J.E.Mercereau, Phys. Rev. Lett., **39**, 826 (1977)

Z1: Zavaritski,N.V., Sov.Phys.JETP, **30**, 412 (1969)